

COHERENT MANIPULATION OF MULTILEVEL ATOMS  
FOR QUANTUM INFORMATION PROCESSING

December 2005

COHERENT MANIPULATION OF MULTILEVEL ATOMS  
FOR QUANTUM INFORMATION PROCESSING

A dissertation submitted in partial fulfillment  
of the requirements for the degree of  
Doctor of Philosophy

By

JUAN DAVID SERNA, B.S., M.S.  
Universidad de Antioquia, 1997  
University of Arkansas, 2004

December 2005  
University of Arkansas

In quantum information processing, quantum cavities play an important role by providing the mechanisms to transfer information between atom qubits and photon qubits, or to couple single atoms with the optical modes of the cavity field. We explore numerically the population transfer in an atom + cavity system by using the  $\pi$ -pulse and adiabatic passage methods. While the first method is very efficient transferring the atomic population for no radiative decay of the intermediate level, the second method shows very interesting nonadiabatic, resonance-like properties that can be used to achieve very large transfer efficiencies without needing very large Rabi frequencies or very long interaction times. We introduce a simple analytical model to explore the origin of these properties and describe “qualitatively” the power-law dependence of the failure probability on the product of the pulse amplitude and the interaction time. We also examine numerically the transfer of interatomic coherence in a two-atom + cavity system by using adiabatic methods. For some specific symmetry conditions, we show that the dynamics of the original system can be studied as the individual evolution of a symmetric and an antisymmetric system, interacting separately with the classical field and the cavity mode, but mutually exchanging the atomic coherence.

This dissertation is approved for  
Recommendation to the  
Graduate Council

Dissertation Director:

---

Dr. Julio Gea-Banacloche

Dissertation Committee:

---

Dr. Luca Capogna

---

Dr. Michael Lieber

---

Dr. Surendra Singh

---

Dr. Min Xiao

# Contents

<b>1</b>	<b>Fundamental Concepts</b>	<b>1</b>
1.1	Introduction . . . . .	1
1.2	The two-level atom . . . . .	2
1.3	$\pi$ -pulses . . . . .	9
1.4	The three-level atom . . . . .	10
1.5	The adiabatic following . . . . .	15
<b>2</b>	<b>Laser-induced population transfer in multilevel systems</b>	<b>18</b>
2.1	The atom-cavity system . . . . .	18
2.1.1	Dark state . . . . .	19
2.1.2	Adiabatic following . . . . .	20
2.1.3	Master equation . . . . .	21
2.2	Numerical results . . . . .	23
<b>3</b>	<b>A simple analytical model</b>	<b>36</b>
3.1	Population transfer . . . . .	36
3.2	Asymptotic behavior of the pulses . . . . .	41
3.2.1	Gaussian pulses . . . . .	42
3.2.2	Hyperbolic secant pulses: . . . . .	44
3.2.3	Lorentzian pulses: . . . . .	45
3.3	The failure probability . . . . .	45
<b>4</b>	<b>Transfer of atomic coherence</b>	<b>51</b>
4.1	The two-atom + cavity system . . . . .	51
4.1.1	Probability amplitude method . . . . .	52
4.1.2	Dark state . . . . .	54

4.1.3	Conditions for adiabatic following . . . . .	54
4.1.4	Density matrix and equations of motion . . . . .	55
4.2	Numerical results . . . . .	57
4.3	An alternative model . . . . .	65
4.3.1	The associated three-level system: EIT . . . . .	65
4.3.2	The associated two-level system: $2\pi$ -pulse coherence transfer . . . . .	68
4.3.3	Transferring the coherence . . . . .	72
<b>Appendix A: Change of variables</b>		<b>77</b>
<b>Appendix B: The instantaneous Hamiltonian eigenstates</b>		<b>79</b>
<b>Appendix C: The forced harmonic oscillator</b>		<b>82</b>

# Chapter 1

## Fundamental Concepts

### 1.1 Introduction

Population transfer in atoms and molecules is one of the most intriguing problems of quantum optics. To carry out successful multilevel excitations is an important task for theoretical and practical purposes. Thus, figuring out different ways of improving the efficiency of those methods used to transfer population between multilevel systems has become an important subject of research during the past years.

In this work, we examine numerically an atom + cavity system with two of the most important methods for transferring population between atomic levels: the  $\pi$ -pulses method and the adiabatic passage scheme. In particular, we explore the possibility of using the nonadiabatic characteristics of the second method to achieve very high transfer efficiencies without using large values of the pulse amplitudes or interaction times.

The  $\pi$ -pulse method takes advantage of the Rabi population oscillations that characterize coherent excitation. By adjusting the laser intensity and the pulse duration so that the time integral of the Rabi frequency (the pulse area) has the value  $\pi$ , it is possible to produce complete population transfer between two states [SBK<sup>+</sup>92]. If the system undergoes no spontaneous emission, transfer efficiencies of 100% are possible to obtain with this method. However, a very accurate control of the pulse area is required, which is a really disadvantage.

The adiabatic passage scheme is an alternative for transferring population between selected quantum states. The population can be transferred between two states by driving the system sufficiently slowly with the appropriate external fields, with the population remaining in an approximate energy eigenstate. This method is quite insensitive to changes in parameters like the laser pulse shapes,

intensity, and frequency modulation, as long as certain easily controllable experimental conditions are satisfied. It is important to note that the adiabatic passage method tends to minimize the population of the intermediate level 2 in a three level system. Normally this level undergoes radiative decay. Therefore, the effects of spontaneous emission are largely reduced. For the adiabatic following solution to be valid, the detuning from the two photon resonance should be small compared to the Rabi frequency  $\Omega_0$ .

The dissertation opens with a mathematical and physical introduction of two- and three-level systems. Concepts like Bloch equations, rotating-wave approximation, the  $\pi$ -pulse method, and the adiabatic following are introduced here. This chapter is based mainly in the Allen and Eberly [AE75], and Scully and Zubairy [SZ97] books.

In the second chapter, we explore numerically an atom + cavity system with four atomic levels and a quantized coupling field. Adiabatic passage and  $\pi$ -pulse methods were used to drive the system classically. We find that for a very particular set of parameters, like Rabi frequency, pulse width, and time delay, we get very large transfer probabilities.

In chapter three, we introduce a simple analytical model based in nonlinear differential equations, that can help to understand why for some nonadiabatic processes we still achieve very high transfer efficiencies. We found that the nonlinear system can be converted into a system of equations relating the angular coordinates of the state vector in the Hilbert space. In this way, we can explore how the state vector follows the adiabatic states of the Hamiltonian governing the evolution of the system.

In the last chapter we consider the problem of coherence transfer of ground state levels, between two atoms inside a quantum microcavity. We proved that adiabatic methods can be used for transferring such coherence. In addition, we examined the system by using an alternative model based on symmetric and antisymmetric eigenstates, finding a connection between the original system and electromagnetic induced transparency and  $2\pi$ -processes.

## 1.2 The two-level atom

Consider the solution to the Schrödinger equation for a two-level atom interacting with a classical coherent driving field. The state of the system is described in terms of the vector  $|\Psi(t)\rangle$ , which obeys the time-dependent Schrödinger equation

$$i\hbar \frac{d}{dt} |\Psi(t)\rangle = H |\Psi(t)\rangle, \quad (1.1)$$



with the Hamiltonian operator  $H$  given by

$$H = H_0 - \boldsymbol{\mu} \cdot \mathbf{E}(\mathbf{r}_0, t). \quad (1.2)$$

Here  $H_0$  is the unperturbed Hamiltonian,  $\boldsymbol{\mu}$  is the atom's dipole moment operator, and  $\mathbf{E}(\mathbf{r}_0, t)$  is the electric field operator evaluated at the position of the dipole.

We assume that the applied electric field is quasi-monochromatic with a frequency nearly coincident with the transition frequency connecting the atomic ground state  $|a\rangle$  and some other level  $|b\rangle$ , as shown in Fig. 1.1.

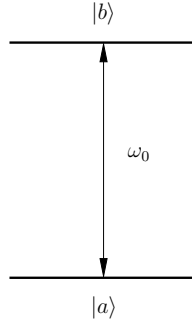


Figure 1.1: The two-level atom coupled by a near-resonant transition.

Because of the effect of the interaction is to mix states  $|a\rangle$  and  $|b\rangle$ , we are only concerned with electric dipole transitions between these two levels. Thus the state vector of the system in the presence of the applied field can be written as

$$|\Psi(t)\rangle = C_a(t)e^{-i\omega_a t}|a\rangle + C_b(t)e^{-i\omega_b t}|b\rangle, \quad (1.3)$$

where  $C_a(t)$  and  $C_b(t)$  represent the probability amplitudes that at time  $t$  the atom is in state  $|a\rangle$  or state  $|b\rangle$ , respectively. Assuming that these states are eigenvectors of the Hamiltonian  $H_0$  with eigenvalues  $\hbar\omega_a$  and  $\hbar\omega_b$ , the matrix elements of the atomic operators can be written as

$$\begin{aligned} \langle a|H_0|a\rangle &= \hbar\omega_a & \langle a|H_0|b\rangle &= 0 \\ \langle b|H_0|a\rangle &= 0 & \langle b|H_0|b\rangle &= \hbar\omega_b, \end{aligned} \quad (1.4)$$

and

$$\begin{aligned}\langle a|\boldsymbol{\mu}|a\rangle &= 0 & \langle a|\boldsymbol{\mu}|b\rangle &= \boldsymbol{\mu}_{ab} \\ \langle b|\boldsymbol{\mu}|a\rangle &= \boldsymbol{\mu}_{ab}^* & \langle b|\boldsymbol{\mu}|b\rangle &= 0.\end{aligned}\tag{1.5}$$

We note that there are no off-diagonal elements of  $H_0$ , because  $|a\rangle$  and  $|b\rangle$  are considered to be *orthonormal* eigenvectors of  $H_0$ ; and there are no diagonal elements of  $\boldsymbol{\mu}$ , because it is a *vector operator* and then has odd parity (we assume that  $|a\rangle$  and  $|b\rangle$  have definite parity).

In general, the dipole matrix elements are complex vectors that can be expressed as

$$\boldsymbol{\mu}_{ab} = \boldsymbol{\mu}_r + i\boldsymbol{\mu}_i, \quad \boldsymbol{\mu}_{ab}^* = \boldsymbol{\mu}_r - i\boldsymbol{\mu}_i;\tag{1.6}$$

where  $\boldsymbol{\mu}_r$  and  $\boldsymbol{\mu}_i$  are real vectors. Therefore, we can represent the *Hermitian* operator  $\boldsymbol{\mu}$  by the two-dimensional off-diagonal matrix:

$$\boldsymbol{\mu} = \begin{bmatrix} 0 & \boldsymbol{\mu}_r + i\boldsymbol{\mu}_i \\ \boldsymbol{\mu}_r - i\boldsymbol{\mu}_i & 0 \end{bmatrix}.\tag{1.7}$$

By introducing the two-dimensional Pauli matrix operators

$$\sigma_1 = \begin{pmatrix} 0 & 1 \\ 1 & 0 \end{pmatrix}, \quad \sigma_2 = \begin{pmatrix} 0 & -i \\ i & 0 \end{pmatrix}, \quad \sigma_3 = \begin{pmatrix} 1 & 0 \\ 0 & -1 \end{pmatrix},\tag{1.8}$$

the unperturbed Hamiltonian and the atom's dipole moment operators can be written as

$$H_0 = \frac{1}{2}(\omega_b + \omega_a)I + \frac{1}{2}(\omega_b - \omega_a)\sigma_3,\tag{1.9}$$

$$\boldsymbol{\mu} = \boldsymbol{\mu}_r\sigma_1 - \boldsymbol{\mu}_i\sigma_2.\tag{1.10}$$

In this way, the Hamiltonian of the system takes the form

$$H = \frac{1}{2}(\omega_b + \omega_a)I + \frac{1}{2}(\omega_b - \omega_a)\sigma_3 - (\boldsymbol{\mu}_r \cdot \mathbf{E})\sigma_1 + (\boldsymbol{\mu}_i \cdot \mathbf{E})\sigma_2.\tag{1.11}$$

Here  $I$  represents the  $2 \times 2$  identity operator.

In the Heisenberg picture, the equation of motion for an operator that does not depend explicitly

on time is given by

$$i\hbar \frac{d}{dt} A = [A, H]. \quad (1.12)$$

Then, by plugging the Pauli matrix operators and Eq. (1.11) into the Heisenberg equation (1.12), we may obtain

$$\dot{\sigma}_1(t) = -\omega_0 \sigma_2(t) + \frac{2}{\hbar} [\boldsymbol{\mu}_i \cdot \mathbf{E}(t)] \sigma_3(t), \quad (1.13a)$$

$$\dot{\sigma}_2(t) = \omega_0 \sigma_1(t) + \frac{2}{\hbar} [\boldsymbol{\mu}_r \cdot \mathbf{E}(t)] \sigma_3(t), \quad (1.13b)$$

$$\dot{\sigma}_3(t) = -\frac{2}{\hbar} [\boldsymbol{\mu}_r \cdot \mathbf{E}(t)] \sigma_2(t) - \frac{2}{\hbar} [\boldsymbol{\mu}_i \cdot \mathbf{E}(t)] \sigma_1(t), \quad (1.13c)$$

where  $\omega_0 = (\omega_b - \omega_a)/\hbar$  represents the atomic transition frequency, and  $\mathbf{E}(t)$  has been taken in the Heisenberg picture.

As we see from Eqs. (1.13), the operator nature of the atom and field variables makes the system very difficult to solve and no general solutions are known. Moreover, if the operator Maxwell equations that govern the electric field are included, the system becomes even more complicated. One way to overcome this problem is by considering an alternative system of equations for which the quantum correlations between field and atom can safely be ignored [AE75]. As a result, the expectation value of any product of two operators of the form  $\mathbf{E}(t)\sigma_i(t)$  can be expressed as the product of the individual expectation values:

$$\langle \mathbf{E}(t)\sigma_i(t) \rangle = \langle \mathbf{E}(t) \rangle \langle \sigma_i(t) \rangle. \quad (1.14)$$

In this way, we can reformulate the semi-classical radiation theory of two-level atoms by applying this factorization systematically to Eqs. (1.13). Now, according to the following notation

$$s_i(t) \equiv \langle \sigma_i(t) \rangle, \quad i = 1, 2, 3 \quad (1.15)$$

$$\overline{\mathbf{E}}(t) \equiv \langle \mathbf{E}(t) \rangle, \quad (1.16)$$

the set of equations (1.13), that represents the general interaction of a two-level atom with an electric

field in the semiclassical theory, takes the form

$$\dot{s}_1(t) = -\omega_0 s_2(t) + \frac{2}{\hbar} [\boldsymbol{\mu}_i \cdot \bar{\mathbf{E}}(t)] s_3(t), \quad (1.17a)$$

$$\dot{s}_2(t) = \omega_0 s_1(t) + \frac{2}{\hbar} [\boldsymbol{\mu}_r \cdot \bar{\mathbf{E}}(t)] s_3(t), \quad (1.17b)$$

$$\dot{s}_3(t) = -\frac{2}{\hbar} [\boldsymbol{\mu}_r \cdot \bar{\mathbf{E}}(t)] s_2(t) - \frac{2}{\hbar} [\boldsymbol{\mu}_i \cdot \bar{\mathbf{E}}(t)] s_1(t). \quad (1.17c)$$

It is well known that the dynamical evolution of an  $N$ -level quantum system can be described by the rotations of a coherent vector [RRS54, FVH57] which is constrained by the existence of high-order constants of motion [Elg80, HE81, HE82]. For the two-dimensional Hilbert space, some of these conservation laws come directly from the properties of the Pauli matrix operators, reflecting the intrinsic symmetry of the vector space. For example  $\sigma_1^2 = \sigma_2^2 = \sigma_3^2 = I$ . Another important constant of motion is derived from the fact that

$$\left( \frac{d}{dt} \right) \sigma_1(t)^2 = 0, \quad \text{so that} \quad \sigma_1^2(t) = \sigma_1^2(0) = I. \quad (1.18)$$

Extending all these ideas to the system of equations (1.17), we may obtain their associated conservation law, which is written as

$$s_1^2(t) + s_2^2(t) + s_3^2(t) = 1. \quad (1.19)$$

This expression means that the probability of the system is conserved over the time, or equivalently, the state of the atom remains normalized in time.

For electric dipole  $\Delta m = 0$  transitions, we can adjust the arbitrary phases of the connected levels so that  $\boldsymbol{\mu}_i$  vanishes. By denoting

$$\frac{2}{\hbar} \boldsymbol{\mu}_r \cdot \bar{\mathbf{E}} = \frac{2\mu E}{\hbar} = \Omega, \quad (1.20)$$

we can write the semiclassical atomic equations (1.17) in the simpler form:

$$\dot{s}_1(t) = -\omega_0 s_2(t), \quad (1.21a)$$

$$\dot{s}_2(t) = \omega_0 s_1(t) + \Omega(t) s_3(t), \quad (1.21b)$$

$$\dot{s}_3(t) = -\Omega(t) s_2(t). \quad (1.21c)$$

Because these equations are the electric-dipole analogues of equations of a spin-1/2 magnetic dipole undergoing precession in a magnetic field [Blo46], the vector  $\mathbf{s}(t)$  is called the electric-dipole “pseudospin.”

The physical meaning of the expectation values  $s_1(t)$ ,  $s_2(t)$ , and  $s_3(t)$  can be interpreted as follows. From Eqs. (1.15) and (1.9), it is clear that  $s_3(t)$  represents the internal energy of the atom in  $\frac{1}{2}\hbar\omega_0$  units; and from Eqs. (1.15) and (1.10), we see that  $s_1(t)$  and  $s_2(t)$  are both manifestations of the atom's dipole moment operator [FVH57, AE75].

The pseudospin Eqs. (1.21) can be rewritten as if they were the equations for the precession of a solid body upon which a known torque  $\mathbf{N}^F$  is acting. The superscript  $F$  stands for the coordinate system of fixed unit vectors  $|1\rangle$ ,  $|2\rangle$ , and  $|3\rangle$ . Thus the set of three equations (1.21) can be expressed as the single equation:

$$\dot{\mathbf{s}}(t) = \mathbf{N}^F(t) \times \mathbf{s}(t), \quad (1.22)$$

where the vector  $\mathbf{s}$  has components  $s_1$ ,  $s_2$ ,  $s_3$ , and the torque vector  $\mathbf{N}^F$  has components

$$\mathbf{N}_1^F(t) = -\Omega(t), \quad (1.23a)$$

$$\mathbf{N}_2^F(t) = 0, \quad (1.23b)$$

$$\mathbf{N}_3^F(t) = \omega_0. \quad (1.23c)$$

We note that the pseudospin precession is originated by the first and third components of the torque vector.

To simplify the mathematics, we define a coordinate reference frame which rotates at the same frequency  $\omega$  of the field. In this way we reduce the number of rapidly oscillating variables of the system and consider only those which change slowly with time. The torque vector is then rewritten as the sum of three torques, one  $\mathbf{N}^0$  along the  $|3\rangle$  direction, and two much smaller torques that lie completely in the  $|1\rangle$ – $|2\rangle$  plane:

$$\mathbf{N}^F = \mathbf{N}^+(t) + \mathbf{N}^-(t) + \mathbf{N}^0, \quad (1.24)$$

where

$$\mathbf{N}^0 = (0, 0, \omega_0), \quad (1.25a)$$

$$\mathbf{N}^- = (-\Omega \cos \omega t, -\Omega \sin \omega t, 0), \quad (1.25b)$$

$$\mathbf{N}^+ = (-\Omega \cos \omega t, +\Omega \sin \omega t, 0), \quad (1.25c)$$

and

$$E(t) = \mathcal{E}(t)[e^{i\omega t} + \text{c.c.}]. \quad (1.26)$$

As we see,  $\mathbf{N}^+$  rotates counterclockwise as  $t$  increases, while  $\mathbf{N}^-$  rotates clockwise. In a coordinate system following  $\mathbf{s}$  and moving to the right at angular velocity  $\omega$ , the vector  $\mathbf{N}^+$  remains constant, and  $\mathbf{N}^-$  is counter-rotating at angular velocity  $2\omega$ . In such a coordinate frame the effect of the torque  $\mathbf{N}^+$  on a spin is steady and cumulative over long times. On the other hand, the effect of the torque  $\mathbf{N}^-$  reverses itself  $10^{15}$ – $10^{16}$  times/s, and is almost completely ineffective [Shi63].

The *rotating-wave approximation* (RWA) consists of ignoring  $\mathbf{N}^-$  for this reason, and writing the pseudospin equations using  $\mathbf{N}^+$  and  $\mathbf{N}^-$  in place of  $\mathbf{N}^F$  [BS40, EWG76]. It then follows that

$$\dot{s}_1 = -\omega_0 s_2 - \Omega s_3 \sin \omega t, \quad (1.27a)$$

$$\dot{s}_2 = \omega_0 s_1 + \Omega s_3 \cos \omega t, \quad (1.27b)$$

$$\dot{s}_3 = -\Omega [s_2 \cos \omega t - s_1 \sin \omega t]. \quad (1.27c)$$

By introducing an appropriate rotation matrix for the vector  $\mathbf{s}$  and defining a nearly stationary vector  $\boldsymbol{\rho}$  in the rotating frame with components  $u$ ,  $v$ , and  $w$ , it is possible to determine what the observer sees in the rotating frame. Thus

$$\begin{bmatrix} u \\ v \\ w \end{bmatrix} = \begin{bmatrix} \cos \omega t & \sin \omega t & 0 \\ -\sin \omega t & \cos \omega t & 0 \\ 0 & 0 & 1 \end{bmatrix} \quad (1.28)$$

The equations of motion obeyed by the components of the pseudospin  $\boldsymbol{\rho}$  in the rotating frame are

$$\dot{u} = -(\omega_0 - \omega)v, \quad (1.29a)$$

$$\dot{v} = +(\omega_0 - \omega)u + \Omega w, \quad (1.29b)$$

$$\dot{w} = -\Omega v, \quad (1.29c)$$

which are the same as the single vector equation

$$\frac{d}{dt} \boldsymbol{\rho} = \mathbf{N} \times \boldsymbol{\rho}, \quad (1.30)$$

if the rotating frame torque vector  $\mathbf{N}$  has the components

$$\mathbf{N} \equiv (-\Omega, 0, \omega_0 - \omega). \quad (1.31)$$

### 1.3 $\pi$ -pulses

By defining a “dimensionless” quantity  $\theta(t)$  as

$$\theta(t) = \int_{-\infty}^t \Omega(t') dt', \quad (1.32)$$

equations (1.29) can be integrated to give

$$u(t; 0) = u_0, \quad (1.33a)$$

$$v(t; 0) = w_0 \sin \theta(t) + v_0 \cos \theta(t), \quad (1.33b)$$

$$w(t; 0) = -v_0 \sin \theta(t) + w_0 \cos \theta(t), \quad (1.33c)$$

where  $u_0 = u(0; 0)$ , and so on. The second zero in the labels  $v(0; 0)$  and  $w(0; 0)$  makes reference to the detuning frequency  $\Delta = \omega_0 - \omega$ .

In the special case when the applied field envelope has a steady state value between  $t_1$  and  $t_2$ , Eq. (1.32) can be integrated to give

$$\theta = \Omega_0(t_2 - t_1), \quad (1.34)$$

where  $\Omega_0$  is called the Rabi frequency on resonance.

The Rabi frequency gives the rate at which transitions are coherently induced between the two atomic levels. If the atom is initially in the ground state ( $w_0 = -1$ ,  $v_0 = 0$ ) then after a time  $\delta t$  such that  $\Omega_0 \delta t = \pi$ , Eq. (1.33c) shows that  $w = +1$ , and the atom is in its upper state. In other words, a “ $\pi$  pulse” of electromagnetic radiation inverts the atom population from the ground state to the excited state. Now, in the spins terminology, the  $\pi$  pulse turns a spin from alignment to anti-alignment with a static magnetic field.

The quantity  $\Omega_0(t_2 - t_1)$  is exactly the area under the curve pulse amplitude-time, and represents the well-known “area theorem” written as

$$A(t) = \int_{-\infty}^t \Omega(t') dt' = \theta(t). \quad (1.35)$$

Resonant pulses with areas  $\pi$ ,  $2\pi$ ,  $3\pi$ , and so on, invert the atomic population one, two, three, and so on, times.

We can also note that solutions (1.33) are the result of a rotation. If the rotating frame Eqs. (1.29)

are written also as a single vector precession equation

$$\frac{d}{dt}\boldsymbol{\rho} = \mathbf{N} \times \boldsymbol{\rho} \quad (1.36)$$

where

$$\boldsymbol{\rho} = (u, v, w), \quad (1.37)$$

and

$$\mathbf{N} = (-\Omega, 0, \Delta), \quad (1.38)$$

then Eq. (1.36) can be represented as

$$\frac{d}{dt} \begin{bmatrix} u \\ v \\ w \end{bmatrix} = \begin{bmatrix} 0 & -\Delta & 0 \\ \Delta & 0 & \Omega \\ 0 & -\Omega & 0 \end{bmatrix} \begin{bmatrix} u \\ v \\ w \end{bmatrix}. \quad (1.39)$$

## 1.4 The three-level atom

Consider the interaction of a two-mode radiation field with the three-level atom shown schematically in Fig. 1.2. Let  $|a\rangle$ ,  $|c\rangle$ , and  $|b\rangle$  represent the initial, excited, and final states of the atom in a  $\Lambda$  configuration. They are eigenstates of the unperturbed part of the Hamiltonian  $H_0$  with the eigenvalues  $\hbar\omega_a$ ,  $\hbar\omega_c$ , and  $\hbar\omega_b$ , respectively ( $\omega_a < \omega_b < \omega_c$ ).

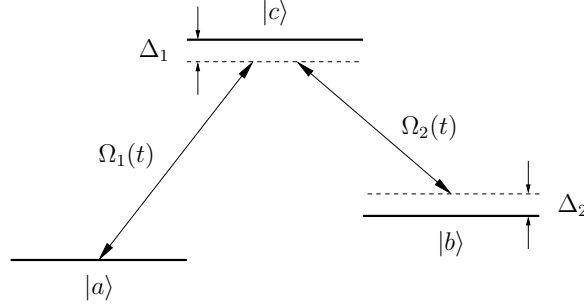


Figure 1.2: The three-level atom in a  $\Lambda$ -configuration.

We are only interested in electric dipole transitions between these three levels, so we can concern ourselves exclusively with the three-dimensional Hilbert space spanned by these eigenstates. Then, the state vector of the system (in the Schödinger picture) can be written as

$$|\psi(t)\rangle = C_a(t)e^{-i\omega_a t}|a\rangle + C_b(t)e^{-i\omega_b t}|b\rangle + C_c(t)e^{-i\omega_c t}|c\rangle, \quad (1.40)$$



where  $C_a$ ,  $C_b$ , and  $C_c$  are the *slowly* varying amplitudes of finding the atom in states  $|a\rangle$ ,  $|b\rangle$ , and  $|c\rangle$ , respectively. The corresponding time-dependent Schrödinger equation is

$$i\hbar \frac{d}{dt}|\psi(t)\rangle = H(t)|\psi(t)\rangle, \quad (1.41)$$

with

$$H(t) = H_0 + H_1(t), \quad (1.42)$$

where  $H_0$  and  $H_1$  represent the unperturbed and interaction parts of the Hamiltonian, respectively. By using the completeness relation

$$|a\rangle\langle a| + |b\rangle\langle b| + |c\rangle\langle c| = I, \quad (1.43)$$

we can write  $H_0$  as follows

$$\begin{aligned} H_0 &= IH_0I \\ &= \hbar\omega_a|a\rangle\langle a| + \hbar\omega_b|b\rangle\langle b| + \hbar\omega_c|c\rangle\langle c|, \end{aligned} \quad (1.44)$$

where we have used  $H_0|j\rangle = \hbar\omega_j|j\rangle$ , with  $j = a, b, c$ . Similarly, the part of the Hamiltonian  $H_1$  that represents the interaction of the atom with the radiation field is described by

$$H_1(t) = -\boldsymbol{\mu} \cdot \mathbf{E}(\mathbf{r}_0, t), \quad (1.45)$$

where  $\boldsymbol{\mu}$  is the atom's dipole moment operator, and  $\mathbf{E}(\mathbf{r}_0, t)$  is the two-mode electric field operator. In the dipole approximation, the electric field is evaluated at the dipole position  $\mathbf{r}_0 = \mathbf{0}$ , and the operator can be written in the form

$$\mathbf{E}(\mathbf{0}, t) = \sum_{k=1}^2 \text{Re}[\hat{\boldsymbol{\epsilon}}_k \mathcal{E}_k(t) e^{i\omega_k t}], \quad (1.46)$$

where  $\hat{\boldsymbol{\epsilon}}_k$  and  $\mathcal{E}_k(t)$  represent the normalized polarization vector and the amplitude of the electric

field, respectively. We can also write  $H_1$  in Dirac notation by using Eq. (1.43)

$$\begin{aligned} H_1(t) &= -I[\boldsymbol{\mu} \cdot \mathbf{E}(\mathbf{0}, t)]I \\ &= -\sum_{i,j} \sum_{k=1}^2 |i\rangle\langle i| \boldsymbol{\mu} \cdot \hat{\mathbf{e}}_k \left[ \frac{\mathcal{E}_k(t)e^{i\omega_k t} + \mathcal{E}_k^*(t)e^{-i\omega_k t}}{2} \right] |j\rangle\langle j|. \end{aligned} \quad (1.47)$$

Assuming that the electric field is linearly polarized along the dipole moment direction, we have

$$\langle i| \boldsymbol{\mu} \cdot \hat{\mathbf{e}}_k |j\rangle = \langle i| \boldsymbol{\mu} |j\rangle = \mu_{ij}, \quad (1.48)$$

and Eq. (1.47) becomes

$$H_1(t) = -\frac{1}{2} \sum_{i,j} \sum_{k=1}^2 \mu_{ij} [\mathcal{E}_k(t)e^{i\omega_k t} + \mathcal{E}_k^*(t)e^{-i\omega_k t}] |i\rangle\langle j|, \quad j = a, b, c. \quad (1.49)$$

In the general case the dipole matrix elements are complex numbers that might be written simply as (see 1.6 for an alternative notation)

$$\mu_{ij} = |\mu_{ij}|e^{i\alpha}. \quad (1.50)$$

In this problem we consider only the relevant dipole transitions  $|a\rangle \leftrightarrow |c\rangle$  and  $|b\rangle \leftrightarrow |c\rangle$ , coupled by the electric fields  $\mathbf{E}_1$  and  $\mathbf{E}_2$ , respectively. The transition  $|a\rangle \leftrightarrow |b\rangle$  is forbidden by the dipole selection rules. Thus, the only matrix elements of the electric dipole moment that survive are:  $\mu_{ac}$ ,  $\mu_{bc}$ , with their respective complex conjugates. Plugging Eq. (1.50) into Eq. (1.49), and considering only the allowed dipole transitions, we get

$$\begin{aligned} H_1(t) &= -\frac{1}{2} [|\mu_{ac}| \mathcal{E}_1 e^{i(\omega_1 t + \alpha)} |a\rangle\langle c| + |\mu_{ca}| \mathcal{E}_1 e^{i(\omega_1 t - \alpha)} |c\rangle\langle a| \\ &\quad + |\mu_{bc}| \mathcal{E}_2 e^{i(\omega_2 t + \beta)} |b\rangle\langle c| + |\mu_{cb}| \mathcal{E}_2 e^{i(\omega_2 t - \beta)} |c\rangle\langle b| + \text{H.c.}] \end{aligned} \quad (1.51)$$

We next derive the equations of motion for the probability amplitudes  $C_a$ ,  $C_b$ , and  $C_c$ . By introducing Eq. (1.40) into Eq. (1.41) and multiplying the resulting equation from the left by  $\langle a|$ , we find that

$$\dot{C}_a = \frac{i}{2} \Omega_1(t) e^{i\alpha} e^{i(\omega_1 - \omega_{ca})t} C_c, \quad (1.52)$$

where the Rabi frequency  $\Omega_1(t)$  is defined as

$$\Omega_1(t) = \frac{|\mu_{ac}|\mathcal{E}_1(t)}{\hbar}, \quad (1.53)$$

and  $\omega_{ca} = \omega_c - \omega_a$  is the atomic transition frequency. In deriving Eq. (1.52), we have ignored counter-rotating terms proportional to  $\exp[\pm i(\omega_1 + \omega_{ca})]$  on the right-hand side in the *rotating-wave approximation* (RWA). Similarly, by multiplying instead by  $\langle b|$  and  $\langle c|$ , we find

$$\dot{C}_b = \frac{i}{2} \Omega_2(t) e^{i\beta} e^{i(\omega_2 - \omega_{cb})t} C_c, \quad (1.54)$$

$$\dot{C}_c = \frac{i}{2} \Omega_1^*(t) e^{-i\alpha} e^{-i(\omega_1 - \omega_{ca})t} C_a + \frac{i}{2} \Omega_2^*(t) e^{-i\beta} e^{-i(\omega_2 - \omega_{cb})t} C_b. \quad (1.55)$$

with the Rabi frequency

$$\Omega_2(t) = \frac{|\mu_{bc}|\mathcal{E}_2(t)}{\hbar}, \quad (1.56)$$

and the atomic transition frequency  $\omega_{cb} = \omega_c - \omega_b$ . Introducing the *detuning* factors

$$\Delta_1 = \omega_1 - \omega_{ca}, \quad (1.57a)$$

$$\Delta_2 = \omega_2 - \omega_{cb} - \Delta_1, \quad (1.57b)$$

the coupled Eqs. (1.52), (1.55), and (1.54) then reduce to the set

$$\dot{C}_a = \frac{i}{2} \Omega_1(t) e^{i\alpha} e^{i\Delta_1 t} C_c, \quad (1.58a)$$

$$\dot{C}_b = \frac{i}{2} \Omega_2(t) e^{i\beta} e^{i(\Delta_1 + \Delta_2)t} C_c, \quad (1.58b)$$

$$\dot{C}_c = \frac{i}{2} \Omega_1^*(t) e^{-i\alpha} e^{-i\Delta_1 t} C_a + \frac{i}{2} \Omega_2^*(t) e^{-i\beta} e^{-i(\Delta_1 + \Delta_2)t} C_b. \quad (1.58c)$$

By making a change of variables and choosing values for the phases (see Appendix 4.3.3), it is possible to eliminate the exponentials from Eqs. (1.58). It then follows that

$$i\dot{C}_a(t) = \Delta_1 C_a(t) + \frac{\Omega_1(t)}{2} C_c(t), \quad (1.59a)$$

$$i\dot{C}_b(t) = (\Delta_1 + \Delta_2) C_b(t) + \frac{\Omega_2(t)}{2} C_c(t), \quad (1.59b)$$

$$i\dot{C}_c(t) = \frac{\Omega_1^*(t)}{2} C_a(t) + \frac{\Omega_2^*(t)}{2} C_b(t). \quad (1.59c)$$

These are the equations of motion for the probability amplitudes of the three-level  $\Lambda$ -system shown

in Fig. 1.2. The Schrödinger equation for these amplitudes in the rotating-wave approximation reads:

$$i\hbar \frac{d}{dt} \mathbf{C}(t) = H(t) \mathbf{C}(t), \quad (1.60)$$

where

$$H(t) = \frac{\hbar}{2} \begin{bmatrix} 2\Delta_1 & 0 & \Omega_1(t) \\ 0 & 2(\Delta_1 + \Delta_2) & \Omega_2(t) \\ \Omega_1^*(t) & \Omega_2^*(t) & 0 \end{bmatrix}, \quad (1.61)$$

and  $\mathbf{C}(t) = [C_a(t), C_b(t), C_c(t)]^T$ .

For the case of two-photon resonance ( $\Delta_1 = \Delta_2 = 0$ ) and real matrix elements of the dielectric dipole moment, Eq. (1.61) takes the simple form

$$H(t) = \frac{\hbar}{2} \begin{bmatrix} 0 & 0 & \Omega_1(t) \\ 0 & 0 & \Omega_2(t) \\ \Omega_1(t) & \Omega_2(t) & 0 \end{bmatrix}. \quad (1.62)$$

It is easy to verify (see Appendix 4.3.3) that the following linear combination of bare states  $|a\rangle$ ,  $|c\rangle$ , and  $|b\rangle$  are eigenstates of the instantaneous RWA Hamiltonian

$$|W^+\rangle = \frac{1}{\sqrt{2}} [\sin \Phi(t) |a\rangle + \cos \Phi(t) |b\rangle + |c\rangle], \quad (1.63a)$$

$$|W^0\rangle = \cos \Phi(t) |a\rangle - \sin \Phi(t) |b\rangle, \quad (1.63b)$$

$$|W^-\rangle = \frac{1}{\sqrt{2}} [\sin \Phi(t) |a\rangle + \cos \Phi(t) |b\rangle - |c\rangle]. \quad (1.63c)$$

where the (time-varying) *mixing angle*  $\Phi$  is defined by the relationship

$$\tan \Phi(t) = \frac{\Omega_1(t)}{\Omega_2(t)}. \quad (1.64)$$

When combined with the related photon numbers in the two radiation fields, the eigenstates given by Eqs. (1.63) are called the “dressed states” of the matter-field system. Although we do not keep track of the photon numbers, we use this name here as well. The (time-dependent) dressed-state eigenvalues are

$$\omega^+ = +\frac{1}{2} \sqrt{\Omega_1^2 + \Omega_2^2}, \quad \omega^0 = 0, \quad \omega^- = -\frac{1}{2} \sqrt{\Omega_1^2 + \Omega_2^2}. \quad (1.65)$$

## 1.5 The adiabatic following

An alternative method for population transfer between two states is based on sweeping the pulse frequency through a resonance. If the sweep is sufficiently slow, then it is possible to produce complete population transfer between the two states that are connected by the resonance [SBK<sup>+</sup>92]. The adiabatic process can be characterized by a steady state process [Mor64]. That is, the rates of change of the varying components of the incident laser fields are assumed to be small enough that a quasi steady state is maintained throughout the process [Hio83]. These processes have the advantage of being insensitive to pulse area, pulse shape, and to the precise location of the resonance. Then they are useful for producing population transfer in an ensemble of atoms that have different Doppler shifts and different dipole moments.

The condition for exact adiabatic following of a system from state  $|a\rangle$  to state  $-|b\rangle$ , without populating an excited state (which normally undergoes spontaneous emission), can be seen from Fig. 1.3.

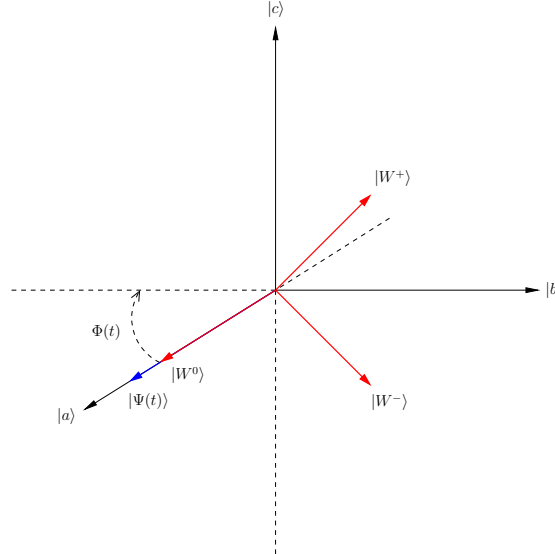


Figure 1.3: Graphic representation of the Hilbert space for the three-level system in the basis  $\{|a\rangle, |b\rangle, |c\rangle\}$ , and in the basis of the dressed states  $\{|W^+\rangle, |W^0\rangle, \text{ and } |W^-\rangle\}$ . The dressed vectors are free to rotate in time following the evolution of the system.

In stimulated Raman scattering processes (STIRAP) the pulses are applied in counterintuitive way, that is, the  $\Omega_2(t)$  pulse precedes the pulse  $\Omega_1(t)$ , though they partially overlap. In other words

$$\lim_{t \rightarrow -\infty} \frac{\Omega_1(t)}{\Omega_2(t)} = 0, \quad \lim_{t \rightarrow +\infty} \frac{\Omega_1(t)}{\Omega_2(t)} = +\infty. \quad (1.66)$$

Assuming that

$$\tan \Phi(t) = \frac{\Omega_1(t)}{\Omega_2(t)}, \quad (1.67)$$

then we have

$$\Phi(-\infty) = 0 \quad \text{and} \quad \Phi(+\infty) = \pi/2. \quad (1.68)$$

Hence the adiabatic state  $|W^0\rangle$  coincides with the state  $|a\rangle$  before the excitation and with state  $-|b\rangle$  after it, so that initially only state  $|W^0\rangle$  among the adiabatic states is populated. If the excitation is adiabatic, then the system will remain in this adiabatic state all time and the population will eventually be completely transferred to state  $|b\rangle$ . Moreover, no appreciable population will reside in the intermediate state  $|c\rangle$  at any time which makes the transfer efficiency insensitive to decay from this state to other states [VS96]. Therefore in the adiabatic process, the evolution of the wave vector  $|\Psi(t)\rangle$  follows closely the evolution of the “dressed state”  $|W^0\rangle$ , which goes from a direction parallel to  $|a\rangle$  to a direction antiparallel to  $|b\rangle$ .

We now consider the conditions under which the system evolves adiabatically. Nonadiabatic coupling between the eigenstates is small when the rate of change of the mixing angle  $\Phi(t)$ , is small compared with the separation of the corresponding eigenvalues [Mes99].

$$|\langle W^+ | \dot{W}^0 \rangle| \ll |\omega^\pm - \omega^0|. \quad (1.69)$$

For no detuning, this separation is given by

$$|\omega^\pm - \omega^0| = \frac{1}{2} \sqrt{\Omega_1^2 + \Omega_2^2} = \Omega_{\text{eff}}. \quad (1.70)$$

In addition, it is easy to find that  $|\langle W^+ | \dot{W}^0 \rangle| = -\dot{\Phi} \sin \Theta$ , and therefore the adiabaticity constraint, with  $\sin \Theta = 1$ , reads

$$|\dot{\Phi}| \ll \Omega_{\text{eff}}. \quad (1.71)$$

By differentiating the above expression with respect to time, we may get

$$\left| \frac{\dot{\Omega}_1 \Omega_2 - \Omega_1 \dot{\Omega}_2}{\Omega_1^2 + \Omega_2^2} \right| \ll \Omega_{\text{eff}}. \quad (1.72)$$

Finally, for a given counterintuitive sequence of pulses  $\Omega_1$  and  $\Omega_2$ , separated by some time delay  $\Delta t/T$  (with  $T$  being the pulse length or interaction time), the adiabatic theorem leads to the

condition

$$\Omega_{\text{eff}} T \gg 1. \tag{1.73}$$

## Chapter 2

# Laser-induced population transfer in multilevel systems

Cavity quantum electrodynamics (QED) is the part of physics that studies the interaction of single atoms and photons coupled to an electromagnetic resonator. Many interesting effects have been observed during the last twenty years. They include the alteration of the atomic radiative rates by the presence of a cavity around an atom, shifts in the atomic energy level due to the coupling with the cavity, manipulation of photons by using the interaction with individual atoms crossing the cavity, creation of non-classical field states, among others [OBRW96].

In the recent few years, and due to the advancements in the technology of high- $Q$  cavities and in atomic beam manipulation, many proposals in the area of quantum information and quantum computation have been made. They include applications to particle teleportation, quantum cryptography, spectroscopy and conditional dynamics.

In this chapter we study numerically the transfer of population in a four-level system by using  $\pi$ -pulse methods and adiabatic passage schemes. We present some examples of the resonance-like features in the failure probability  $p$ . We show that the features appear for Gaussian, hyperbolic secant, and Lorentzian pulse profiles.

### 2.1 The atom-cavity system

Consider a three-level atom consisting of two ground states  $|g_1\rangle$  and  $|g_2\rangle$ , and an excited state  $|e\rangle$ , interacting with a coherent driving field  $\Omega(t)$  of frequency  $\omega_L$  and a cavity-mode field  $g(t)$  of frequency  $\omega$ , as indicated in Fig. 2.1.



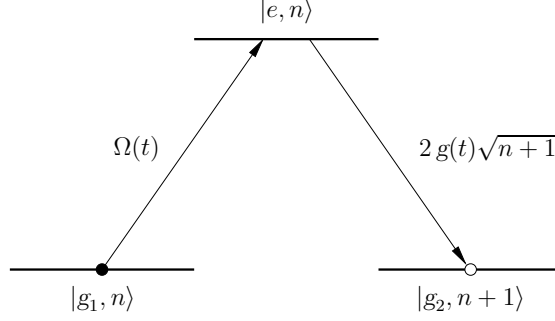


Figure 2.1: A Three-level atom in a cavity.

The state vector describing the three-level atom can be written in the form

$$|\Psi(t)\rangle = \sum_n [C_{g_1,n}(t)|g_1, n\rangle + C_{e,n}(t)|e, n\rangle + C_{g_2,n}(t)|g_2, n\rangle], \quad (2.1)$$

where  $C_{g_1,n}$ ,  $C_{e,n}$ , and  $C_{g_2,n}$  are the probability amplitudes of finding the atom in states  $|g_1, n\rangle$ ,  $|e, n\rangle$ , and  $|g_2, n\rangle$ , respectively. The ket  $|g_1, n\rangle \equiv |g_1\rangle \otimes |n\rangle$  represents the state in which the atom is in the ground state  $|g_1\rangle$  and the cavity field has  $n$  photons. Similar descriptions exist for the other two states.

The time evolution of the system is described by the Schrödinger equation

$$i\hbar |\dot{\Psi}(t)\rangle = H(t)|\Psi(t)\rangle \quad (2.2)$$

with the Hamiltonian operator  $H(t)$  given by

$$\begin{aligned} H(t) = & \hbar\omega a^\dagger a + \omega_{eg}|e\rangle\langle e| - i\hbar g(t)(|e\rangle\langle g_2|a - \text{H.c.}) \\ & + i\hbar\Omega(t)(|e\rangle\langle g_1|e^{-i\omega_L t} - \text{H.c.}). \end{aligned} \quad (2.3)$$

Here  $a$  represents the annihilator operator for the cavity mode. The time dependence of  $\Omega(t)$  and  $g(t)$  may be provided simply by the motion of the atom across the laser- and cavity-field profiles.

### 2.1.1 Dark state

It is interesting to observe that the interaction part of the Hamiltonian (2.3) can only cause transitions between states within the family

$$\{|g_1, n\rangle, |e, n\rangle, |g_2, n+1\rangle\}, \quad (2.4)$$

Therefore, in the rotating-wave approximation, the adiabatic energy eigenvalues of the Hamiltonian associated with a particular family of states are [PMZK93]

$$E_n = n\hbar\omega, \quad (2.5)$$

$$E_n^\pm = n\hbar\omega + \frac{\hbar}{2} \left[ \Delta \pm \sqrt{\Delta^2 + 4g(t)^2(n+1) + \Omega(t)^2} \right], \quad (2.6)$$

where we have assumed that  $\omega = \omega_L$ , and  $\Delta = \omega_{eg} - \omega$  is the detuning. We are interested in the eigenstate corresponding to  $E_n = n\hbar\omega$ , which is given by

$$|E_n(t)\rangle = \frac{2g(t)\sqrt{n+1}|g_1, n\rangle + \Omega(t)|g_2, n+1\rangle}{\sqrt{\Omega(t)^2 + 4g(t)^2(n+1)}}. \quad (2.7)$$

This eigenstate is, at all times, free of any contribution from the excited state  $|e, n\rangle$ , and is independent of the detuning  $\Delta$ .

### 2.1.2 Adiabatic following

If we assume that only level  $|g_1, n\rangle$  is initially populated, complete population transfer occurs if [KGHB89]

$$\left. \frac{\Omega(t)}{g(t)} \right|_{t \rightarrow -\infty} = 0 \quad \text{and} \quad \left. \frac{g(t)}{\Omega(t)} \right|_{t \rightarrow +\infty} = 0, \quad (2.8)$$

where  $t \rightarrow -\infty$  and  $t \rightarrow +\infty$  corresponds to times before and after the interaction with the fields, respectively. Consequently, for the pulse sequence in which the pulse  $\Omega(t)$  is delayed with respect to  $g(t)$ , the dark state is the appropriate vehicle for transferring population from state  $|g_1, n\rangle$  to state  $|g_2, n+1\rangle$  without populating state  $|e, n\rangle$ .

If the condition for adiabaticity [Mes99]

$$\Omega_0 T, 2g_0\sqrt{n+1}T \gg 1 \quad (2.9)$$

is satisfied (with  $\Omega_0$  and  $g_0$  representing peak intensities for the respective fields) then the state vector of the system remains very nearly an eigenvector of the time-dependent Hamiltonian at all times, that is

$$|\Psi(t)\rangle \approx |E_n(t)\rangle. \quad (2.10)$$

### 2.1.3 Master equation

We can generalize the previous ideas to more complicated and realistic atomic-level structures. For example, this time we may consider Zeeman ground state levels, and include in our analysis the spontaneous emission  $\Gamma$ , and the cavity decay  $\kappa$ .

Consider the case of an atomic  $J_g = 1 \rightarrow J_e = 0$  transition in a four-level  $\Lambda$  atom, as indicated in Fig. 2.2. The transition  $|g_1, 1\rangle \rightarrow |e, 0\rangle$  is strongly connected to a  $\pi$ -polarized cavity-mode field

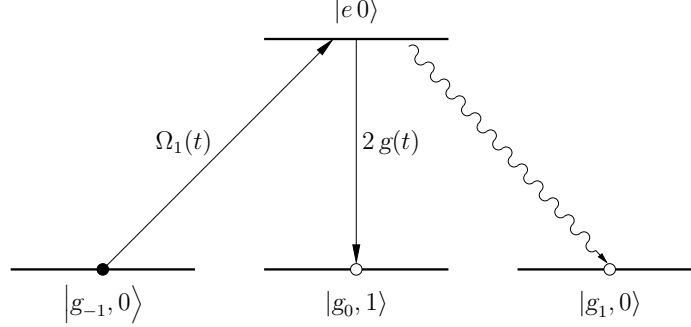


Figure 2.2:  $\Lambda$  four-level atom in a cavity.

with coupling strength  $g(t)$ . The transition  $|g_{-1}, 0\rangle \rightarrow |e, 0\rangle$  is coupled to a coherent  $\sigma^+$ -polarized laser field with frequency  $\omega_L$  and Rabi frequency  $\Omega(t)$ . The excited state is assumed to be able to decay to the three ground states with the same decaying rate  $\Gamma/3$ .

In the short period of time compared to the natural decay times, the dynamical evolution of the density matrix  $\rho(t)$  of the atomic system is given by the Liouville equation

$$\frac{\partial \rho}{\partial t} = -i[H_{\text{eff}} \rho - \text{H.c.}] + \Gamma \sum_{\sigma=0,\pm 1} A_{\sigma} \rho A_{\sigma}^{\dagger} + \kappa a \rho a^{\dagger}, \quad (2.11)$$

where  $\rho(t)$  is the reduced density operator of the system, and

$$\begin{aligned} H_{\text{eff}} = & (\Delta - i\Gamma/2) \sum_{m_e} |J_e m_e\rangle \langle J_e m_e| - i\frac{\kappa}{2} a^{\dagger} a \\ & - i\Omega(t)(A_{+1} - A_{+1}^{\dagger}) - ig(t)(a^{\dagger} A_0 - A_0^{\dagger} a), \end{aligned} \quad (2.12)$$

is the effective non-Hermitian Hamiltonian in the rotating-wave approximation [PMZ<sup>+</sup>95]. For the two-photon resonance problem ( $\Delta = 0$ ) this Hamiltonian reduces to

$$\begin{aligned} H_{\text{eff}} = & -i\frac{\Gamma}{2} |e\rangle \langle e| - i\frac{\kappa}{2} a^{\dagger} a \\ & - i\Omega(t)(A_{+1} - A_{+1}^{\dagger}) - ig(t)(a^{\dagger} A_0 - A_0^{\dagger} a), \end{aligned} \quad (2.13)$$

where the atomic lowering operators  $A_\sigma$  are given by

$$A_\sigma = \sum_{m_e, m_g} |J_g m_g\rangle \langle J_g m_g; 1\sigma | J_e m_e\rangle \langle J_e m_e|, \quad (2.14)$$

with  $\langle J_g m_g; 1\sigma | J_e m_e\rangle$  the Clebsch-Gordan coefficient for the dipole transition  $|e\rangle \rightarrow |g\rangle$  with polarization  $\sigma = 0, \pm 1$ . Working out these coefficients, we may have

$$A_1 = \frac{1}{\sqrt{3}} |g_{-1}\rangle \langle e|, \quad A_0 = -\frac{1}{\sqrt{3}} |g_0\rangle \langle e|, \quad A_{-1} = \frac{1}{\sqrt{3}} |g_1\rangle \langle e|. \quad (2.15)$$

Upon substitution of Eqs. (2.13) and (2.15) into Eq. (2.11), we find that

$$\begin{aligned} \frac{\partial \rho}{\partial t} = & -\frac{1}{2} (\Gamma |e\rangle \langle e| \rho + \kappa a^\dagger a \rho + \text{H.c.}) - \frac{\Omega(t)}{\sqrt{3}} (|g_{-1}\rangle \langle e| \rho - |e\rangle \langle g_{-1}| \rho + \text{H.c.}) \\ & - \frac{g(t)}{\sqrt{3}} (a^\dagger |g_0\rangle \langle e| \rho - |e\rangle \langle g_0| a \rho + \text{H.c.}) + \kappa a \rho a^\dagger \\ & + \frac{\Gamma}{3} (|g_1\rangle \langle e| \rho |e\rangle \langle g_1| + |g_0\rangle \langle e| \rho |e\rangle \langle g_0| + |g_{-1}\rangle \langle e| \rho |e\rangle \langle g_{-1}|). \end{aligned} \quad (2.16)$$

We can see from Eq. (2.16) that only the following family of eigenstates survive:

$$|g_{-1}, 0\rangle, \quad |e, 0\rangle, \quad |g_0, 1\rangle, \quad |g_0, 0\rangle, \quad \text{and} \quad |g_1, 0\rangle. \quad (2.17)$$

This means that in our density matrix approach, we have up to 25 matrix elements of the form  $\dot{\rho}_{ij} = \langle i | \dot{\rho} | j \rangle$ . However, we can get rid of some of these matrix elements because they are electric dipole forbidden or make no physical sense. In this way, the total number of matrix elements can be reduced from 25 to only eight, which corresponds to the number of differential equations describing the evolution of the system.

By introducing the following notation for the atomic levels:

$$|a\rangle = |g_{-1}\rangle, \quad |b\rangle = |g_0\rangle, \quad |c\rangle = |g_1\rangle; \quad (2.18)$$

and calling  $\rho_{ij} \equiv \text{Re}[\langle i | \rho | j \rangle]$ , we can write the equations of motion for the density matrix elements in the form

$$\dot{\rho}_{a0a0} = -2\Omega(t)\rho_{a0e0} + \frac{\Gamma}{3}\rho_{e0e0}, \quad (2.19a)$$

$$\dot{\rho}_{b0b0} = \frac{\Gamma}{3}\rho_{e0e0} + \kappa\rho_{b1b1}, \quad (2.19b)$$

$$\dot{\rho}_{b1b1} = -\kappa \rho_{b1b1} - 2g(t) \rho_{b1e0}, \quad (2.19c)$$

$$\dot{\rho}_{c0c0} = \frac{\Gamma}{3} \rho_{e0e0}, \quad (2.19d)$$

$$\dot{\rho}_{e0e0} = -\Gamma \rho_{e0e0} + 2\Omega(t) \rho_{a0e0} + 2g(t) \rho_{b1e0}, \quad (2.19e)$$

$$\dot{\rho}_{a0e0} = -\frac{\Gamma}{2} \rho_{a0e0} - \Omega(t)(\rho_{e0e0} - \rho_{a0a0}) + g(t) \rho_{a0b1}, \quad (2.19f)$$

$$\dot{\rho}_{a0b1} = -\frac{\kappa}{2} \rho_{a0b1} - \Omega(t) \rho_{b1e0} - g(t) \rho_{a0e0}, \quad (2.19g)$$

$$\dot{\rho}_{b1e0} = -\frac{1}{2}(\Gamma + \kappa) \rho_{b1e0} + \Omega(t) \rho_{b1a0} - g(t)(\rho_{e0e0} - \rho_{b1b1}). \quad (2.19h)$$

## 2.2 Numerical results

In this section we have studied numerically two different methods for transferring the population between two atomic levels: the  $\pi$ -pulses and the adiabatic passage methods. The calculation of the transfer efficiencies was done by numerically integrating the system of equations (2.19) using the Runge-Kutta method of fifth order with an adaptive mesh. By using Gaussian, hyperbolic secant, and Lorentzian pulse shapes, we obtained the coherent transfer efficiencies for the four-level system in a cavity, including radiative decay from the excited states. For simplicity, we have considered a high- $Q$  cavity with no decay ( $\kappa = 0$ ). Five different parameters were considered in our simulations: the Rabi frequency and the width of the pulses, the time delay (for intuitive and counterintuitive configurations), and the spontaneous emission of the excited states.

Because of the big volume of data manipulated during the simulations (necessary to obtain results with some degree of accuracy) the computations were performed in a cluster of four heterogeneous computers running Parallel Virtual Machine (PVM). Surfaces of the logarithm of the failure probability were plotted for some physically reasonable intervals for the Rabi frequencies and widths of the pulses. For example, most of the time we studied widths in the interval  $[0, 10]$ . We also explored time delays in intervals between  $[0, 50]$  for Gaussian pulses, and  $[0, 100]$  for Sech and Lorentzian pulses. The figures obtained for all these parameters were given in “absolute” numbers (no units). We did it in this way because we wanted to examine the ratios between quantities with same dimensions rather than individual values taken by the parameters themselves. This is why most of the graphs were plotted in terms of  $\Omega/g$ , and  $\Delta t/\sigma$ . During the numerical simulations we also fixed the value  $g$  to unity for many of them. This allowed us to have a point of comparison between the pulses’ energies (Rabi frequencies) and widths for the different failure probabilities obtained, and then to

conclude which set of parameters achieved the maximum transfer efficiency.

Our analysis starts with the  $\pi$ -pulses method. An intuitive sequence of these pulses can, in principle, produce a complete population transfer between two atomic levels [SBK<sup>+</sup>92]. Here, we adjust the laser intensities and pulses' duration so that the time integral of the Rabi frequencies (the pulse area) have the value of  $\pi$ . The first pulse  $\Omega$ , takes the system from the initially populated level  $|g_{-1} 0\rangle$  to the excited level  $|e 0\rangle$ ; then the cavity-mode field  $g$  takes the system to the target level  $|g_0 0\rangle$ . For this to be possible the excitation has to be coherent. Results for the time delay and failure probability are shown in Table 2.1 for different values of the Rabi frequency and the width of the pulses.

Table 2.1:  $\pi$ -pulses method.

Pulse profile	$\Gamma$	$\Omega$	$\sigma$	$g$	$\sigma_g$	$\Delta t$	$\log_{10} p$
Gaussian	0.01	2.14	0.29	1.00	0.63	1.26	-2.05
	0.02	2.15	0.29	1.00	0.63	1.16	-1.78
	0.05	2.03	0.31	1.00	0.63	1.01	-1.44
	0.10	2.11	0.30	1.00	0.63	0.89	-1.19
	0.20	2.18	0.29	1.00	0.63	0.75	-0.95
Sech	0.01	1.84	0.26	1.00	0.50	1.52	-1.94
	0.02	2.01	0.25	1.00	0.50	1.35	-1.69
	0.05	2.16	0.23	1.00	0.50	1.11	-1.37
	0.10	2.26	0.22	1.00	0.50	0.94	-1.13
	0.20	2.43	0.21	1.00	0.50	0.77	-0.91
Lorentzian	0.01	5.71	0.09	1.00	0.50	2.28	-1.63
	0.02	5.53	0.09	1.00	0.50	1.80	-1.43
	0.05	5.56	0.09	1.00	0.50	1.32	-1.16
	0.10	5.80	0.09	1.00	0.50	1.04	-0.96
	0.20	6.28	0.08	1.00	0.50	0.82	-0.77

As is well known, this method presents the most efficiency (100%) when the system undergoes no

spontaneous emission. However, when the system decays radiatively, the efficiency of the method decreases gradually as the spontaneous emission rate increases. We observe that, when the spontaneous emission is  $\Gamma = 0.01$ , the Gaussian pulses have an efficiency of 99.1%, while the secant and Lorentzian pulses presented maximum efficiencies of 98.9% and 97.7%, respectively. These values were the best obtained for a wide range of the examined pulse amplitudes and pulse widths. Fig. 2.3 shows that for greater values of the spontaneous emission, the transfer efficiency reduces in a considerable way. The time delay between the pulses also reduces to shorter times for bigger spontaneous

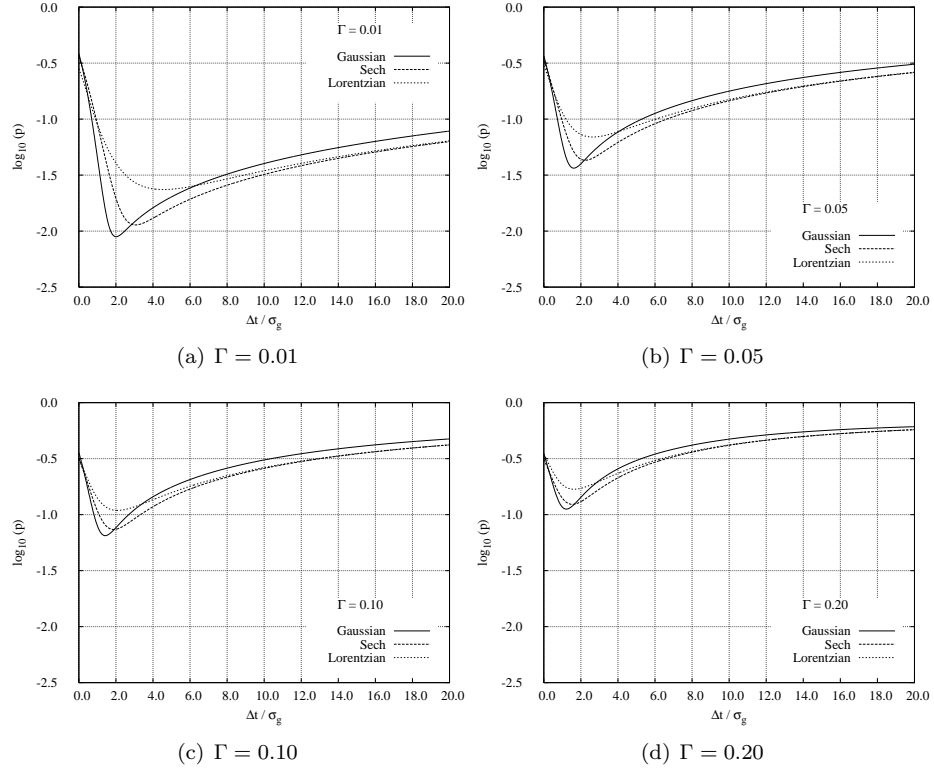


Figure 2.3:  $\pi$ -pulses failure probability for four different values of spontaneous emission. The values of the Rabi frequencies, widths, and time delay can be found in Table 2.1

emission values. This is understandable because more overlap between the pulses is required to neutralize the decay rate of the excited states.

It is interesting to note that in this *intuitive* sequence of pulses (as it is the case for the  $\pi$ -pulses method), good transfer efficiencies were achieved when the driving classical field (laser) was stronger than the quantized cavity mode, as shown in Fig. 2.4. Even though the ratio of the Gaussian pulses ( $\Omega/g$ ) was bigger than the ratio of the Sech pulses, less interaction time ( $\Delta t/\sigma_g$ ) was required for the Gaussian pulses to obtain a bigger efficiency. The Lorentzian pulses required the biggest energy (Rabi frequency) to achieve even less efficiency than the other two types of pulses, as observed from

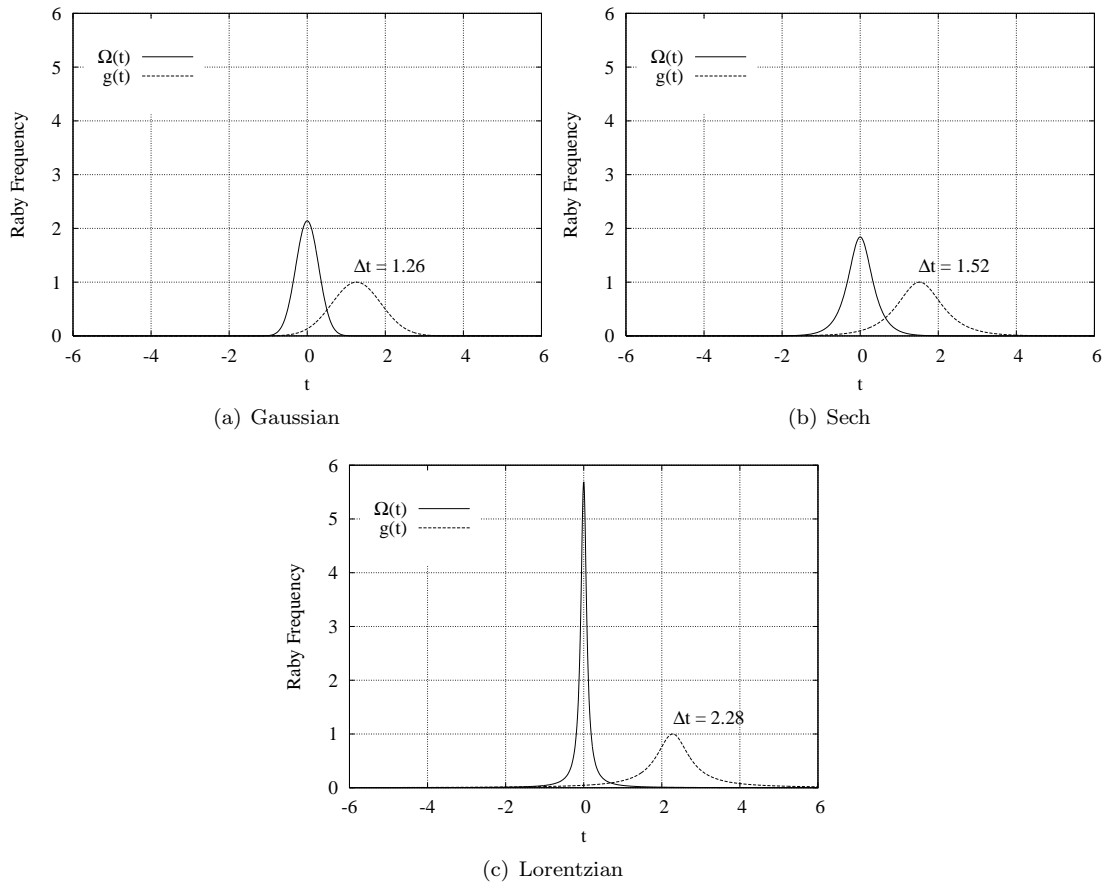


Figure 2.4:  $\pi$ -pulses' profiles for the best set of parameters when  $\Gamma = 0.01$ .



the ratio of the pulses shown in 2.4.

The  $\pi$ -pulses method is a good and efficient technique to transfer the population in atomic systems, but we will see that the adiabatic passage scheme overtakes considerably the  $\pi$ -pulses performance for some very interesting and particular situations.

The next method we studied numerically was the adiabatic passage scheme. Table 2.2 shows the values of time delay and failure probability we obtained for different values of the spontaneous emission.

Table 2.2: Adiabatic passage scheme

Pulse profile	$\Gamma$	$\Omega$	$\sigma$	$g$	$\sigma_g$	$\Delta t$	$\log_{10} p$
Gaussian	0.00	2.00	1.00	2.00	1.00	1.31	-4.88
		4.00	1.00	19.20	1.00	1.90	-4.53
		6.00	1.00	5.70	1.00	1.50	-6.83
		6.70	1.50	2.00	1.00	2.72	-5.67
	0.10	3.39	3.23	1.00	2.45	5.85	-1.99
		2.75	3.09	1.00	2.48	5.29	-2.00
	0.20	3.30	3.30	1.00	2.50	5.90	-1.73
		2.40	3.30	1.00	3.00	5.38	-1.80
		2.30	4.20	1.00	4.48	6.62	-1.96
		2.10	4.60	1.00	5.00	7.09	-2.01
	Sech	0.00	2.00	1.00	2.00	1.00	0.80
		0.10	2.60	1.40	1.00	1.20	2.70
			5.00	1.50	1.00	2.00	3.80
			4.50	1.70	1.00	2.40	4.10
			4.20	1.80	1.00	2.60	4.30
			6.30	3.40	1.00	4.01	12.01

Table 2.2: Adiabatic passage scheme

	0.20	14.70	5.00	1.00	7.00	21.40	-2.06
Lorentzian	0.00	2.00	1.00	2.00	1.00	0.32	-4.46
	0.10	9.20	0.60	1.00	2.00	2.29	-1.05

Here, it is important to emphasize that the figures shown in the table do not necessarily correspond to the best possible values of the transfer efficiency achieved by the system. It happens that the efficiency can be optimized as much as we want by increasing the values of the Rabi frequencies, or equivalently, the widths of the pulses. Thus, for bigger Rabi frequencies, bigger efficiencies. This is something that has no experimental worth. What we want to examine here are those values of the Rabi frequency and time delay that can be reproduced in a laboratory, and for which very good transfer efficiency values can be obtained. So we have decided to consider a reasonable value of  $\log_{10} p = -2.00$  for our numerical exploration.

We analyze first the case of no spontaneous emission, when the system is driven by Gaussian pulses. Fig. 2.5 shows that for the particular set of parameters  $\{\Omega = 2.00, \sigma = 1.00, g = 2.00, \sigma_g = 1.00, \Delta t = 1.31\}$  a tremendous efficiency of 99.9% or higher is obtained. We observe that, while the failure probability remains almost the same over a wide region of the pulses' amplitudes, there is one particular sector for which a sudden fall in the failure probability occurs. A very sharp, deep, and unexpected well just appears on the probability surface. Intriguingly, an even more sharper and deeper well emerges when the driving pulses are hyperbolic secants, and the set of parameter is  $\{\Omega = 2.00, \sigma = 1.00, g = 2.00, \sigma_g = 1.00, \Delta t = 0.80\}$ , as shown in Fig. 2.6. For this case we observe that the region nearby to the sharp dip is deformed a little bit forming a valley of good values for the transfer efficiency. Fig. 2.7 shows another efficient set of parameters, this time for Lorentzian pulses.

We observe from Fig. 2.8 that, with a shorter interaction time ( $\Delta t/\sigma_g$ ) than the Gaussian pulses (but longer than Lorentzian pulses), the Sech pulses achieved the best transfer efficiency. Here, all the profiles have the same ratio for the pulses ( $\Omega/g = 1.0$ ).

When we consider spontaneous emission, the situation changes a little bit. We are looking for good efficiencies of the order of  $\log_{10} p = -2.00$ . Figs. 2.9 and 2.10 show the failure probability

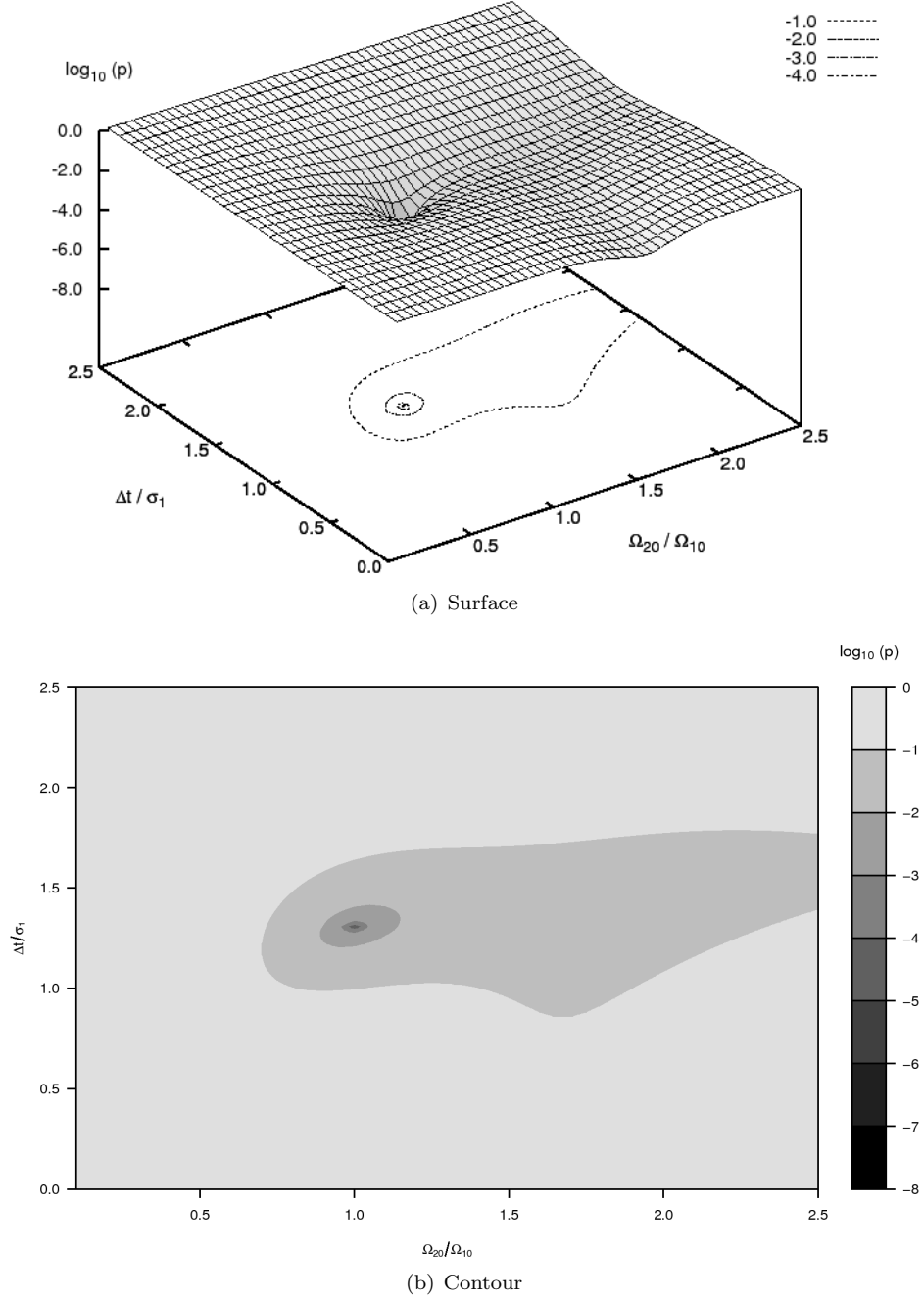


Figure 2.5: Gaussian surface and contour for  $\Gamma = 0.00$ . Here  $\Omega = 2.00$ ,  $\sigma = 1.00$ ,  $g = 2.00$ ,  $\sigma_g = 1.00$ ,  $\Delta t = 1.31$ , and  $\log_{10} p = -4.88$ .

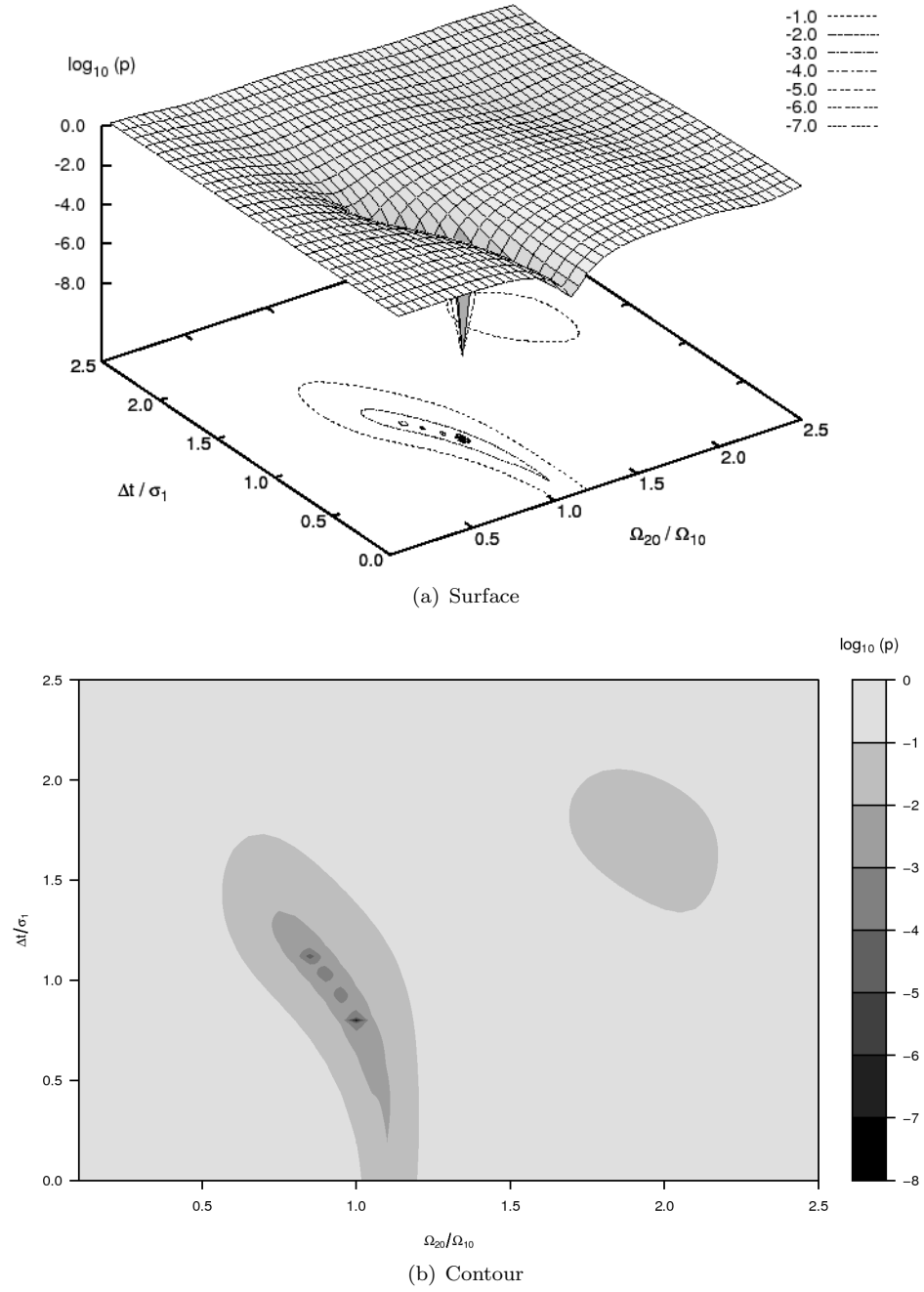


Figure 2.6: Hyperbolic secant surface and contour for  $\Gamma = 0.00$ . Here  $\Omega = 2.00$ ,  $\sigma = 1.00$ ,  $g = 2.00$ ,  $\sigma_g = 1.00$ ,  $\Delta t = 0.80$ , and  $\log_{10} p = -7.79$ .

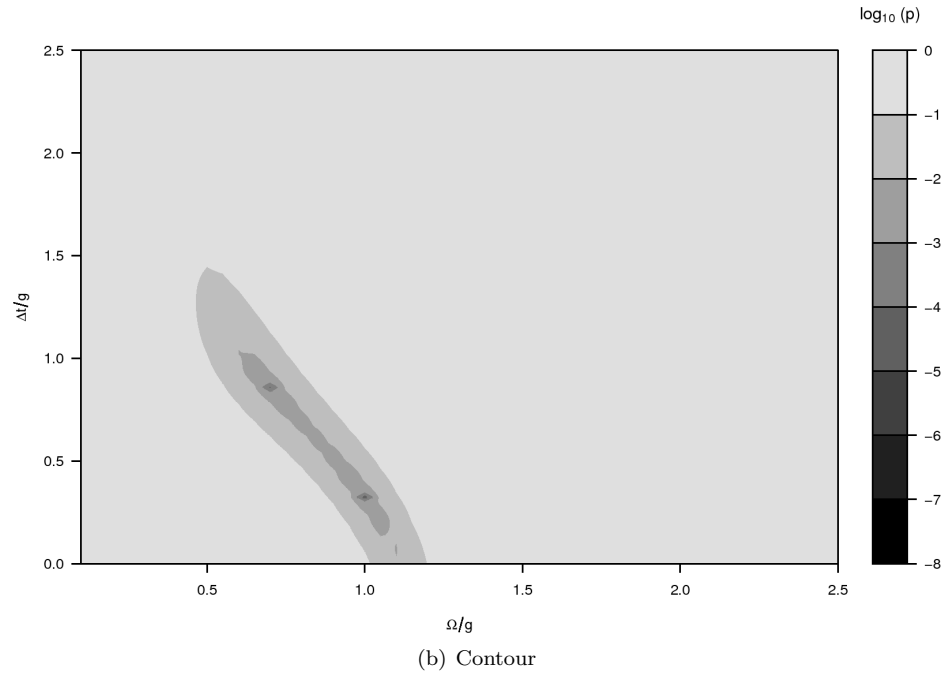
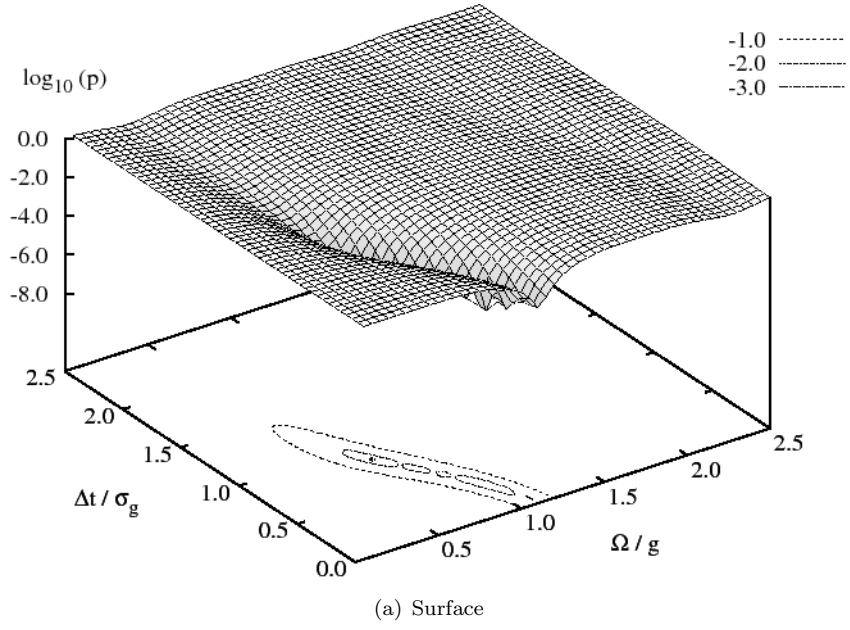


Figure 2.7: Lorentzian secant surface and contour for  $\Gamma = 0.00$ . Here  $\Omega = 2.00$ ,  $\sigma = 1.00$ ,  $g = 2.00$ ,  $\sigma_g = 1.00$ ,  $\Delta t = 0.32$ , and  $\log_{10} p = -4.46$ .

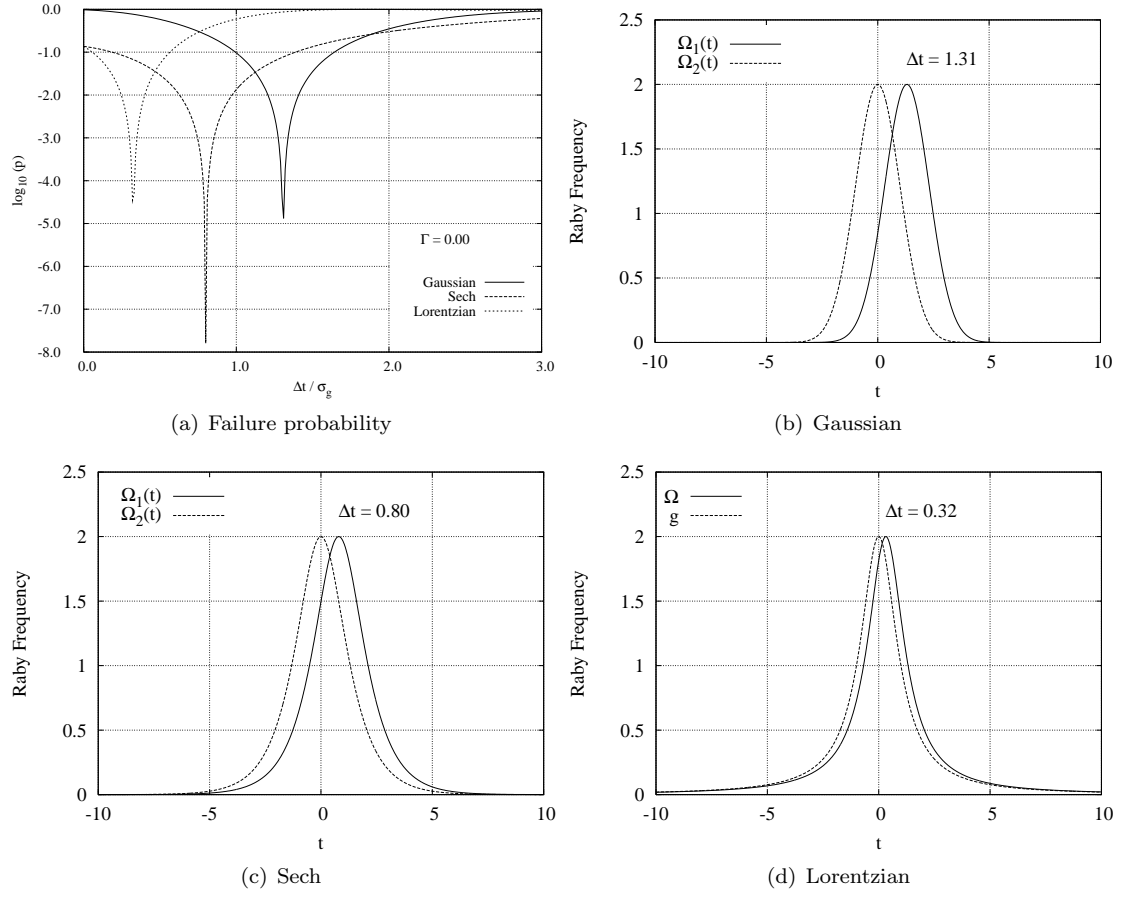


Figure 2.8: (a) Cross-sections of  $\log_{10} p$  as a function of  $\Delta t / \sigma_g$  for  $\Gamma = 0$ . (b)-(d) Pulses' profiles.

for two different values of the spontaneous emission, when Gaussian and secant pulses are used for driving the system. In this case, we focus our attention in the Rabi frequencies, the pulses' widths

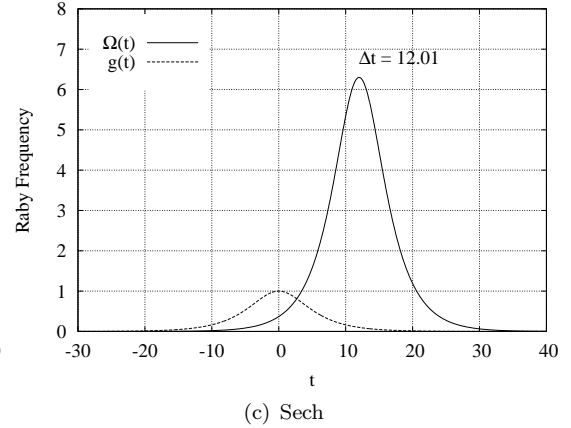
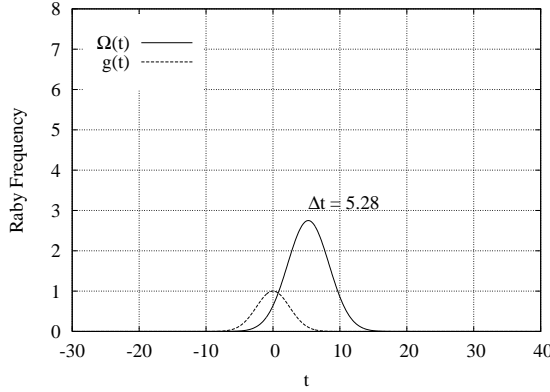
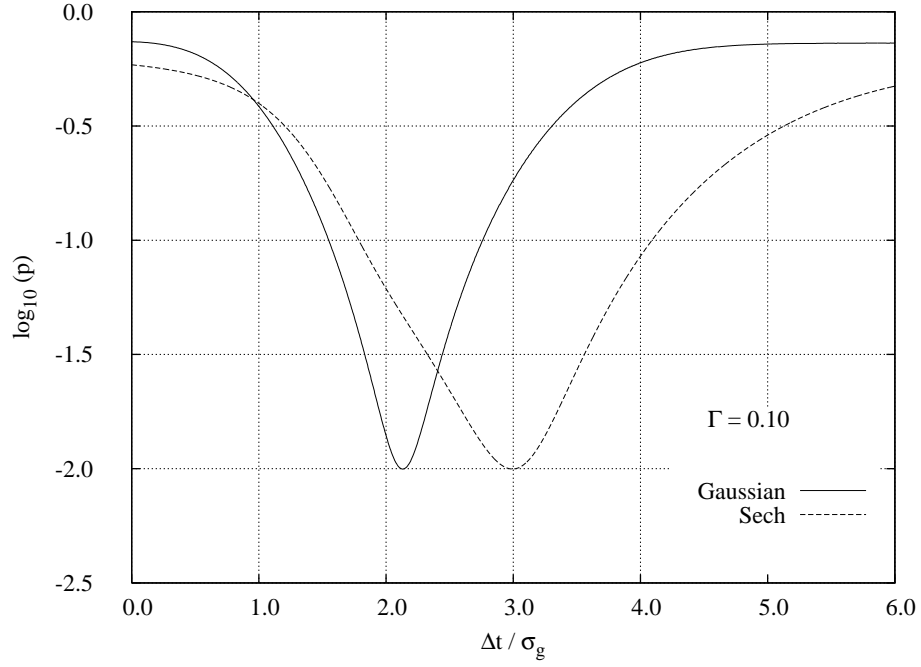
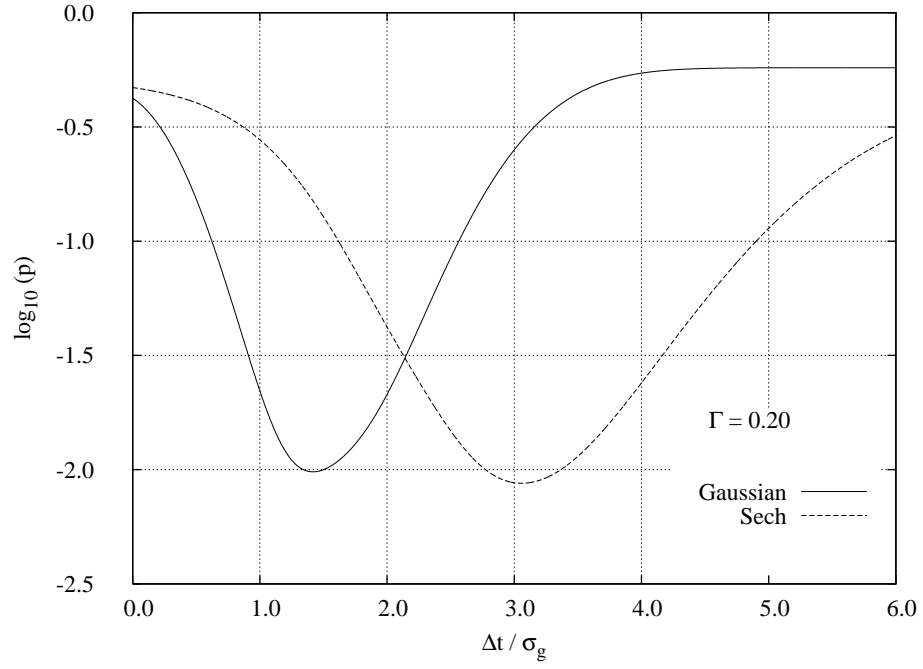


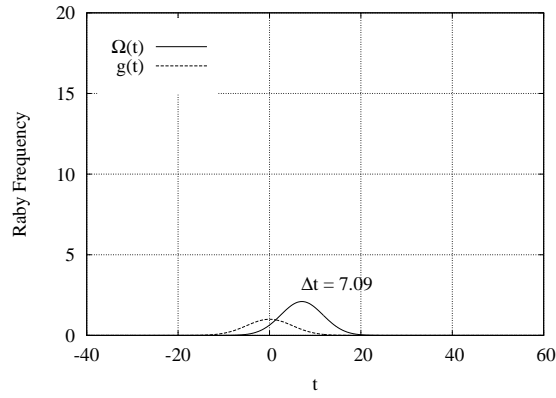
Figure 2.9: Adiabatic passage for  $\Gamma = 0.10$

and the time delay. We immediately observe from the figures that a bigger energy and a longer time delay is required by the Sech pulses to obtain the same efficiency than that achieved by Gaussian pulses. We also see that a considerable overlapping of the pulses is necessary to obtain good transfer efficiencies. Gaussian pulses seem to be more effective this time, as the comparison between the ratio of the pulses and the interaction time confirms.

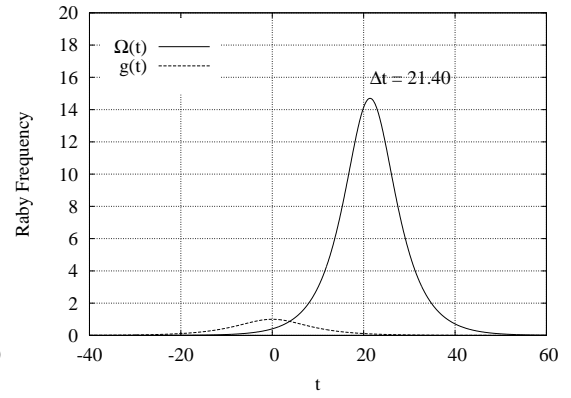
Unfortunately, it was very difficult to obtain results for the Lorentzian pulses for values of the spontaneous emission different from zero. These pulses are very wide, and their numerical integration



(a) Failure probability



(b) Gaussian



(c) Sech

Figure 2.10: Adiabatic passage for  $\Gamma = 0.20$



is a very complicated task. However, it is possible to see from Table 2.2, that for bigger values of the spontaneous emission, bigger values of the Rabi frequency are needed.

## Chapter 3

# A simple analytical model

In this chapter we introduce a simple analytical model that explains qualitatively the origin of the nonadiabatic, resonance-like features observed in adiabatic passage methods. We also present a mathematical description of the three different pulse shapes used in our numerical simulations of chapters two and three, including the nonadiabatic coupling terms. By using the analytical model, we study the dependence of the failure probability  $p$  on the system parameters  $\Omega T$ , showing the exact solution of a simple problem. Although the analytical results here reported have been obtained by others, the method is somewhat different from those in the literature.

### 3.1 Population transfer

Consider a three-level  $\Lambda$  system driven by a two-mode classical coherent field, as shown in Fig. 3.1.

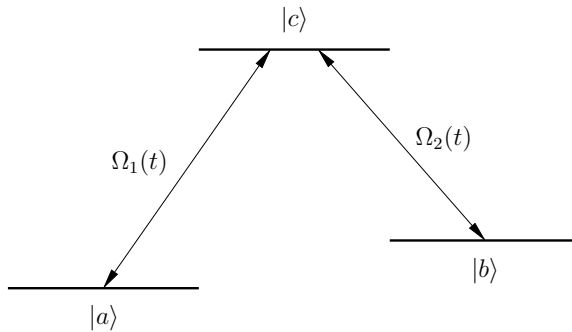


Figure 3.1: Three-level  $\Lambda$  system driven by two lasers. The Rabi frequencies for the *pump* and *Stokes* laser are  $\Omega_1$  and  $\Omega_2$ , respectively.

We want to study the problem of coherent population transfer from the initially populated state  $|a\rangle$  to the final state  $|b\rangle$  by using a pump laser coupling states  $|a\rangle$  and  $|c\rangle$ , and a Stokes laser coupling

states  $|c\rangle$  and  $|b\rangle$  (see [KGHB89]).

Under two-photon resonance condition and by using the rotating-wave approximation, the evolution of the system is described by

$$\dot{C}_a = -\frac{\Omega_1(t)}{2} C_c, \quad (3.1a)$$

$$\dot{C}_b = -\frac{\Omega_2(t)}{2} C_c, \quad (3.1b)$$

$$\dot{C}_c = \frac{\Omega_1(t)}{2} C_a + \frac{\Omega_2(t)}{2} C_b, \quad (3.1c)$$

where  $C_a$ ,  $C_b$ , and  $C_c$  are the probability amplitudes of finding the system in states  $|a\rangle$ ,  $|b\rangle$ , and  $|c\rangle$ , respectively.

To obtain approximate solutions to this system, we may proceed as follows. Let us first consider the normalized state vector  $|\Psi(t)\rangle$  in spherical coordinates, as indicated in Fig. 3.2. The state vector

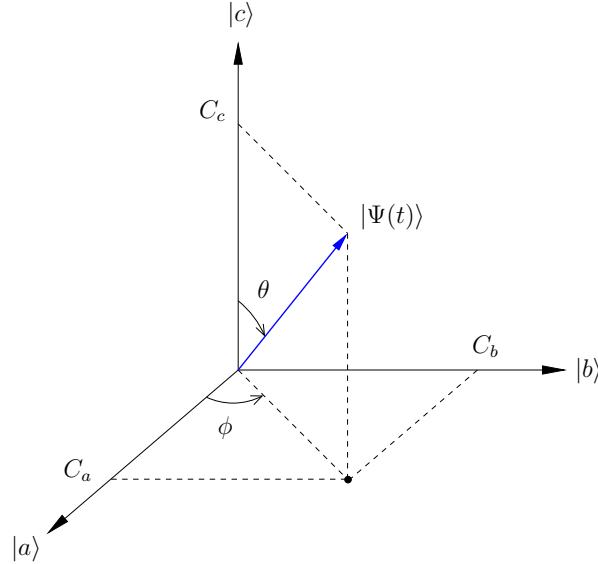


Figure 3.2: Graphic representation of the Hilbert space for the three-level system in the eigenbasis  $\{|a\rangle, |b\rangle, |c\rangle\}$ . The state vector  $|\Psi(t)\rangle$  is represented by its three Cartesian components  $C_a$ ,  $C_b$ , and  $C_c$ , corresponding to the probability amplitudes.

components  $C_a$ ,  $C_b$ , and  $C_c$  (probability amplitudes) can be written in the form

$$C_a = \sin \theta \cos \phi, \quad (3.2a)$$

$$C_b = \sin \theta \sin \phi, \quad (3.2b)$$

$$C_c = \cos \theta, \quad (3.2c)$$

with time derivatives given by

$$\dot{C}_a = \dot{\theta} \cos \theta \cos \phi - \dot{\phi} \sin \theta \sin \phi, \quad (3.3a)$$

$$\dot{C}_b = \dot{\theta} \cos \theta \sin \phi + \dot{\phi} \sin \theta \cos \phi, \quad (3.3b)$$

$$\dot{C}_c = -\dot{\theta} \sin \theta. \quad (3.3c)$$

Now, plugging Eqs. (3.2) and (3.3) into Eqs. (3.1), and by using the *mixing angle*

$$\tan \Phi(t) = \frac{\Omega_1(t)}{\Omega_2(t)}, \quad (3.4)$$

it is simple to verify that Eqs. (3.1) reduce to a system of two coupled nonlinear differential equations given by

$$\dot{\phi}(t) = \frac{\tan[\theta - \pi/2]}{2} \Omega(t) \cos[\phi + \Phi(t)], \quad (3.5a)$$

$$\dot{\theta}(t) = -\frac{\Omega(t)}{2} \sin[\phi + \Phi(t)]. \quad (3.5b)$$

Here  $\Omega(t) = \sqrt{\Omega_1^2(t) + \Omega_2^2(t)}$ .

Taking a look at the asymptotic behavior of Eqs. (3.1), we see that at very early times ( $t \rightarrow -\infty$ ) when the state vector is parallel to the initially populated state  $|a\rangle$ , the probability amplitude coefficients take the values

$$\begin{aligned} C_a(-\infty) &= 1 = \sin \theta(-\infty) \cos \phi(-\infty), \\ C_b(-\infty) &= 0 = \sin \theta(-\infty) \sin \phi(-\infty), \\ C_c(-\infty) &= 0 = \cos \theta(-\infty). \end{aligned} \quad (3.6)$$

This implies that before the interaction with the lasers, the angular coordinates of the state vector are

$$\theta(-\infty) = \pi/2 \quad \text{and} \quad \phi(-\infty) = 0. \quad (3.7)$$

Similarly, for very late times ( $t \rightarrow +\infty$ ) when the state vector is antiparallel to the final state  $|b\rangle$

(see Sec. 1.5), the probability amplitudes are

$$\begin{aligned} C_a(\infty) &= 0 = \sin \theta(\infty) \cos \phi(\infty), \\ C_b(\infty) &= -1 = \sin \theta(\infty) \sin \phi(\infty), \\ C_c(\infty) &= 0 = \cos \theta(\infty). \end{aligned} \tag{3.8}$$

From these equations, we may conclude that after the interaction with the lasers

$$\theta(\infty) = \pi/2 \quad \text{and} \quad \phi(\infty) = -\pi/2. \tag{3.9}$$

Since we are interested in transferring population from the initial state  $|a\rangle$  to the final state  $|b\rangle$  without populating the leaking excited state  $|c\rangle$  (which we assume undergoes radiative decay), then the state vector  $|\Psi(t)\rangle$  should evolve adiabatically by closely following the “dressed state”  $|W^0\rangle$  of the Hamiltonian of system (3.1). Thus the angular coordinates of the state vector can be written as

$$\theta_{ad}(t) = \pi/2 \quad \text{and} \quad \phi_{ad}(t) = -\Phi(t), \tag{3.10}$$

where the label “*ad*” accounts for an *adiabatic following* of these angles to the corresponding angular coordinates of the dressed state.

If we assume small deviations from conditions (3.10), the system (3.5) can be linearized. By plugging the equations

$$\theta = \theta_{ad} + \delta\theta = \pi/2 + \delta\theta, \tag{3.11a}$$

$$\phi = \phi_{ad} + \delta\phi = -\Phi(t) + \delta\phi, \tag{3.11b}$$

and their time derivatives

$$\dot{\theta} = \dot{\delta\theta}, \tag{3.12a}$$

$$\dot{\phi} = -\dot{\Phi}(t) + \dot{\delta\phi}, \tag{3.12b}$$

into Eqs. (3.5), we obtain

$$\dot{\delta\phi} = \frac{\Omega(t)}{2} \delta\theta + \dot{\Phi}(t), \tag{3.13a}$$

$$\dot{\delta\theta} = -\frac{\Omega(t)}{2} \delta\phi. \tag{3.13b}$$

To integrate Eqs. (3.13), we need to make a change of variables by defining a “dimensionless phase”  $\tau$  in the form

$$\tau(t) = \int_{-\infty}^t \frac{\Omega(t')}{2} dt'. \quad (3.14)$$

This phase will play the role of a rescaled time in the following. Then, by using the chain rule

$$\frac{d}{dt} = \frac{d\tau}{dt} \frac{d}{d\tau} = \frac{\Omega(t)}{2} \frac{d}{d\tau}, \quad (3.15)$$

we can rewrite Eqs. (3.13) in the form

$$\frac{d}{d\tau} \delta\phi[\tau] = \delta\theta[\tau] + \frac{d}{d\tau} \Phi[\tau], \quad (3.16a)$$

$$\frac{d}{d\tau} \delta\theta[\tau] = -\delta\phi[\tau]. \quad (3.16b)$$

Now, by differentiating the second equation and plugging it into the first, we obtain the equation of an *undamped driven harmonic oscillator*

$$\frac{d^2}{d\tau^2} \delta\theta[\tau] + \delta\theta[\tau] = -\frac{d}{d\tau} \Phi[\tau]. \quad (3.17)$$

The general solution to this equation is very well known and given by (see Appendix 4.3.3)

$$\delta\theta[\tau] = A \sin[\tau] + B \cos[\tau] - \int_0^\tau \sin[\tau - \tau'] \frac{d\Phi[\tau']}{d\tau'} d\tau'. \quad (3.18)$$

The lower limit of the integral results when the time is  $-\infty$  giving

$$\tau[-\infty] = \int_{-\infty}^{-\infty} \frac{\Omega(t)}{2} dt = 0. \quad (3.19)$$

In addition, we have that the difference between phases can be written as

$$\tau - \tau' = \int_{t'}^t \frac{\Omega(t'')}{2} dt''. \quad (3.20)$$

Now, returning to the original time scale in Eq. (3.18), we get

$$\begin{aligned} \delta\theta(t) = & A \sin \left[ \int_{-\infty}^t \frac{\Omega(t')}{2} dt' \right] + B \cos \left[ \int_{-\infty}^t \frac{\Omega(t')}{2} dt' \right] \\ & - \int_{-\infty}^t \sin \left[ \int_{t'}^t \frac{\Omega(t'')}{2} dt'' \right] \frac{d\Phi(t')}{dt'} dt'; \end{aligned} \quad (3.21)$$

and by inserting Eq. (3.21) into (3.13b), we can solve for  $\delta\phi$  obtaining

$$\begin{aligned}\delta\phi(t) = & -A \cos\left[\int_{-\infty}^t \frac{\Omega(t')}{2} dt'\right] + B \sin\left[\int_{-\infty}^t \frac{\Omega(t')}{2} dt'\right] \\ & + \int_{-\infty}^t \cos\left[\int_{t'}^t \frac{\Omega(t'')}{2} dt''\right] \frac{d\Phi(t')}{dt'} dt'.\end{aligned}\quad (3.22)$$

The initial conditions for the linearized system are

$$\delta\theta(-\infty) = 0, \quad (3.23a)$$

$$\dot{\delta\theta}(-\infty) = -\Omega(-\infty)\Phi(-\infty)/2, \quad (3.23b)$$

$$\delta\phi(-\infty) = \Phi(-\infty), \quad (3.23c)$$

$$\dot{\delta\phi}(-\infty) = \dot{\Phi}(-\infty). \quad (3.23d)$$

And finally, by evaluating the constants of integration  $A$  and  $B$ , we may obtain

$$\delta\phi(t) = \Phi(-\infty) \cos\left[\int_{-\infty}^t \frac{\Omega(t')}{2} dt'\right] + \int_{-\infty}^t \cos\left[\int_{t'}^t \frac{\Omega(t'')}{2} dt''\right] \frac{d\Phi(t')}{dt'} dt', \quad (3.24a)$$

$$\delta\theta(t) = -\Phi(-\infty) \sin\left[\int_{-\infty}^t \frac{\Omega(t')}{2} dt'\right] - \int_{-\infty}^t \sin\left[\int_{t'}^t \frac{\Omega(t'')}{2} dt''\right] \frac{d\Phi(t')}{dt'} dt'. \quad (3.24b)$$

The two terms in each of the equations (3.24) represent different things. The first term represents a coherent mixing of the adiabatic states that occurs when the initial state of the system is not one of the eigenstates of the interaction Hamiltonian. The second term, on the other hand, represents corrections to the adiabatic approximation.

## 3.2 Asymptotic behavior of the pulses

In the present work, we used three different kinds of pulse shapes for the numerical computations

$$\text{Gaussian pulses:} \quad \Omega(t) = \Omega_0 \exp(-t^2/2\sigma^2), \quad (3.25a)$$

$$\text{Hyperbolic Secant pulses:} \quad \Omega(t) = \Omega_0 \operatorname{sech}(t/\sigma), \quad (3.25b)$$

$$\text{Lorentzian pulses:} \quad \Omega(t) = \Omega_0 \sigma^2 / (t^2 + \sigma^2). \quad (3.25c)$$

Here  $\Omega_0$  is the Rabi amplitude of the pulse, and  $\sigma$  is a scale parameter (width) describing the extent of the pulse. The different shapes are illustrated in Fig. 3.3.

It is important to consider the asymptotic behavior of functions (3.25) because this determines if

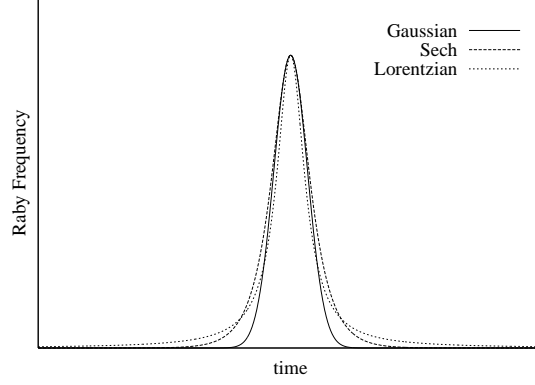


Figure 3.3: Profiles of the three pulses used in this work.

a sequence of pulses satisfies the adiabatic conditions, and then the system can evolve adiabatically. In addition, the *nonadiabatic coupling* matrix element

$$\dot{\Phi}(t) = \frac{\dot{\Omega}_1 \Omega_2 - \Omega_1 \dot{\Omega}_2}{\Omega_1^2 + \Omega_2^2}, \quad (3.26)$$

can be used as a “local” adiabaticity criterion for a given shape of the laser pulses.

### 3.2.1 Gaussian pulses

Consider two Gaussian pulses of the form

$$\Omega_1(t) = \Omega_{10} \exp[-(t - \Delta t)^2 / 2\sigma_1^2], \quad (3.27a)$$

$$\Omega_2(t) = \Omega_{20} \exp(-t^2 / 2\sigma_2^2). \quad (3.27b)$$

These two pulses are in a *counterintuitive* configuration, where the pulse 2 precedes the pulse 1, and their separation is given by the *time delay*  $\Delta t$ .

The ratio of the pulses can be written as

$$\frac{\Omega_1(t)}{\Omega_2(t)} = \frac{\Omega_{10}}{\Omega_{20}} \exp \left[ -\frac{(\Delta t)^2}{2\sigma_1^2} - \frac{\sigma_2^2 - \sigma_1^2}{2(\sigma_1 \sigma_2)^2} t^2 + \frac{\Delta t}{\sigma_1^2} t \right]. \quad (3.28)$$

We observe that at very early or very late times, the behavior of this ratio depends on the pulses’



widths as follows

$$\sigma_1 > \sigma_2 : \quad \Omega_1/\Omega_2 \rightarrow +\infty \text{ when } t \rightarrow \pm\infty, \quad (3.29a)$$

$$\sigma_1 = \sigma_2 : \quad \Omega_1/\Omega_2 \rightarrow \begin{cases} 0 & \text{when } t \rightarrow -\infty, \\ +\infty & \text{when } t \rightarrow +\infty, \end{cases} \quad (3.29b)$$

$$\sigma_1 < \sigma_2 : \quad \Omega_1/\Omega_2 \rightarrow 0 \text{ when } t \rightarrow \pm\infty. \quad (3.29c)$$

Equation (3.29b) shows that for pulses with equal widths ( $\sigma_1 = \sigma_2$ ) the adiabatic conditions for the system are satisfied (that is, the external field and the coupling field go to zero when the time goes to  $-\infty$  and  $+\infty$ , respectively) and the adiabatic theorem supports the population inversion between the initial and the target levels. On the other hand, for unequal widths ( $\sigma_1 \neq \sigma_2$ ) the adiabatic conditions are not *fully* satisfied by the system, and the adiabatic theorem *alone* cannot validate the transferring process. In this case we need additional arguments to help us to understand why, in some situations like these, large transfer probabilities are still achieved. Fig. 3.4 shows the asymptotic response of the pulses' ratio.

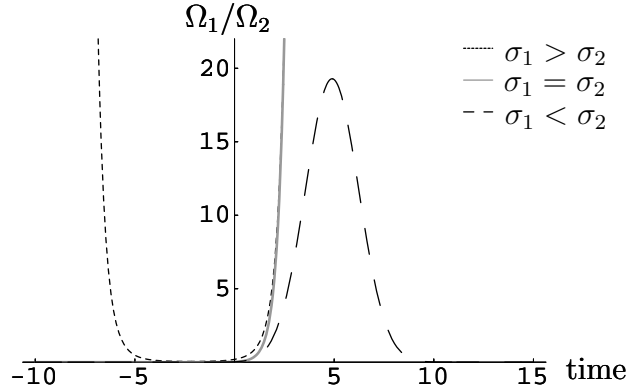


Figure 3.4: Behavior of the Gaussian pulses ratio as a function of time, and for different pulse widths.

The nonadiabatic coupling for these Gaussian pulses is given by

$$\dot{\Phi}(t) = \frac{[\Omega_{10}\Omega_{20}/(\sigma_1\sigma_2)^2][\sigma_2\Delta t - (\sigma_2^2 - \sigma_1^2)t]}{\Omega_{10}^2 \exp(t^2/\sigma_2^2) + \Omega_{20}^2 \exp[(t - \Delta t)^2/\sigma_2^2]} \exp\left[\frac{(t - \Delta t)^2}{2\sigma_1^2} + \frac{t^2}{2\sigma_2^2}\right]. \quad (3.30)$$

### 3.2.2 Hyperbolic secant pulses:

Consider two Sech pulses of the form

$$\Omega_1(t) = \Omega_{10} \operatorname{sech}[(t - \Delta t)/\sigma_1], \quad (3.31a)$$

$$\Omega_2(t) = \Omega_{20} \operatorname{sech}(t/\sigma_2). \quad (3.31b)$$

The ratio of the two pulses is given by

$$\frac{\Omega_1(t)}{\Omega_2(t)} = \left( \frac{\Omega_{10}}{\Omega_{20}} \right) \frac{\exp(t/\sigma_2) + \exp(-t/\sigma_2)}{\exp[(t - \Delta t)/\sigma_1] + \exp[-(t - \Delta t)/\sigma_1]}, \quad (3.32)$$

and the asymptotic behavior of the pulses can be expressed as:

$$\sigma_1 > \sigma_2 : \quad \Omega_1/\Omega_2 \rightarrow +\infty \text{ when } t \rightarrow \pm\infty, \quad (3.33a)$$

$$\sigma_1 = \sigma_2 : \quad \Omega_1/\Omega_2 \rightarrow \begin{cases} (\Omega_{10}/\Omega_{20}) \exp(-\Delta t/\sigma) & \text{when } t \rightarrow -\infty, \\ (\Omega_{10}/\Omega_{20}) \exp(\Delta t/\sigma) & \text{when } t \rightarrow +\infty, \end{cases} \quad (3.33b)$$

$$\sigma_1 < \sigma_2 : \quad \Omega_1/\Omega_2 \rightarrow 0 \text{ when } t \rightarrow \pm\infty. \quad (3.33c)$$

From these relations we observe that hyperbolic secant pulses behave like Gaussian pulses when the widths are unequal ( $\sigma_1 \neq \sigma_2$ ). In contrast, for equal widths ( $\sigma_1 = \sigma_2$ ), the ratio of the pulses reaches constant values different to zero or infinity. In both situations the adiabatic conditions are not satisfied by the system. However, we will see in Ch. 2 that Sech pulses still allow us to get very good transfer efficiencies.

For Sech pulses, the nonadiabatic coupling is given by the function

$$\begin{aligned} \dot{\Phi}(t) = & \frac{[\Omega_{10}\Omega_{20}/\sigma_1\sigma_2] \operatorname{sech}[(t - \Delta t)/\sigma_1] \operatorname{sech}[t/\sigma_2]}{\Omega_{10}^2 \operatorname{sech}^2[(t - \Delta t)/\sigma_1] + \Omega_{20}^2 \operatorname{sech}^2[t/\sigma_2]} \\ & \times \left[ \sigma_1 \tanh\left(\frac{t}{\sigma_2}\right) - \sigma_2 \tanh\left(\frac{t - \Delta t}{\sigma_1}\right) \right]. \end{aligned} \quad (3.34)$$

### 3.2.3 Lorentzian pulses:

Finally, let us consider two Lorentzian pulses of the form

$$\Omega_1(t) = \Omega_{10} \sigma_1^2 / [(t - \Delta t)^2 + \sigma_1^2], \quad (3.35a)$$

$$\Omega_2(t) = \Omega_{20} \sigma_2^2 / (t^2 + \sigma_2^2). \quad (3.35b)$$

The ratio of the two pulses is given by

$$\frac{\Omega_1(t)}{\Omega_2(t)} = \left( \frac{\Omega_{10} \sigma_1^2}{\Omega_{20} \sigma_2^2} \right) \frac{t^2 + \sigma_2^2}{(t - \Delta t)^2 + \sigma_1^2}, \quad (3.36)$$

and the asymptotic behavior expressed as

$$\sigma_1 > \sigma_2 : \quad \Omega_1/\Omega_2 \rightarrow \Omega_{10} \sigma_1^2 / \Omega_{20} \sigma_2^2 \quad \text{when } t \rightarrow \pm\infty, \quad (3.37a)$$

$$\sigma_1 = \sigma_2 : \quad \Omega_1/\Omega_2 \rightarrow \Omega_{10}/\Omega_{20} \quad \text{when } t \rightarrow \pm\infty, \quad (3.37b)$$

$$\sigma_1 < \sigma_2 : \quad \Omega_1/\Omega_2 \rightarrow \Omega_{10} \sigma_1^2 / \Omega_{20} \sigma_2^2 \quad \text{when } t \rightarrow \pm\infty. \quad (3.37c)$$

These equations show a very interesting property: whatever the time delay of the pulses is, their ratio is the same constant in both directions ( $\pm t$ ). Lorentzian pulses behave in a very strange and sometimes unpredictable way. Ch. 2 will show some numerical results obtained when Lorentzian pulses were used to drive a quantum system.

The nonadiabatic coupling of the Lorentzian pulses is given by

$$\dot{\Phi}(t) = \frac{2 \Omega_{10} \Omega_{20} \sigma_1^2 \sigma_2^2 \{ t [(t - \Delta t)^2 + \sigma_1^2] - (t - \Delta t) (t^2 + \sigma_2^2) \}}{\Omega_{10}^2 \sigma_1^4 (t^2 + \sigma_2^2)^2 + \Omega_{20}^2 \sigma_2^4 [(t - \Delta t)^2 + \sigma_1^2]^2}. \quad (3.38)$$

## 3.3 The failure probability

To determine the degree of efficiency in the process of transferring atomic population from the initial state  $|a\rangle$  to the final state  $|b\rangle$ , we define the “failure probability” as

$$p = 1 - |C_b(\infty)|^2. \quad (3.39)$$

This quantity gives us information about how much the process fails to get the population transferred to the target state. If we substitute Eqs. (3.2b) and (3.11) into Eq. (3.39), and consider only the

lowest order in  $\delta\theta$  and  $\delta\phi$ , the probability failure can be written in the form

$$p = [(\delta\phi)^2 + (\delta\theta)^2]_{t \rightarrow \infty}. \quad (3.40)$$

Let us first consider the case of two Gaussian pulses driving the three-level system described by equations (3.1). If the pulses' widths are considered equal ( $\sigma_1 = \sigma_2$ ) then the system satisfies the adiabatic conditions and the mixing angle takes the values  $\Phi(-\infty) = 0$  and  $\Phi(\infty) = \pi/2$ . Solutions for the small angle deviations (3.24) can now be written as

$$\delta\phi(t) = \int_{-\infty}^t \cos\left[\int_{t'}^t \frac{\Omega(t'')}{2} dt''\right] \frac{d\Phi(t')}{dt'} dt', \quad (3.41a)$$

$$\delta\theta(t) = - \int_{-\infty}^t \sin\left[\int_{t'}^t \frac{\Omega(t'')}{2} dt''\right] \frac{d\Phi(t')}{dt'} dt'. \quad (3.41b)$$

Upon substitution of these equations into Eq. (3.40), and by using the relation

$$|\delta\phi \pm i \delta\theta|^2 = (\delta\phi)^2 + (\delta\theta)^2, \quad (3.42)$$

we find the following closed-form expression for the failure probability

$$p = \left| \int_{-\infty}^{\infty} \exp\left(i \int_t^{\infty} \frac{\Omega(t')}{2} dt'\right) \frac{d\Phi}{dt} dt \right|^2. \quad (3.43)$$

It can be readily seen that integral (3.43) is small enough to explain the large transfer probabilities observed in adiabatic passage processes. As long as the adiabatic conditions are satisfied ( $\Omega\sigma \gg 1$ ), the exponential term in the integrand can oscillate rapidly over the interval of integration, making the integral to take small values. The local adiabaticity criterion also suggests that the nonadiabatic coupling  $d\Phi/dt$  remains small over that interval, contributing with a small value to the integrand. Similarly, we note that the very sharp and profound dips found in the Ch. 2 simulations for some particular choices of the pulses' parameters (see Figs. 2.5 and 2.9) correspond to zeros, or near-zeros of Eq. (3.43).

By making the change of variable

$$\tau(t) = \int_{-\infty}^t \frac{\Omega(t')}{2} dt', \quad (3.44)$$

the probability failure (3.43) can be written in the form

$$p = \left| \int_0^{\tau(\infty)} e^{-i\tau} \frac{d\Phi}{dt} dt \right|^2. \quad (3.45)$$

This expression can be interpreted as the Fourier transform of a function equal to  $d\Phi/d\tau$  between  $\tau = 0$  and  $\tau(\infty)$ , and zero elsewhere. This accounts for the oscillatory character of integral (3.43), and explains the existence of zeros (or near-zeros) for certain values of the parameters.

By way of example, let us consider a simple case for which integral (3.43) can be evaluated analytically. If the pulses are given by the equations

$$\begin{aligned} \Omega_1(t) &= \Omega_0 \sin(t/T), \\ \Omega_2(t) &= \begin{cases} \Omega_0 \cos(t/T) & \text{if } -T\pi/2 \leq t \leq T\pi/2, \\ 0 & \text{elsewhere,} \end{cases} \end{aligned}$$

we may have that

$$\Phi(t) = \frac{t}{T}, \quad \text{and} \quad \Omega(t) = \Omega_0.$$

Plugging these values into Eq. (3.43), we find that

$$p = \left| \lim_{a \rightarrow \infty} \frac{1}{T} \int_{-\infty}^{\infty} e^{-i\Omega_0(t-a)/2} dt \right|^2 = \frac{16 \sin^2(\pi \Omega_0 T/4)}{\Omega_0^2 T^2}.$$

This result reveals a power-law decay of the failure probability in the form  $1/(\Omega_0 T)^2$ , and also shows zeros for this function when  $\Omega_0 T = 4n$ .

Although it is well known that adiabatic passage produces very large transfer efficiencies provided the adiabatic conditions are satisfied, the dependence on  $\Omega T$  of the failure probability is complicated. A “perfect adiabatic transfer” is characterized by a probability failure that decreases exponentially as a function of  $\Omega T$  (this is called the DDP result [DP76]). Recent results have shown that this exponential behavior is no longer satisfied for sufficiently large values of  $\Omega T$ , giving instead a power-law decay of the probability failure with respect to these parameters [LS96, VS96]. In addition to this power-law, oscillations of the failure probability have been also observed coming from a nonadiabatic component of the total transition amplitude [DH98].

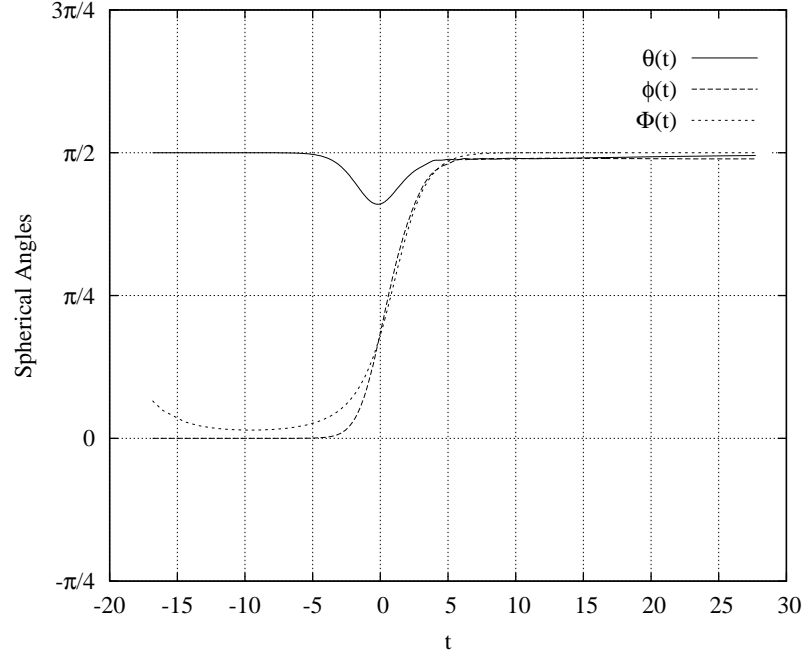
Now, let us explore a bit what happens when the conditions for adiabaticity are not fully satisfied, for example, the case of hyperbolic secant pulses. As before, we want to transfer population from the initial level to the target level by closely following the evolution of the dressed (adiabatic) state

of the system. If the pulses' widths are in such a way that the ratio  $\Omega_1/\Omega_2$  goes to constant values at very early or very late times (see Eq. (3.33b)), the adiabatic conditions are obviously not satisfied by the system. Then an adiabatic following of the dressed state by the state vector is not possible, at least under those *initial* conditions, because these two vectors are not parallel to each other before the interaction with the lasers takes place. In other words, the state vector is parallel to the initially populated level, while the dressed vector is somewhere else (see Fig. 1.3 for a representation of these vectors in the Hilbert space). However, it happens that at some moment during the evolution of the system, the dressed state approaches the initial state and the target state close enough to take sufficient population from the initial level, evolve parallel to the state vector for a moment, leave the population in the target state, and finally continue with its own evolution to some other place in the Hilbert state. Although the system does not evolve in an adiabatic manner, strictly speaking, there is a region in time (not too early, not too late) for which this evolution resembles that of an adiabatic process. In this “near-adiabatic” process, large transfer efficiencies are still achieved.

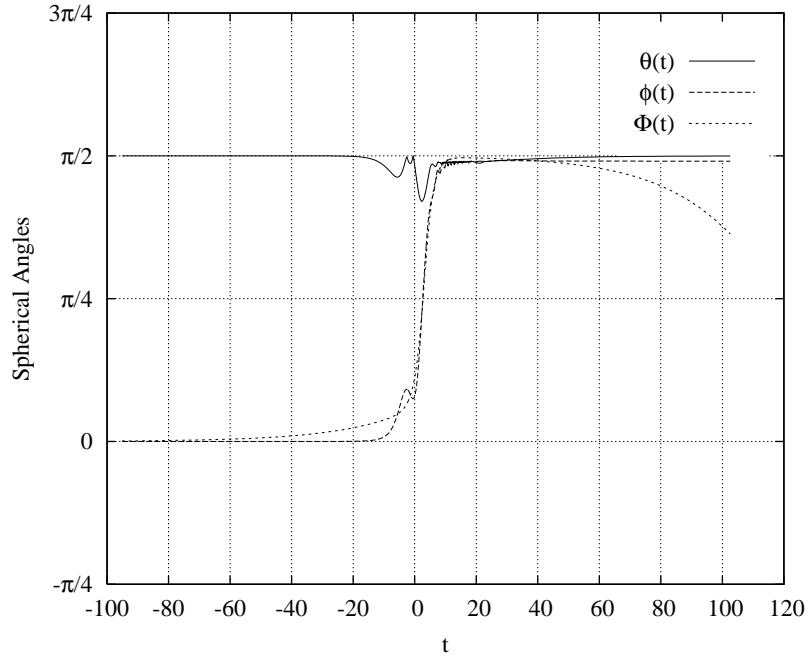
Fig. 3.5 shows the evolution of the system for two particular set of parameters corresponding to Gaussian and Sech pulses. We observe from these figures that the mixing angle is close to zero for a short period of time before the interaction, and nearly  $\pi/2$  for a short period of time after the interaction. When  $t \rightarrow -\infty$ , the dressed state  $|W^0\rangle$  is parallel to the empty bare state  $|b\rangle$  and carries no population. However, the dressed “unstable” states  $|W^+\rangle$  and  $|W^-\rangle$  (see Sec. 1.5) have components along the bare state  $|a\rangle$  (which has the initial entire population) and each one carry half of the total population. These two dressed states also have components along the excited state  $|c\rangle$  which decays radiatively. The adiabatic frame of reference rotates faster than the frequency of the lasers (and perhaps than the decay rate itself) and the coupling classical field  $\Omega(t)$  has not populated enough the decaying level. Then the system is not going to lose too much population at the beginning of the interaction with the cavity-mode  $g$ . By the time in which  $\Omega(t)$  starts to act upon the levels, the adiabatic state  $|W^0\rangle$  is almost parallel to the initial state  $|a\rangle$ . At this point, this adiabatic state will carry mostly the entire population of the initial state (not all of it because the other unstable adiabatic states have already contributed with population to the target state) and the wave vector will follow adiabatically the evolution of this adiabatic state.

Our simple analytical model can also explain the behavior of the system for those near-adiabatic conditions. Since the goal is to have

$$\phi(\infty) = -\frac{\pi}{2}, \quad \text{and} \quad \theta(\infty) = \frac{\pi}{2}, \quad (3.46)$$



(a) Gaussian



(b) Sech

Figure 3.5: Spherical angles. For the Gaussian pulses we have  $\Omega = 2.75$ ,  $\sigma = 3.09$ ,  $g = 1.00$ ,  $\sigma_g = 2.48$ ,  $\Delta t = 5.28$ , and  $\log_{10} p = -2.00$ . For the sech pulses we have  $\Omega = 6.30$ ,  $\sigma = 3.40$ ,  $g = 1.00$ ,  $\sigma_g = 4.01$ ,  $\Delta t = 12.01$ , and  $\log_{10} p = -2.00$ . In both cases the spontaneous emission was  $\Gamma = 0.10$

we see from equations (3.24) that the condition

$$\int_{-\infty}^{\infty} \frac{\Omega(t)}{2} dt = n\pi, \quad \text{with } n \text{ odd} \quad (3.47)$$

must be satisfied. This ensures that the sine in the first term of the  $\delta\theta$  equation cancels out. The second terms of equations (3.24), which are proportional to  $\dot{\Phi}$ , can be ignored for a moment (we will retake these components later on). Therefore  $\delta\phi \simeq -\Phi(-\infty)$ . By plugging this result into Eq. (3.11b), and considering the simple case in which  $\Omega_{10} = \Omega_{20}$ , we may obtain

$$\begin{aligned} \phi(\infty) &\simeq -\Phi(\infty) - \Phi(-\infty) \\ &\simeq -[\Phi(\infty) + \Phi(-\infty)] \\ &\simeq -[\arctan(e^{\Delta t/\sigma}) + \arctan(e^{-\Delta t/\sigma})] \\ &\simeq -\pi/2. \end{aligned} \quad (3.48)$$

Now, we have to examine what happens with the second terms in (3.24). Since those terms are typically small, because of the near-adiabatic condition (that is, they are inversely proportional to  $\Omega\sigma$ ), a small deviation from the parameter values that make the first terms in (3.24) vanish exactly may be enough to, instead, make the first and second terms (nearly) cancel each other, and this is, in fact, what we observe in our numerical calculations.



## Chapter 4

# Transfer of atomic coherence

The concepts of atomic coherence and interference has been extensively studied and applied to many areas of atomic physics and quantum optics for the last fifteen years. Applications of these ideas include electromagnetically induced transparency (EIT), electromagnetically induced absorption (EIA), lasing without inversion (LWI), sensitive spectroscopy in coherent media, among other things [FYL00].

Recent developments in quantum information and quantum computation have stimulated interest in processes that can prepare entangled states, as well as perform conditional quantum dynamics and logic gates. The coherent manipulation of these entangled states are fundamental to realizing a quantum computer, and promises a novel atomic spectroscopy with resolution better than the standard quantum limit [PGCZ95].

In this chapter we present a numerical analysis of the Zeeman coherence transfer between two atoms by using adiabatic passage methods. We also present a simplified model for the two-atom + cavity system that help us to better understand the process of coherence transfer between two atoms coupled with a cavity.

### 4.1 The two-atom + cavity system

We consider a system consisting of a single-mode cavity containing two three-level atoms in the  $\Lambda$  configuration, as shown in Fig. 4.1. The atoms are fixed inside the cavity at distances apart much larger than the wavelength of the cavity mode and interacting individually with laser beams. The transitions  $|a\rangle_j \rightarrow |c\rangle_j$  of both atoms ( $j = 1, 2$ ) are coupled to separate classical coherent driving fields with frequency  $\omega_L$  and Rabi frequencies  $\Omega_j$ . The transitions  $|b\rangle_j \rightarrow |c\rangle_j$  are strongly coupled

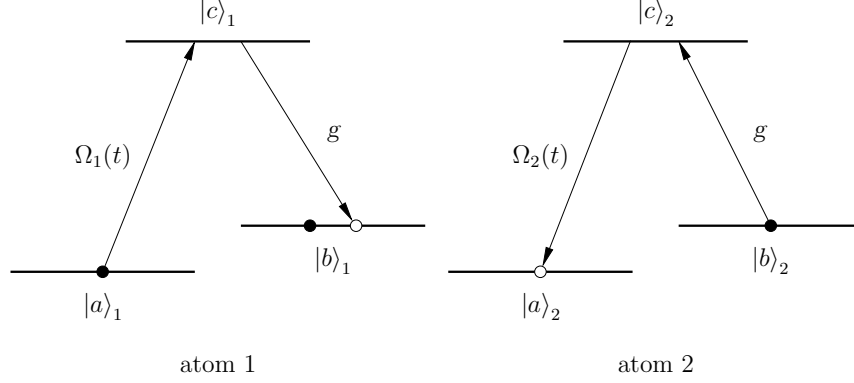


Figure 4.1: Transfer of atomic coherence between two  $\Lambda$  systems.

to the *same* quantized cavity-mode field with coupling strength  $g$  and frequency  $\omega$ . The dynamics of this system is described by the interaction Hamiltonian:

$$H_I = \frac{\hbar}{2} \sum_{j=1,2} [\Omega_j(t) e^{-i\omega_L t} |c\rangle_{jj} \langle a| + g |c\rangle_{jj} \langle b| a] + \text{H.c.}, \quad (4.1)$$

where  $a$  is the annihilation operator for the cavity mode and  $g$  gives the coupling strength between the atoms and the field mode (vacuum Rabi-frequency).

#### 4.1.1 Probability amplitude method

We are interested in transferring the atomic coherence according to

$$(A|a\rangle_1 + B|b\rangle_1) |b\rangle_2 |0\rangle_c \longrightarrow |b\rangle_1 (A|a\rangle_2 + B|b\rangle_2) |0\rangle_c, \quad (4.2)$$

where  $A$  and  $B$  are arbitrary coefficients. If we consider the particular case in which the system evolves without populating the dark state  $|b\rangle_1 |b\rangle_2 |0\rangle_c$  (that is, for  $B = 0$ ) then the evolution of the quantum system takes place as follows:

$$\begin{array}{ccc} |a\rangle_1 |b\rangle_2 |0\rangle_c & & |b\rangle_1 |a\rangle_2 |0\rangle_c \\ \downarrow \Omega_1(t) & & \uparrow \Omega_2(t) \\ |c\rangle_1 |b\rangle_2 |0\rangle_c & \xrightarrow{g} & |b\rangle_1 |b\rangle_2 |1\rangle_c \xrightarrow{g} |b\rangle_1 |c\rangle_2 |0\rangle_c \end{array} \quad (4.3)$$

The state vector of the system can be constructed as a linear superposition of these *basis* eigenvectors in the form

$$\begin{aligned} |\Psi(t)\rangle = & C_{ab}(t) |a b 0\rangle + C_{cb}(t) |c b 0\rangle + C_{bb}(t) |b b 1\rangle \\ & + C_{bc}(t) |b c 0\rangle + C_{ba}(t) |b a 0\rangle, \end{aligned} \quad (4.4)$$

with the probability amplitudes given by

$$\begin{aligned} C_{ab}(t) = \langle a b 0 | \Psi(t) \rangle, \quad C_{cb}(t) = \langle c b 0 | \Psi(t) \rangle, \quad C_{bb}(t) = \langle b b 1 | \Psi(t) \rangle, \\ C_{bc}(t) = \langle b c 0 | \Psi(t) \rangle, \quad C_{ba}(t) = \langle b a 0 | \Psi(t) \rangle. \end{aligned} \quad (4.5)$$

The corresponding time-dependent Schrödinger equation is

$$i\hbar|\dot{\Psi}(t)\rangle = H_I|\Psi(t)\rangle, \quad (4.6)$$

with

$$\begin{aligned} H_I = & \frac{\Omega_1(t)}{2} |c\rangle_{11}\langle a| + \frac{g}{2} |c\rangle_{11}\langle b|a + \frac{\Omega_2(t)}{2} |c\rangle_{22}\langle a| + \frac{g}{2} |c\rangle_{22}\langle b|a \\ & + \frac{\Omega_1^*(t)}{2} |a\rangle_{11}\langle c| + \frac{g^*}{2} a^\dagger |b\rangle_{11}\langle c| + \frac{\Omega_2^*(t)}{2} |a\rangle_{22}\langle c| + \frac{g^*}{2} a^\dagger |b\rangle_{22}\langle c|. \end{aligned} \quad (4.7)$$

By introducing Eqs. (4.4) and (4.7) into Eq. (4.6), and multiplying the resulting equation by every bra vector of the basis (4.3), we find that

$$\dot{C}_{ab} = -\frac{\Omega_1^*(t)}{2} \tilde{C}_{cb}, \quad (4.8a)$$

$$\dot{\tilde{C}}_{cb} = -\frac{\Gamma}{2} \tilde{C}_{cb} + \frac{\Omega_1(t)}{2} C_{ab} + \frac{g}{2} C_{bb}, \quad (4.8b)$$

$$\dot{C}_{bb} = -\frac{g^*}{2} (\tilde{C}_{cb} + \tilde{C}_{bc}), \quad (4.8c)$$

$$\dot{\tilde{C}}_{bc} = -\frac{\Gamma}{2} \tilde{C}_{bc} + \frac{\Omega_2(t)}{2} C_{ba} + \frac{g}{2} C_{bb}, \quad (4.8d)$$

$$\dot{C}_{ba} = -\frac{\Omega_2^*(t)}{2} \tilde{C}_{bc}. \quad (4.8e)$$

These are the equations of motion for the probability amplitudes of the two-atom + cavity system. Here we have considered the spontaneous emission of the excited levels by adding phenomenological decay terms  $\Gamma$  to the equations. We have also avoided the complex character resulting in some of

the equations by introducing the notation

$$\tilde{C}_{bc} = i C_{bc} \quad \text{and} \quad \dot{\tilde{C}}_{bc} = i \dot{C}_{bc}. \quad (4.9)$$

#### 4.1.2 Dark state

Under two-photon resonance condition, and by using the rotating-wave approximation, the evolution of system (4.8) is governed by the non-Hermitian Hamiltonian

$$H' = \frac{\hbar}{2} \begin{bmatrix} 0 & -\Omega_1^* & 0 & 0 & 0 \\ \Omega_1 & -\Gamma & g & 0 & 0 \\ 0 & -g^* & 0 & -g^* & 0 \\ 0 & 0 & g & -\Gamma & \Omega_2 \\ 0 & 0 & 0 & -\Omega_2^* & 0 \end{bmatrix}. \quad (4.10)$$

This operator has a *dark* state with eigenvalue zero given by

$$|D\rangle = \frac{\Omega_2 g |a b 0\rangle - \Omega_1 \Omega_2 |b b 1\rangle + \Omega_1 g |b a 0\rangle}{\sqrt{\Omega_0^2 g^2 + \Omega_1^2 \Omega_2^2}}, \quad (4.11)$$

where  $\Omega_0 = \sqrt{\Omega_1^2 + \Omega_2^2}$ .

We observe that states of the type given by Eq. (4.11) are immune against decay from the excited atomic levels, since they have no contribution of such states. Therefore, the dark state  $|D\rangle$  becomes the right mechanism to transfer, from one atom to the other, the Zeeman coherence of the ground state levels by using adiabatic passage [PGCZ95].

#### 4.1.3 Conditions for adiabatic following

If the pulses are applied in a counterintuitive sequence, that is the pulse on atom 2 preceding the pulse on atom 1, an adiabatic transfer of the dark state between the atomic levels  $|a b 0\rangle$  and  $|b a 0\rangle$  may be achieved. To see clearly how this happens, let define the mixing angle  $\Phi$  by the relationship

$$\tan \Phi(t) = \frac{\Omega_1(t)}{\Omega_2(t)}, \quad (4.12)$$

and express the dark state (4.11) in the form

$$|D\rangle = K \left[ \cos \Phi |a b 0\rangle - \frac{\Omega_0}{g} \sin \Phi \cos \Phi |b b 1\rangle + \sin \Phi |b a 0\rangle \right], \quad (4.13)$$

where  $K = \Omega_0 g / \sqrt{\Omega_0^2 g^2 + \Omega_1^2 \Omega_2^2}$ . At very early times, just before the interaction with the pulses, the condition  $\Omega_1/\Omega_2 \rightarrow 0$  is satisfied, and the dark state  $|D\rangle \rightarrow |a b 0\rangle$ , as  $\Phi(-\infty) \rightarrow 0$  and  $K \rightarrow 1$ . Then, at very late times, the pulses satisfy the condition  $\Omega_2/\Omega_1 \rightarrow 0$ , and the dark state  $|D\rangle \rightarrow |b a 0\rangle$ , as  $\Phi(+\infty) \rightarrow \pi/2$  and  $K \rightarrow 1$ .

It is important to note that the strength  $g$  of the quantized cavity mode (which is assumed to be constant for simplicity) plays an important role here. If the condition  $g \gg \Omega_0$  is satisfied, then  $K \rightarrow 1$  for all times, and the intermediate level  $|b b 1\rangle$  is never populated ( $\Omega_0/g \rightarrow 0$ ). This reduces the probability of finding a photon roaming inside the cavity, decreasing the chances for cavity decay. In addition, if the conditions for adiabatic evolution are fulfilled [TRK92, MYM94], that is

$$gT, \Omega_0 T \gg 1 \quad \text{and} \quad g\Omega_0 \gg \Gamma, \kappa, \quad (4.14)$$

with  $T$  the laser pulse duration,  $\Gamma$  the radiative decay, and  $\kappa$  the cavity decay; then the state vector of the system  $|\Psi(t)\rangle$  may evolve adiabatically, following closely the dark state  $|D\rangle$ .

#### 4.1.4 Density matrix and equations of motion

For a realistic description of the two-atom + cavity system, in which dissipative channels are accounted for, we must employ a master equation description. The time evolution of the system is described by the following Liouville equation:

$$\dot{\rho} = -i[H_{\text{eff}}\rho - \rho H_{\text{eff}}^\dagger] + \sum_{j=1}^2 J_{\Gamma_j}\rho + J_\kappa\rho, \quad (4.15)$$

where, in the interaction picture and on resonance

$$H_{\text{eff}} = -i\kappa a^\dagger a - i\frac{\Gamma}{2} \sum_{j=1}^2 |c\rangle_{jj}\langle c| + \sum_{j=1}^2 \left( \frac{\Omega_j(t)}{2} |c\rangle_{jj}\langle a| + \frac{g}{2} |c\rangle_{jj}\langle b|a + \text{H.c.} \right) \quad (4.16)$$

is a non-Hermitian Hamiltonian including decay terms from spontaneous emission and cavity decay. The superoperator  $J_{\Gamma_j}$  describes the return of the electron to the atomic ground states after a spontaneous emission, and  $J_\kappa$  the corresponding term for the cavity decay [PGCZ95].

The decay  $\Gamma$  terms can be obtained by doing a simple analysis of the spontaneous emission rates of the excited levels. For example, the initially populated state  $|a b 0\rangle \equiv |a\rangle_1 |b\rangle_2 |0\rangle_c$  can only have contributions from the radiative decay of states  $|c b 0\rangle$  and  $|a c 0\rangle$ . However, the state  $|c b 0\rangle$  is the only level which really contributes to the decay, since the state  $|a c 0\rangle$  never happens in this scheme.

In addition, this state can also spontaneously emit to other two different states: the state  $|b b 1\rangle$  and some other arbitrary state which is not taken into account in our system evolution. Therefore, the contribution made by state  $|c b 0\rangle$  is  $\Gamma/3$ . A similar analysis applies to the other possibilities.

By constructing a density operator with the elements of basis (4.3), plugging it into Eq. (4.15), and left- and right-multiplying the resulting equation by the elements of the basis, we find

Diagonal matrix elements:

$$\dot{\rho}_{abab} = \frac{\Omega_1(t)}{2}(\tilde{\rho}_{abcb} - \tilde{\rho}_{cbab}) + \frac{\Gamma}{3}\rho_{cbcb}, \quad (4.17a)$$

$$\dot{\rho}_{cbcb} = \frac{\Omega_1(t)}{2}(\tilde{\rho}_{cbab} - \tilde{\rho}_{abcb}) + \frac{g}{2}(\tilde{\rho}_{cbbb} - \tilde{\rho}_{bbcb}) - \Gamma\rho_{cbcb}, \quad (4.17b)$$

$$\dot{\rho}_{bbbb} = \frac{g}{2}(\tilde{\rho}_{bbcb} + \tilde{\rho}_{bbbc} - \tilde{\rho}_{cbbb} - \tilde{\rho}_{bcbb}) + \frac{\Gamma}{3}(\rho_{cbcb} + \rho_{bcbc}), \quad (4.17c)$$

$$\dot{\rho}_{bcbc} = \frac{\Omega_2(t)}{2}(\tilde{\rho}_{bcba} - \tilde{\rho}_{babc}) + \frac{g}{2}(\tilde{\rho}_{bcbb} - \tilde{\rho}_{bbbc}) - \Gamma\rho_{bcbc}, \quad (4.17d)$$

$$\dot{\rho}_{baba} = \frac{\Omega_2(t)}{2}(\tilde{\rho}_{babc} - \tilde{\rho}_{bcba}) + \frac{\Gamma}{3}\rho_{bcbc}, \quad (4.17e)$$

Off-diagonal matrix elements:

$$\dot{\tilde{\rho}}_{abcb} = \frac{\Omega_1(t)}{2}(\rho_{cbcb} - \rho_{abab}) - \frac{g}{2}\rho_{abbb} - \frac{\Gamma}{2}\tilde{\rho}_{abcb}, \quad (4.17f)$$

$$\dot{\rho}_{abbb} = -\frac{\Omega_1(t)}{2}\tilde{\rho}_{cbbb} + \frac{g}{2}(\tilde{\rho}_{abcb} + \tilde{\rho}_{abbc}), \quad (4.17g)$$

$$\dot{\tilde{\rho}}_{abbc} = \frac{\Omega_1(t)}{2}\rho_{cbbc} - \frac{\Omega_2(t)}{2}\rho_{abba} - \frac{g}{2}\rho_{abbb} - \frac{\Gamma}{2}\tilde{\rho}_{abbc}, \quad (4.17h)$$

$$\dot{\rho}_{abba} = -\frac{\Omega_1(t)}{2}\tilde{\rho}_{cbba} + \frac{\Omega_2(t)}{2}\tilde{\rho}_{abbc}, \quad (4.17i)$$

$$\dot{\tilde{\rho}}_{cbab} = \frac{\Omega_1(t)}{2}(\rho_{abab} - \rho_{cbcb}) + \frac{g}{2}\rho_{bbab} - \frac{\Gamma}{2}\tilde{\rho}_{cbab}, \quad (4.17j)$$

$$\dot{\tilde{\rho}}_{cbbb} = \frac{\Omega_1(t)}{2}\rho_{abbb} + \frac{g}{2}(\rho_{bbbb} - \rho_{cbcb} - \rho_{cbbc}) - \frac{\Gamma}{2}\tilde{\rho}_{cbbb}, \quad (4.17k)$$

$$\dot{\rho}_{cbbc} = -\frac{\Omega_1(t)}{2}\tilde{\rho}_{abbc} + \frac{\Omega_2(t)}{2}\tilde{\rho}_{cbba} + \frac{g}{2}(\tilde{\rho}_{cbbb} - \rho_{bbbc}) - \Gamma\rho_{cbbc}, \quad (4.17l)$$

$$\dot{\tilde{\rho}}_{cbba} = \frac{\Omega_1(t)}{2}\rho_{abba} - \frac{\Omega_2(t)}{2}\rho_{cbbc} + \frac{g}{2}\rho_{bbba} - \frac{\Gamma}{2}\tilde{\rho}_{cbba}, \quad (4.17m)$$

$$\dot{\rho}_{bbab} = \frac{\Omega_1(t)}{2}\rho_{bbcb} - \frac{g}{2}(\tilde{\rho}_{cbab} + \tilde{\rho}_{bcab}), \quad (4.17n)$$

$$\dot{\tilde{\rho}}_{bbcb} = -\frac{\Omega_1(t)}{2}\rho_{bbab} + \frac{g}{2}(\rho_{cbcb} + \rho_{bccb} - \rho_{bbbb}) - \frac{\Gamma}{2}\tilde{\rho}_{bbcb}, \quad (4.17o)$$

$$\dot{\tilde{\rho}}_{bbbc} = -\frac{\Omega_2(t)}{2}\rho_{bbba} + \frac{g}{2}(\rho_{cbbc} + \rho_{bcbc} - \rho_{bbbb}) - \frac{\Gamma}{2}\tilde{\rho}_{bbbc}, \quad (4.17p)$$

$$\dot{\rho}_{bbba} = \frac{\Omega_2(t)}{2}\tilde{\rho}_{bbbc} - \frac{g}{2}(\tilde{\rho}_{cbba} + \tilde{\rho}_{bcba}), \quad (4.17q)$$

$$\dot{\tilde{\rho}}_{bcab} = -\frac{\Omega_1(t)}{2} \rho_{bccb} + \frac{\Omega_2(t)}{2} \rho_{baab} + \frac{g}{2} \rho_{bbab} - \frac{\Gamma}{2} \tilde{\rho}_{bcab}, \quad (4.17r)$$

$$\dot{\rho}_{bccb} = \frac{\Omega_1(t)}{2} \tilde{\rho}_{bcab} - \frac{\Omega_2(t)}{2} \tilde{\rho}_{bacb} + \frac{g}{2} (\tilde{\rho}_{bccb} - \tilde{\rho}_{bbcb}) - \Gamma \rho_{bccb}, \quad (4.17s)$$

$$\dot{\tilde{\rho}}_{bccb} = \frac{\Omega_2(t)}{2} \rho_{babb} + \frac{g}{2} (\rho_{bbbb} - \rho_{bccb} - \rho_{bcbc}) - \frac{\Gamma}{2} \tilde{\rho}_{bccb}, \quad (4.17t)$$

$$\dot{\tilde{\rho}}_{bcb a} = \frac{\Omega_2(t)}{2} (\rho_{baba} - \rho_{bcbc}) + \frac{g}{2} \rho_{bbba} - \frac{\Gamma}{2} \tilde{\rho}_{bcb a}, \quad (4.17u)$$

$$\dot{\rho}_{baab} = \frac{\Omega_1(t)}{2} \tilde{\rho}_{bacb} - \frac{\Omega_2(t)}{2} \tilde{\rho}_{bcab}, \quad (4.17v)$$

$$\dot{\tilde{\rho}}_{bacb} = -\frac{\Omega_1(t)}{2} \rho_{baab} + \frac{\Omega_2(t)}{2} \rho_{bccb} - \frac{g}{2} \rho_{babb} - \frac{\Gamma}{2} \tilde{\rho}_{bacb}, \quad (4.17w)$$

$$\dot{\rho}_{babb} = -\frac{\Omega_2(t)}{2} \tilde{\rho}_{bccb} + \frac{g}{2} (\tilde{\rho}_{bacb} + \tilde{\rho}_{babc}), \quad (4.17x)$$

$$\dot{\tilde{\rho}}_{babc} = \frac{\Omega_2(t)}{2} (\rho_{bcbc} - \rho_{baba}) - \frac{g}{2} \rho_{babb} - \frac{\Gamma}{2} \tilde{\rho}_{babc}. \quad (4.17y)$$

These are the density matrix equations of motion of the two-atom + cavity system, where  $\rho_{pqrs} \equiv \langle p|q\rangle\langle r|s\rangle$ . As before, we have avoided the complex nature of some of these equations by introducing the notation

$$\tilde{\rho}_{pqrs} = i\rho_{pqrs}, \quad \dot{\tilde{\rho}}_{pqrs} = i\dot{\rho}_{pqrs}. \quad (4.18)$$

## 4.2 Numerical results

This section presents numerical results obtained by integration of the system of differential equations (4.17) using the Runge-Kutta method. Basically, we studied the adiabatic passage method for transferring interatomic coherence, when Gaussian and Sech pulses were used to drive a two-atom + cavity system. For simplicity, we considered a high- $Q$  cavity with constant coupling strength  $g$ , and no cavity decay ( $\kappa = 0$ ). For this problem, six different parameters were considered in our simulations: the Rabi frequency and the width of the pulses, the time delay, the coupling strength of the cavity mode, and the spontaneous emission of the excited states.

Numerical results corresponding to different values of the Rabi frequency, the pulse width, the coupling constant, and the time delay are shown in Table 4.1.

Table 4.1: Transfer of coherence. Adiabatic passage

Pulse profile	$\Gamma$	$\Omega_{10}$	$\sigma_1$	$\Omega_{20}$	$\sigma_2$	$g$	$\Delta t$	$\log_{10} p$
Gaussian	0.00	2.60	10.00	1.00	1.00	1.00	6.50	-0.68

Table 4.1: Transfer of coherence. Adiabatic passage

		14.40	10.10	1.00	4.00	1.00	25.29	-1.54
		0.70	7.00	1.00	2.00	2.00	3.48	-2.19
	0.01	1.10	4.50	1.00	1.00	1.00	0.00	-0.61
		15.00	10.20	1.00	4.00	1.00	25.70	-1.40
		14.80	13.60	1.00	7.00	1.00	36.10	-2.13
	0.10	2.50	7.30	1.00	4.00	2.00	11.69	-1.09
		2.00	6.80	1.00	4.00	4.00	9.80	-1.10
		1.90	6.70	1.00	4.00	6.00	9.40	-1.10
		25.00	30.00	1.00	30.00	1.00	80.50	-1.76
Sech	0.00	0.90	2.30	1.00	2.00	1.00	0.00	-1.14
		3.80	4.40	1.00	5.00	1.00	11.51	-3.71
	0.01	3.80	4.40	1.00	5.00	1.00	11.48	-2.06
	0.02	5.20	4.10	1.00	5.00	2.00	11.00	-1.85
		6.90	4.10	1.00	5.00	3.00	11.80	-1.85

As in Ch. 2, we were looking for values of the failure probability of  $\log_{10} p = -2.00$  or better. During the simulations we fixed the value of  $\Omega_{20}$  to unity. In this way, we could compare the pulses' energies (Rabi frequencies) and widths for the different failure probabilities obtained, and then to conclude for which set of parameters we achieved the maximum transfer efficiency. The other parameters of the system were allowed to take values from physically reasonable intervals. For example, we studied widths in the interval  $[0, 10]$  most of the time, going a little bit further in some special cases. We also explored time delays in intervals between  $[0, 50]$  for Gaussian pulses, and  $[0, 100]$  for Sech and Lorentzian pulses.

We first studied the case of no spontaneous emission. We observed from Fig. 4.2 that this time there are no sharp dips, but instead we found a long and profound valley consisting of very



good transfer of efficiency parameters. It is interesting to note that for Gaussian pulses and no spontaneous emission, a good transfer efficiency was achieved for a small value of the pulse amplitude compared with its width (see Table 4.1). Fig. 4.3 shows again that Sech pulses are very efficient when there is no spontaneous emission. However, bigger pulse amplitudes and longer time delays were required, making them less efficient than Gaussians. We tried to extrapolate numerically the apparent *exponential* behavior of these valleys formed by the maximum probability surface, but the results we obtained showed no easy connections with the parameters of the system.

We did not consider Lorentzian pulses in this analysis because they were very computationally demanding.

For spontaneous emission values of  $\Gamma = 0.01$  and  $0.02$ , Figs. 4.4, 4.5, and 4.6 showed that Sech pulses performed this time better than Gaussian pulses. This was also checked by comparison with the ratio of the pulses and the interaction times. This time, the valleys were shallower than those for no decay.

It is very important to note that bigger values of the coupling strength  $g$  increased the coherence transfer efficiency for no spontaneous emission. However, when the system underwent radiative decay, an increment in the magnitude of the cavity mode showed no effect in the failure probability. Instead, if the width of the pulses was increased, so was the transfer efficiency.

In the case of Gaussian pulses, for bigger values of the spontaneous emission, we needed really big values of the pulse amplitudes and time delays to get a good transfer efficiency. However, we still did not reach the minimum value of the failure probability we were looking for, as shown in Table 4.1.

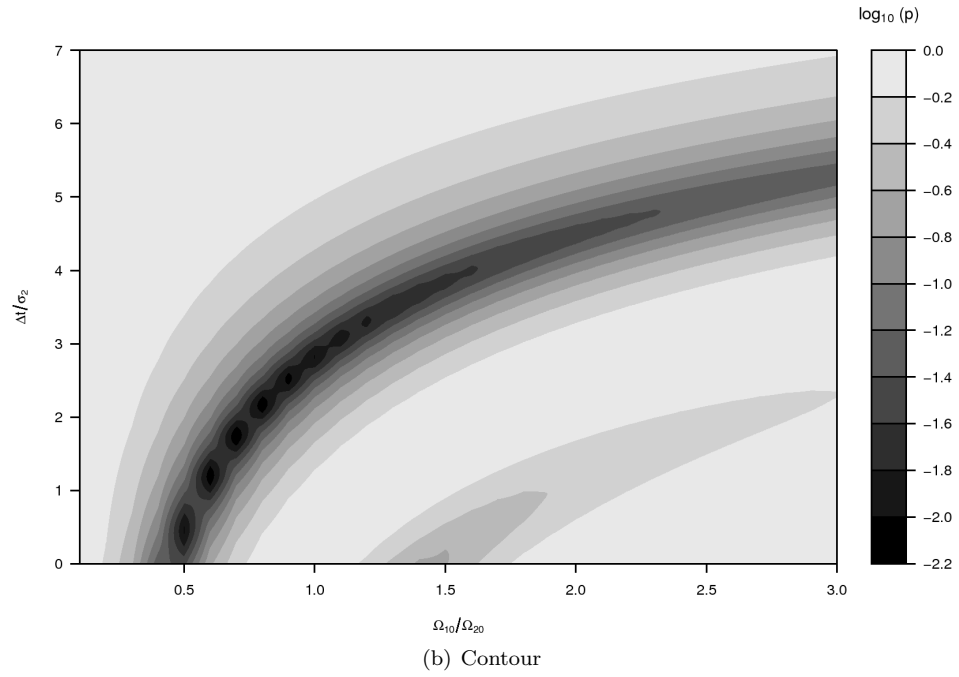
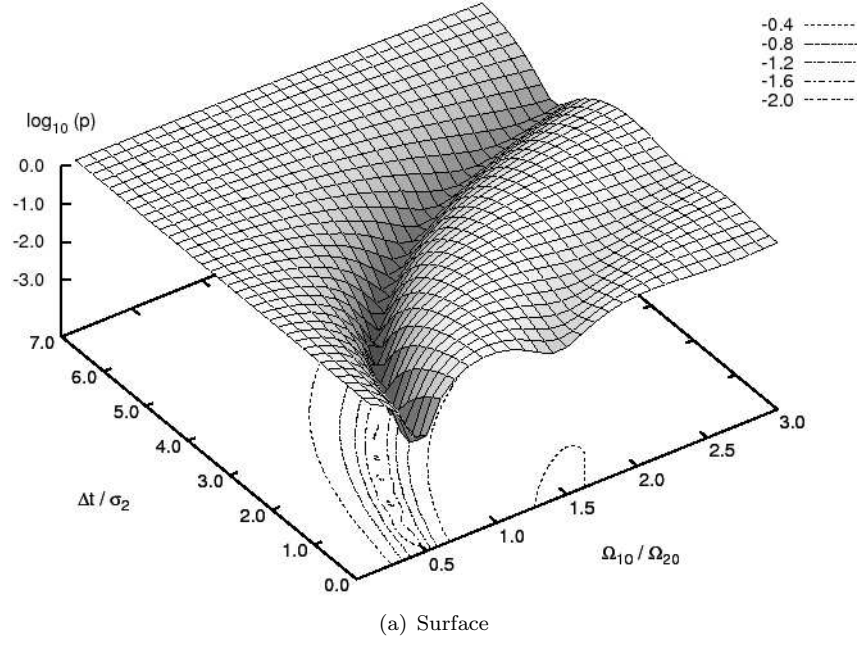


Figure 4.2: Gaussian surface and contour for  $\Gamma = 0.00$ . Here we have  $\Omega_{10} = 0.70$ ,  $\sigma_1 = 7.00$ ,  $\Omega_{20} = 1.00$ ,  $\sigma_2 = 2.00$ ,  $g = 2.00$ ,  $\Delta t = 3.48$ , and  $\log_{10} p = -2.19$ .

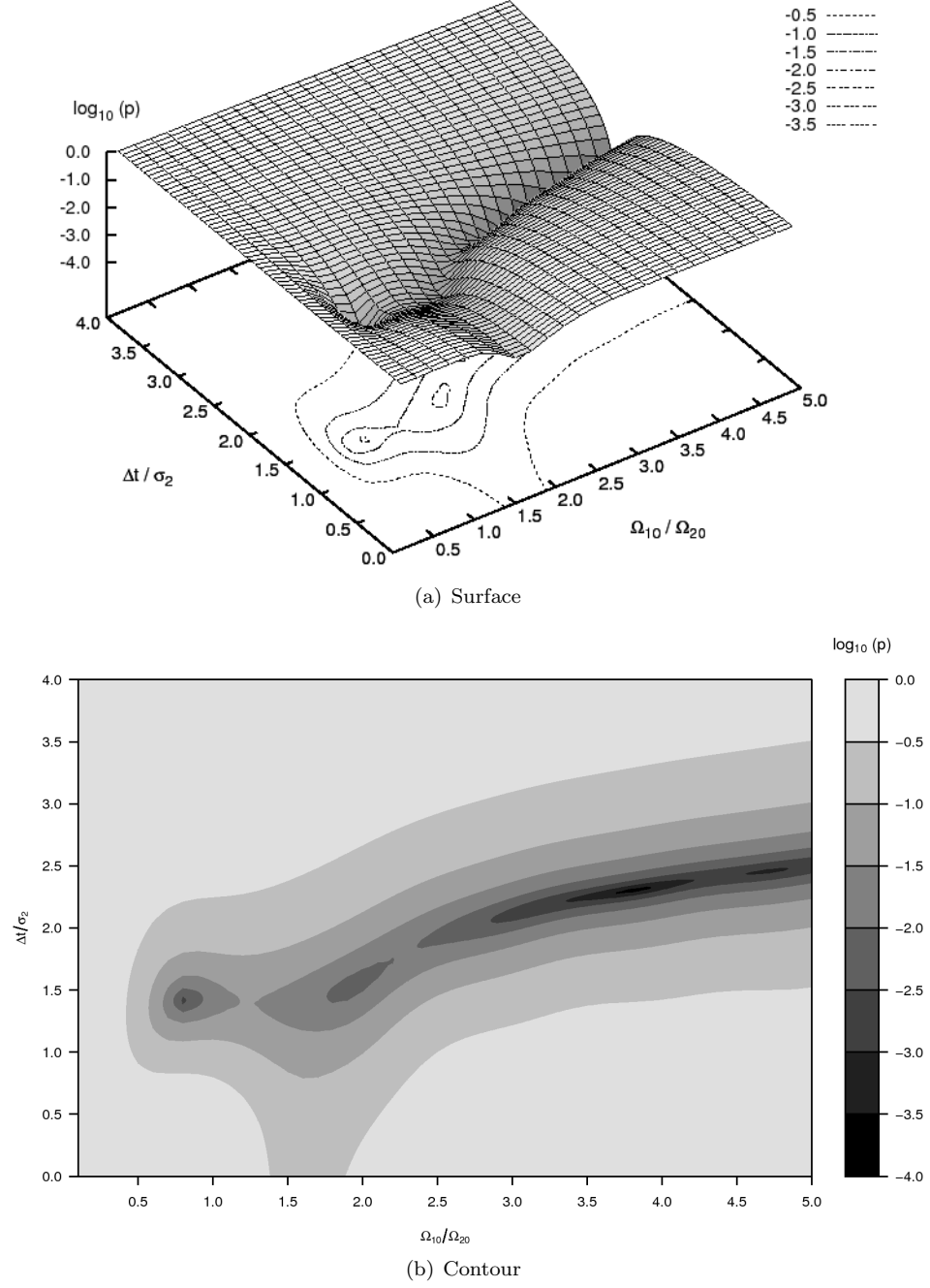


Figure 4.3: Sech surface and contour for  $\Gamma = 0.00$ . Here we have  $\Omega_{10} = 3.80$ ,  $\sigma_1 = 4.40$ ,  $\Omega_{20} = 1.00$ ,  $\sigma_2 = 5.00$ ,  $g = 1.00$ ,  $\Delta t = 11.51$ , and  $\log_{10} p = -3.71$ .

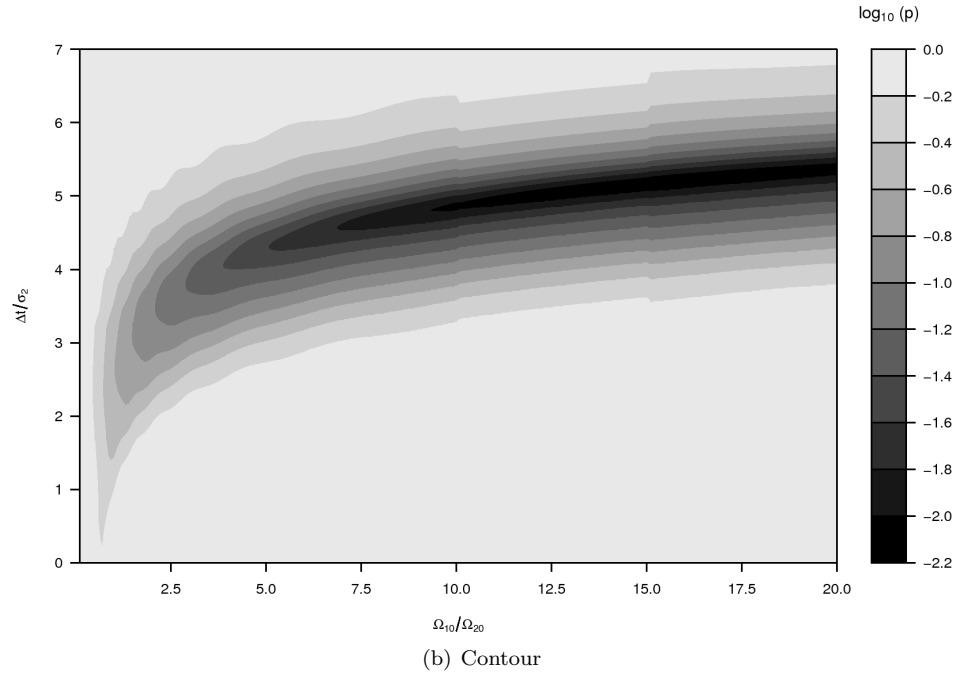
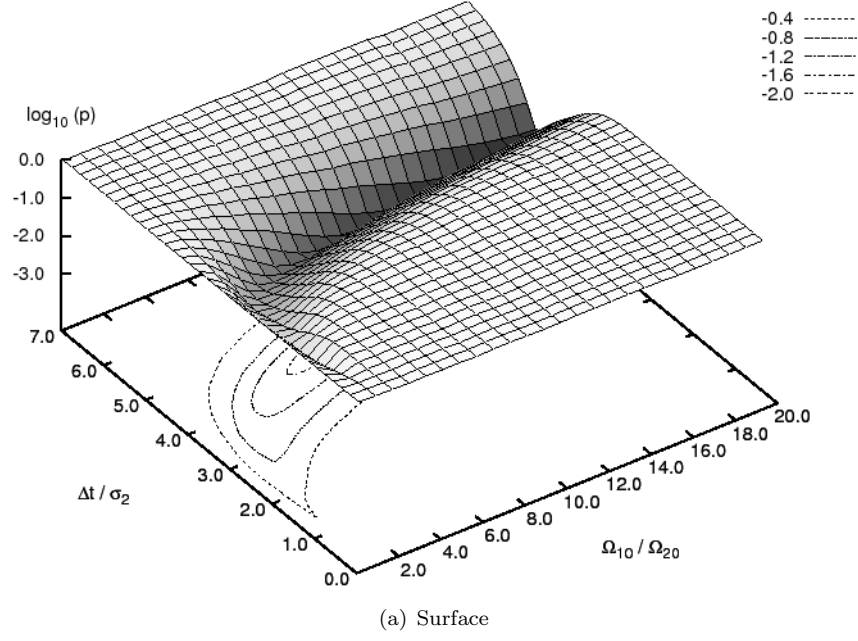


Figure 4.4: Gaussian surface and contour for  $\Gamma = 0.01$ . Here we have  $\Omega_{10} = 15.10$ ,  $\sigma_1 = 13.60$ ,  $\Omega_{20} = 1.00$ ,  $\sigma_2 = 7.00$ ,  $g = 1.00$ ,  $\Delta t = 36.20$ , and  $\log_{10} p = -2.14$ .

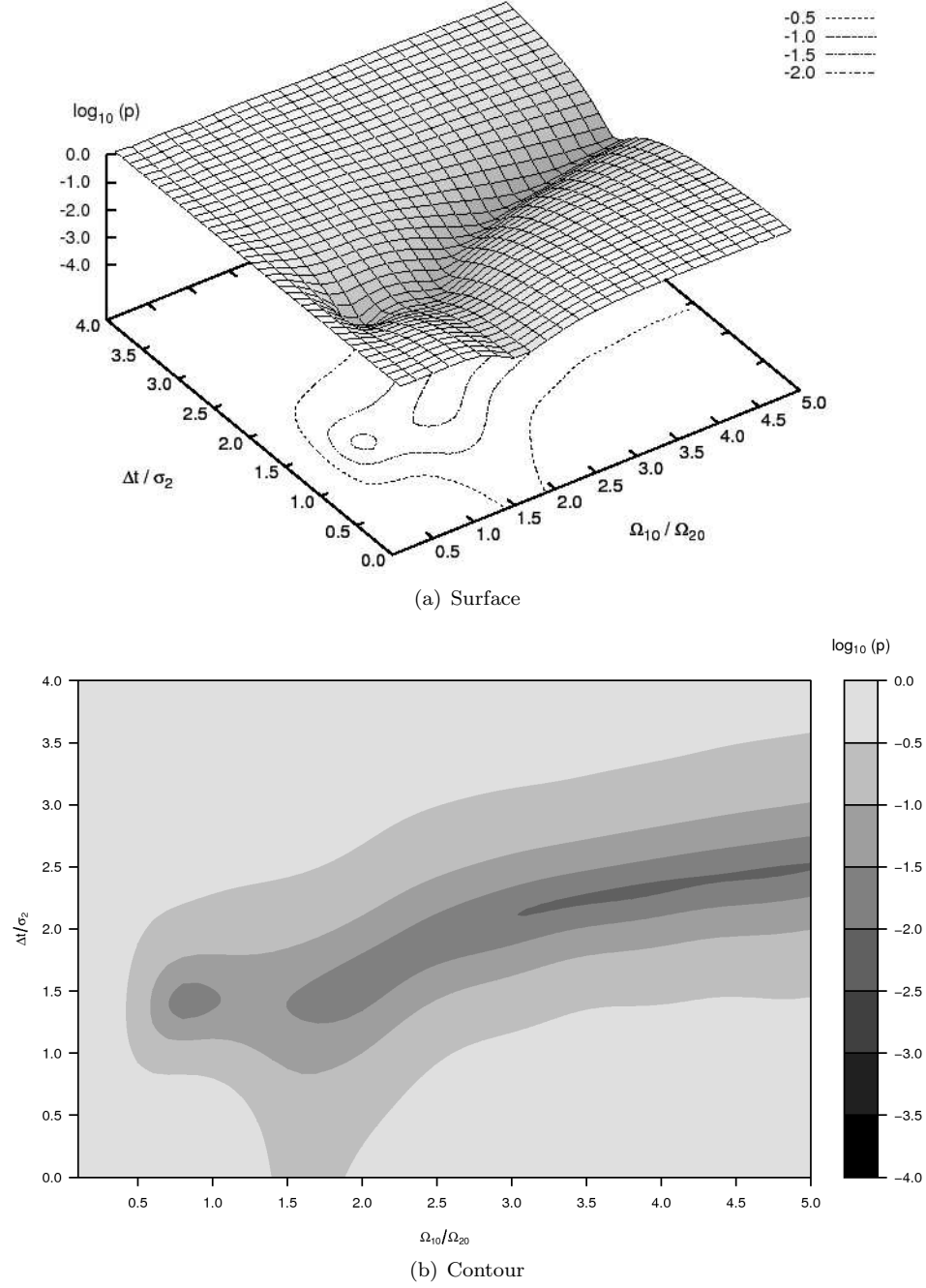


Figure 4.5: Sech surface and contour for  $\Gamma = 0.01$ . Here we have  $\Omega_{10} = 3.80$ ,  $\sigma_1 = 4.40$ ,  $\Omega_{20} = 1.00$ ,  $\sigma_2 = 5.00$ ,  $g = 1.00$ ,  $\Delta t = 11.48$ , and  $\log_{10} p = -2.06$ .

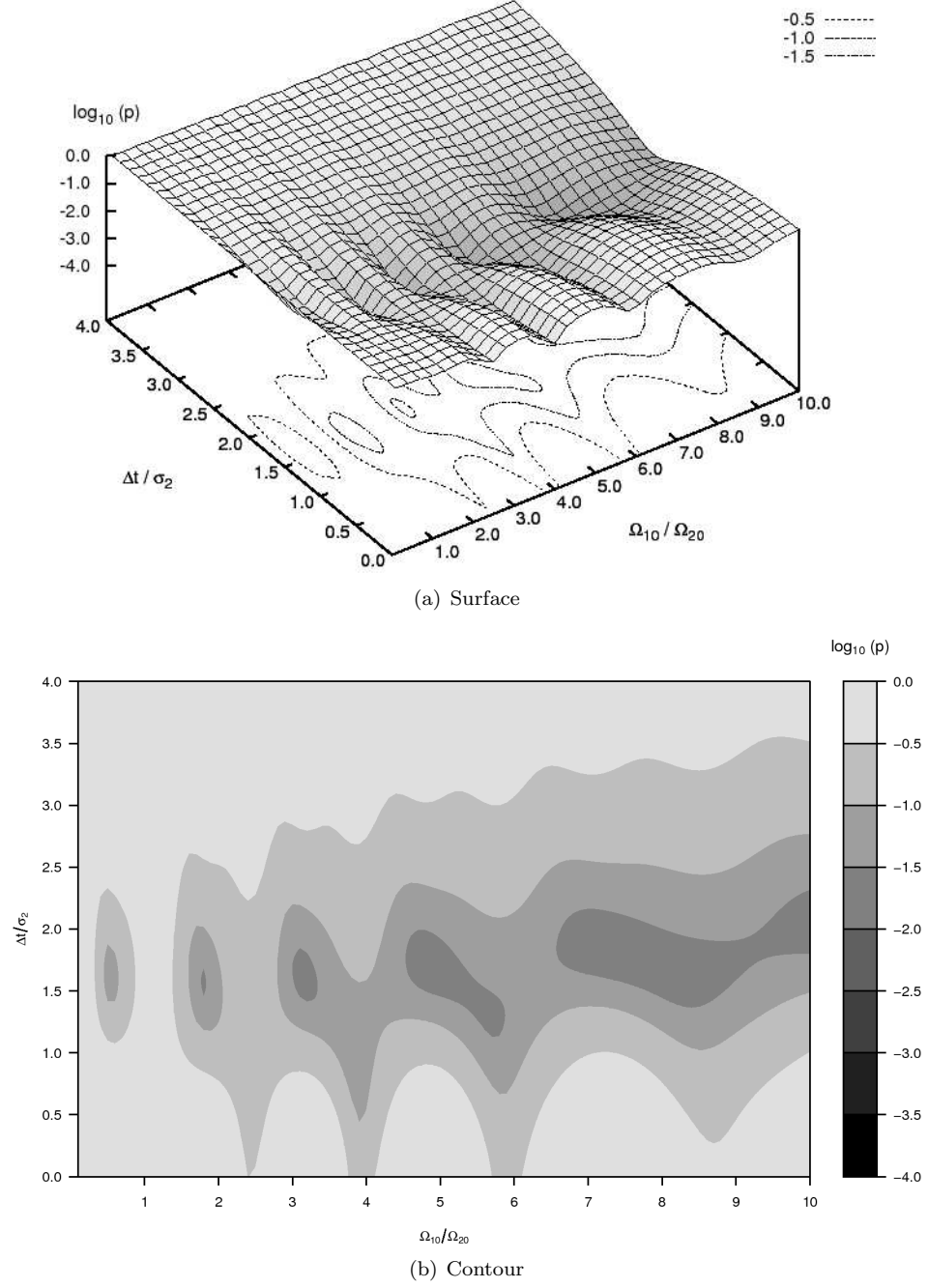


Figure 4.6: Sech surface and contour for  $\Gamma = 0.02$ . Here we have  $\Omega_{10} = 7.30$ ,  $\sigma_1 = 5.00$ ,  $\Omega_{20} = 1.00$ ,  $\sigma_2 = 8.00$ ,  $g = 3.00$ ,  $\Delta t = 14.70$ , and  $\log_{10} p = -1.96$ .

### 4.3 An alternative model

Consider for simplicity the case in which the two Rabi-frequencies are the same, that is  $\Omega_1(t) = \Omega_2(t) = \Omega(t)$ . We assume that the interatomic distance is much less than the wavelength of the coherent classical fields, so that the intracavity registration of a photon cannot be used to identify which atom is the source of this radiation. The system now has *some* kind of symmetry and can be considered as one consisting of two *identical* particles interacting with a laser field with Rabi-frequency  $\Omega(t)$  and a quantized cavity mode with coupling strength  $g$ . The situation is illustrated in Fig. 4.7.

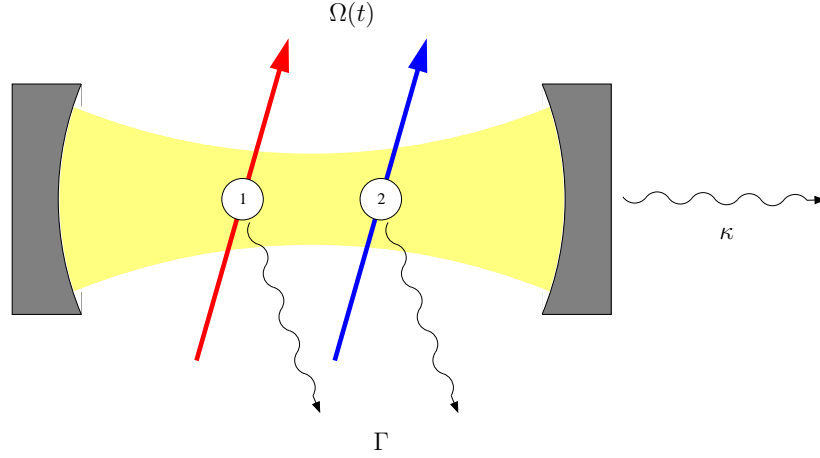


Figure 4.7: Schematic representation of two qubits interacting with a classical coherent field  $\Omega(t)$  and a microcavity mode. The qubits and the cavity can decay with rates  $\Gamma$  and  $\kappa$ , respectively.

It is interesting to observe that in view of the symmetry of the couplings, the dynamics of the two-atom + cavity system can be examined as the evolution of two different systems (one symmetric and the other antisymmetric) interacting individually with the classical coherent field and the quantum cavity mode, but reciprocally exchanging the interatomic coherence.

#### 4.3.1 The associated three-level system: EIT

By adding Eqs. (4.8a) and (4.8e), we obtain

$$\frac{d}{dt}[C_{ab} + C_{ba}] = -\frac{\Omega(t)}{2}[\tilde{C}_{cb} + \tilde{C}_{bc}]. \quad (4.19)$$

Then, by adding Eqs. (4.8b) and (4.8d), we have

$$\frac{d}{dt}[\tilde{C}_{cb} + \tilde{C}_{bc}] = -\frac{\Gamma}{2}[\tilde{C}_{cb} + \tilde{C}_{bc}] + \frac{\Omega(t)}{2}[C_{ab} + C_{ba}] + gC_{bb}. \quad (4.20)$$

And finally, from Eq. (4.8c), we get

$$\frac{d}{dt} C_{bb} = -\frac{g}{2} [\tilde{C}_{cb} + \tilde{C}_{bc}]. \quad (4.21)$$

If we assume that the evolution of the system takes place in the Hilbert space spanned by the *symmetric* eigenvectors

$$|\psi_1\rangle = \frac{1}{\sqrt{2}}(|a\ b\ 0\rangle + |b\ a\ 0\rangle), \quad (4.22a)$$

$$|\psi_2\rangle = \frac{1}{\sqrt{2}}(|c\ b\ 0\rangle + |b\ c\ 0\rangle), \quad (4.22b)$$

$$|\psi_3\rangle = |b\ b\ 1\rangle, \quad (4.22c)$$

then we define the state vector of the system as the linear superposition

$$|\Psi_S(t)\rangle = B_1(t)|\psi_1\rangle + B_2(t)|\psi_2\rangle + B_3(t)|\psi_3\rangle. \quad (4.23)$$

Here  $B_1$ ,  $B_2$ , and  $B_3$  represent the probability amplitudes of finding the system in the symmetric states  $|\psi_1\rangle$ ,  $|\psi_2\rangle$ , and  $|\psi_3\rangle$ , respectively. These coefficients can be expressed in terms of the individual probability amplitudes (4.5) as follows:

$$\begin{aligned} B_1(t) &= \langle\psi_1|\Psi_S(t)\rangle \\ &= \frac{1}{\sqrt{2}}[\langle a\ b\ 0|\Psi_S(t)\rangle + \langle b\ a\ 0|\Psi_S(t)\rangle] \\ &= \frac{1}{\sqrt{2}}[C_{ab} + C_{ba}]. \end{aligned} \quad (4.24a)$$

Similarly

$$B_2(t) = \frac{1}{\sqrt{2}}[\tilde{C}_{cb} + \tilde{C}_{bc}], \quad (4.24b)$$

$$B_3(t) = C_{bb}. \quad (4.24c)$$



On inserting Eqs. (4.24) into Eqs. (4.19), (4.20), and (4.21), we obtain

$$\dot{B}_1 = -\frac{\Omega(t)}{2} B_2, \quad (4.25a)$$

$$\dot{B}_2 = +\frac{\Omega(t)}{2} B_1 - \frac{\Gamma}{2} B_2 + \frac{g}{\sqrt{2}} B_3, \quad (4.25b)$$

$$\dot{B}_3 = -\frac{g}{\sqrt{2}} B_2. \quad (4.25c)$$

These equations represent the dynamics of a three-level  $\Lambda$  system with states  $|\psi_1\rangle$  and  $|\psi_3\rangle$  coupled to an excited state  $|\psi_2\rangle$  via, respectively, a classical laser field  $\Omega(t)$  and a cavity mode field  $\sqrt{2}g$  (see Fig. 4.8).

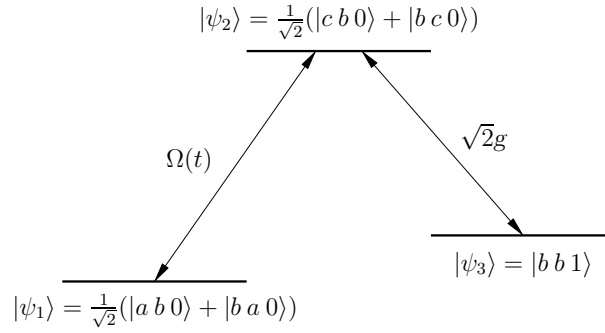


Figure 4.8: The associated three-level  $\Lambda$  system driven by a classical field with Rabi frequency  $\Omega(t)$  and interacting with a quantum field of strength  $\sqrt{2}g$ .

The evolution of system (4.25) is controlled by the non-Hermitian Hamiltonian

$$H_S = \frac{\hbar}{2} \begin{bmatrix} 0 & -\Omega & 0 \\ \Omega & -\Gamma & \sqrt{2}g \\ 0 & -\sqrt{2}g & 0 \end{bmatrix}, \quad (4.26)$$

which has a *dark* state given by

$$|D\rangle = \frac{-\sqrt{2}g|\psi_1\rangle + \Omega|\psi_3\rangle}{\sqrt{2g^2 + \Omega^2}}. \quad (4.27)$$

By defining the mixing angle as

$$\Phi(t) = \tan^{-1} \left[ \frac{\sqrt{2}g}{\Omega(t)} \right], \quad (4.28)$$

we can write Eq. (4.27) in the form

$$|D\rangle = -\sin \Phi(t)|\psi_1\rangle + \cos \Phi(t)|\psi_3\rangle. \quad (4.29)$$

As before, we can transfer population between states  $|\psi_1\rangle$  and  $|\psi_3\rangle$  without populating the leaking state  $|\psi_2\rangle$  by employing adiabatic passage via the dark state of the system. The process of coherence transfer in this system is illustrated in Fig. 4.9.

We note that, if  $\sqrt{2}g \gg \Omega$ , then the state  $|D\rangle$  corresponds almost identically to the state  $|\psi_1\rangle$ . This means that a single photon excitation is shared among the atoms, favoring the transfer of coherence. In addition, the effect of cavity decay is reduced, since the state with a cavity photon is not populated. In this limit, a superposition given by the dark state contains only a very small component of the single-photon state  $|b\ b\ 1\rangle$ . This increases the lifetime of the combined atom-cavity system and is the essential feature of intracavity electromagnetically induced transparency (EIT) [FYL00].

### 4.3.2 The associated two-level system: $2\pi$ -pulse coherence transfer

On the other hand, by subtracting Eq. (4.8e) from (4.8a), we get

$$\frac{d}{dt}[C_{ab} - C_{ba}] = -\frac{\Omega}{2}[\tilde{C}_{cb} - \tilde{C}_{bc}]; \quad (4.30)$$

and by subtracting Eq. (4.8d) from (4.8b), we obtain

$$\frac{d}{dt}[\tilde{C}_{cb} - \tilde{C}_{bc}] = -\frac{\Gamma}{2}[\tilde{C}_{cb} - \tilde{C}_{bc}] - \frac{\Omega}{2}[C_{ab} - C_{ba}]. \quad (4.31)$$

Now, if we assume that the evolution of the system takes place in the Hilbert space spanned by the *antisymmetric* eigenvectors

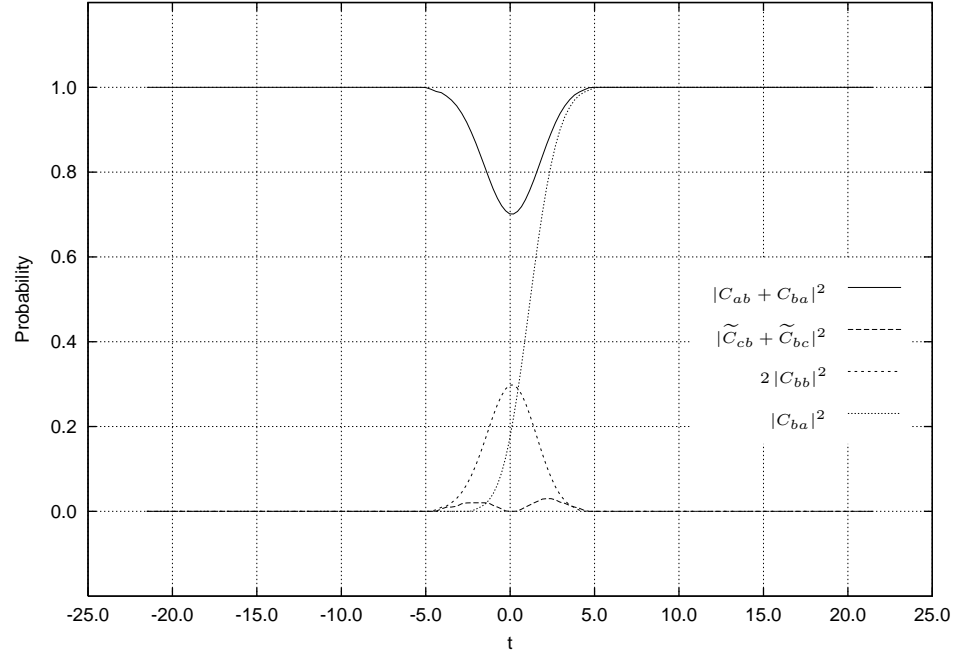
$$|\varphi_1\rangle = \frac{1}{\sqrt{2}}[|a\ b\ 0\rangle - |b\ a\ 0\rangle], \quad (4.32a)$$

$$|\varphi_2\rangle = \frac{1}{\sqrt{2}}[|c\ b\ 0\rangle - |b\ c\ 0\rangle], \quad (4.32b)$$

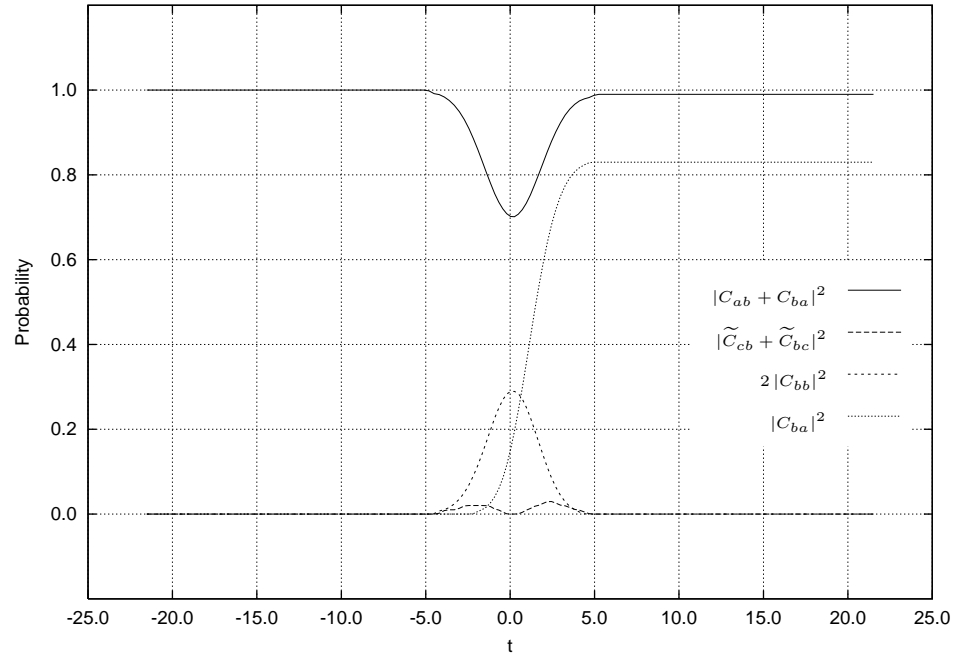
then we define the state vector of the system as the linear superposition

$$|\Psi_A(t)\rangle = A_1(t)|\varphi_1\rangle + A_2(t)|\varphi_2\rangle. \quad (4.33)$$

Here  $A_1$  and  $A_2$  represent the probability amplitudes of finding the system in the antisymmetric states  $|\varphi_1\rangle$  and  $|\varphi_2\rangle$ , respectively. As before, these coefficients can be expressed in terms of the



(a)  $\Gamma = 0.00$



(b)  $\Gamma = 0.10$

Figure 4.9: Transferring of coherence in the associated three-level system.

individual probability amplitudes (4.5) as follows:

$$\begin{aligned}
A_1(t) &= \langle \varphi_1 | \Psi_A(t) \rangle \\
&= \frac{1}{\sqrt{2}} [\langle a b 0 | \Psi_A(t) \rangle - \langle b a 0 | \Psi_A(t) \rangle] \\
&= \frac{1}{\sqrt{2}} [C_{ab} - C_{ba}].
\end{aligned} \tag{4.34a}$$

Similarly

$$A_2(t) = \frac{1}{\sqrt{2}} [\tilde{C}_{cb} - \tilde{C}_{bc}]. \tag{4.34b}$$

On inserting Eqs. (4.34) into Eqs. (4.30) and (4.31), we obtain

$$\dot{A}_1 = -\frac{\Omega(t)}{2} A_2, \tag{4.35a}$$

$$\dot{A}_2 = +\frac{\Omega(t)}{2} A_1 - \frac{\Gamma}{2} A_2. \tag{4.35b}$$

These equations represent the evolution of a two-level system with ground state  $|\varphi_1\rangle$  and excited state  $|\varphi_2\rangle$  coupled by a classical laser field  $\Omega(t)$ , as illustrated in Fig. 4.10.

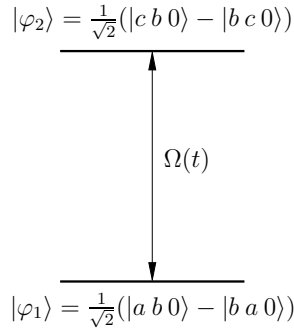
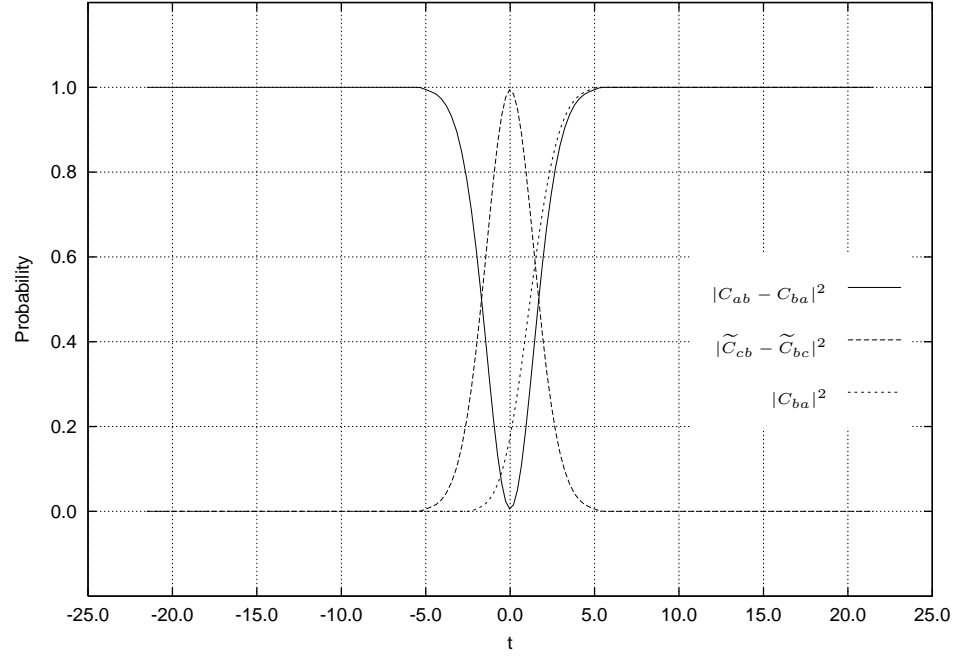


Figure 4.10: The associated two-level atom driven by a classical field with Rabi frequency  $\Omega(t)$ .

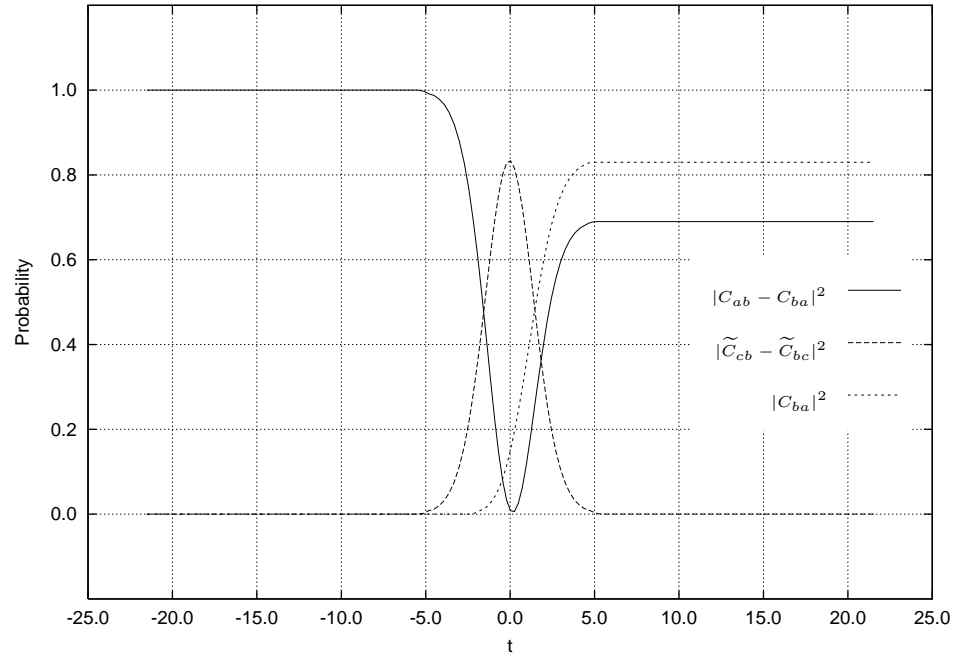
The evolution of system (4.35) is governed by the non-Hermitian Hamiltonian

$$H_A = \frac{\hbar}{2} \begin{bmatrix} 0 & -\Omega \\ \Omega & -\Gamma \end{bmatrix}. \tag{4.36}$$

Here the process of coherence transfer is achieved by a  $2\pi$ -pulse process, as illustrated in Fig. 4.11.



(a)  $\Gamma = 0.00$



(b)  $\Gamma = 0.10$

Figure 4.11: Transferring of coherence in the associated two-level system.

### 4.3.3 Transferring the coherence

By using the symmetric and antisymmetric eigenvectors defined in Eqs. (4.22a) and (4.32a), the evolution of the system  $|a\ b\ 0\rangle \rightarrow |b\ a\ 0\rangle$  can be written in the form

$$\frac{1}{\sqrt{2}}[|\psi_1\rangle + |\varphi_1\rangle] \rightarrow \frac{1}{\sqrt{2}}[|\psi_1\rangle - |\varphi_1\rangle]. \quad (4.37)$$

In this way, the transfer of atomic coherence can be viewed as a combination of two different processes: an adiabatic passage acting on the symmetric eigenstate  $|\psi_1\rangle$ , and a  $2\pi$ -pulse process acting on the antisymmetric eigenstate  $|\varphi_1\rangle$ .

# Conclusions

In this work, we explored numerically two of the most useful methods for transferring population:  $\pi$ -pulse and adiabatic passage schemes. In particular, we applied these methods to transfer population in an atom + cavity system, and to transfer the atomic coherence in a two-atom + cavity system. We discussed some important characteristics, as well as advantages and disadvantages of these two methods.

The numerical simulations revealed very interesting resonance-like features in the adiabatic passage scheme. By choosing appropriately some parameters of the system, like the ratio of the pulses and the pulse delay, we achieved very high transfer efficiencies. To find out different ways of choosing the right values for these parameters and reduce the failure probability was the main goal of this dissertation.

It is well known that when a system undergoes *no* spontaneous emission, we can obtain transfer efficiencies of 100% by using  $\pi$ -pulses methods. However, when the system undergoes spontaneous emission, the transfer efficiency of the method decreases as the radiative decay rate increases. Our numerical results showed that efficiencies near to 100% were possible to obtain by using adiabatic passage methods for a particular set of parameters, with or without radiative decay.

For the atom + cavity system and no spontaneous emission, we obtained efficiencies of 99.9% transferring the population via adiabatic passage. The Sech pulses showed to be more effective than the Gaussian pulses, since they required less relative energy ( $\Omega/g$ ) and less interaction time ( $\Delta t/\sigma_g$ ). When we consider the effects of spontaneous emission, the transfer efficiency of the  $\pi$ -pulses method decreased accordingly to the increment in the rate of radiative decay. In particular, for  $\Gamma = 0.10$ , the Gaussian pulses had an efficiency of 93.5%, while the Sech pulses presented a maximum efficiency of 92.6%. However, in the adiabatic passage scheme was possible to find a set of parameters for which the transfer efficiency achieved a 99.0%. This set was  $\{\Omega = 2.75, \sigma = 3.09, g = 1.00, \sigma_g = 2.48, \Delta t = 5.29\}$ . Gaussian pulses proved to be more efficient this time than Sech pulses.

By comparing the ratio of the Gaussian pulses in adiabatic passage, with the ratio of the Gaussian

pulses in the  $\pi$ -pulses method, and their respective interaction times, we observed that adiabatic passage was more efficient transferring population than  $\pi$ -pulses. For Sech pulses to achieve the same transfer efficiency, it is required to use more energy and more time delay.

We also observed that, in adiabatic passage methods, the efficiency can be optimized as much as we want by increasing the values of the Rabi frequencies, or equivalently, the widths of the pulses. Thus, for bigger Rabi frequencies, bigger efficiencies. Because this is something that has no experimental worth, we examined here those values of the Rabi frequency and time delay that can be reproduced in a laboratory, and for which very good transfer efficiency values could be obtained. So we considered a *reasonable* value of  $\log_{10} p = -2.00$  as a goal for our numerical simulations.

We obtained also interesting results transferring the coherence in the two-atom + cavity system. With no spontaneous emission, efficiencies of 99.9% were achieved by using the adiabatic passage scheme with Gaussian and Sech pulses. However this time, Gaussian pulses required less energy and less interaction time than Sech pulses to obtain such transfer efficiency. When spontaneous emission was included, Sech showed a better performance than Gaussian pulses with a comparatively small ratio of the pulses. A transfer efficiency of 99.1% was achieved for the set of parameters  $\{\Omega_{10} = 3.80, \sigma_1 = 4.40, \Omega_{20} = 1.00, \sigma_2 = 5.00, g = 1.00, \Delta t = 11.48\}$ .

A simple but very useful analytical model used to better understand the transfer efficiencies in the adiabatic passage scheme was introduced in Ch. 3. When the widths of the pulses are unequal, we do not expect adiabatic passage to work. However, we still found some cases for which a high transfer efficiency were obtained. This model described “qualitatively” the dependence of the failure probability on the product of parameters  $\Omega T$ . We confirmed that for large values of  $\Omega T$  the probability failure power-law decreased.

Finally, we examined the two-atom + cavity system by using an alternative and simplified model based on the superposition of symmetric and antisymmetric eigenstates. We found possible to qualitatively explain the transfer of the Zeeman coherence between two atoms, by using an adiabatic passage method for the symmetric state, and a  $2\pi$ -pulses process for the antisymmetric state.



# Bibliography

- [AE75] Leslie Allen and J. H. Eberly, *Optical resonance and two-level atoms*, Wiley, New York, 1975.
- [Blo46] F. Bloch, *Nuclear induction*, Phys. Rev. **70** (1946), no. 7, 460–474.
- [BS40] F. Bloch and A. Siegert, *Magnetic resonance for nonrotating fields*, Phys. Rev. **57** (1940), 522–527.
- [DH98] K. Drese and M. Holthaus, *Perturbative and nonperturbative processes in adiabatic population transfer*, Eur. Phys. J. D. **3** (1998), 73–86.
- [DP76] Jon P. Davis and Philip Pechukas, *Nonadiabatic transitions induced by a time-dependent hamiltonian in the semiclassical/adiabatic limit: The two-state case*, J. Chem. Phys. **64** (1976), no. 8, 3129–3137.
- [Elg80] J. N. Elgin, *Semiclassical formalism for the treatment of three-level systems*, Phys. Lett. **80A** (1980), no. 2, 140–142.
- [EWG76] T. H. Einwohner, J. Wong, and J. C. Garrison, *Analytical solutions for laser excitation of multilevel systems in the rotating-wave approximation*, Phys. Rev. A **14** (1976), no. 4, 1452–1456.
- [FVH57] Richard P. Feynman, Frank L. Vernon, and Robert W. Hellwarth, *Geometrical representation of the schrödinger equation for solving maser problems*, J. Appl. Phys. **28** (1957), no. 1, 49–52.
- [FYL00] M. Fleischhauer, S. F. Yelin, and M. D. Lukin, *How to trap photons? storing single-photon quantum states in collective atomic excitations*, Opt. Commun. **179** (2000), 395–410.
- [HE81] F. T. Hioe and J. H. Eberly, *N-level coherence vector and higher conservation laws in quantum optics and quantum mechanics*, Phys. Rev. Lett. **47** (1981), no. 12, 838–841.
- [HE82] ———, *Nonlinear constants of motion for three-level quantum systems*, Phys. Rev. A **25** (1982), no. 4, 2168–2171.
- [Hio83] F. T. Hioe, *Theory of generalized adiabatic following in multilevel systems*, Phys. Lett. **99A** (1983), no. 4, 150–155.
- [KGHB89] J. R. Kuklinski, U. Gaubatz, F. T. Hioe, and K. Bergmann, *Adiabatic population transfer in a three-level system driven by delayed laser pulses*, Phys. Rev. A **40** (1989), no. 11, 6741–6744.
- [LS96] Timo A. Laine and Stig Stenholm, *Adiabatic processes in three-level systems*, Phys. Rev. A **53** (1996), no. 4, 2501–2512.
- [Mes99] Albert Messiah, *Quantum mechanics*, Dover, Mineola, New York, 1999.
- [Mor64] R. J. Morris, *Theory of adiabatic rapid passage for three equally spaced levels*, Phys. Rev. **133** (1964), no. 3A, A740–A750.

- [MT95] Jerry B. Marion and Stephen T. Thornton, *Classical dynamics of particles and systems*, fourth ed., Saunders College Pub., Fort Worth, 1995.
- [MYM94] S. E. Morin, C. C. Yu, and T. W. Mossberg, *Strong atom-cavity coupling over large volumes and the observation of subnatural intracavity atomic linewidths*, Phys. Rev. Lett. **73** (1994), no. 11, 1489–1492.
- [OBRW96] G-L Oppo, S. M. Barnett, E. Riis, and M. Wilkinson (eds.), *Quantum dynamics of simple systems: the forty-fourth scottish universities summer school in physics*, Scottish Universities Summer School in Physics, Edinburgh, 1996.
- [PGCZ95] T. Pellizzari, S. A. Gardiner, J. I. Cirac, and P. Zoller, *Decoherence, continuous observation, and quantum computing: a cavity qed model*, Phys. Rev. Lett. **75** (1995), no. 21, 3788–3791.
- [PMZ<sup>+</sup>95] A. S. Parkins, P. Marte, P. Zoller, O. Carnal, and H. J. Kimble, *Quantum-state mapping between multilevel atoms and cavity light fields*, Phys. Rev. A **51** (1995), no. 2, 1578–1596.
- [PMZK93] A. S. Parkins, P. Marte, P. Zoller, and H. J. Kimble, *Synthesis of arbitrary quantum states via adiabatic transfer of zeeman coherence*, Phys. Rev. Lett. **71** (1993), no. 19, 3095–3098.
- [RRS54] I. I. Rabi, N. F. Ramsey, and J. Schwinger, *Use of rotating coordinates in magnetic resonance problems*, Rev. Mod. Phys. **26** (1954), no. 2, 167–171.
- [SBK<sup>+</sup>92] Bruce W. Shore, K. Bergmann, A. Kuhn, S. Schiemann, J. Oreg, and J. H. Eberly, *Laser-induced population transfer in multistate systems: A comparative study*, Phys. Rev. A **45** (1992), no. 7, 5297–5300.
- [Shi63] Jon H. Shirley, *Some causes of resonant frequency shifts in atomic beam machines. i. shifts due to other frequencies of excitation*, J. Appl. Phys. **34** (1963), no. 4, 783–788.
- [SZ97] Marlan O. Scully and M. Suhail Zubairy, *Quantum optics*, University Press, Cambridge, 1997.
- [TRK92] R. J. Thompson, G. Rempe, and H. J. Kimble, *Observation of normal-mode splitting for an atom in an optical cavity*, Phys. Rev. Lett. **68** (1992), no. 8, 1132–1137.
- [VS96] N. V. Vitanov and S. Stenholm, *Non-adiabatic effects in population transfer in three-level systems*, Opt. Commun. **127** (1996), 215–222.

# Appendix A: Change of variables

Let us consider the system of three coupled linear differential equations

$$\dot{C}_a = \frac{i}{2} \Omega_1(t) e^{i\alpha} e^{i\Delta_1 t} C_c, \quad (38a)$$

$$\dot{C}_b = \frac{i}{2} \Omega_2(t) e^{i\beta} e^{i(\Delta_1 + \Delta_2)t} C_c, \quad (38b)$$

$$\dot{C}_c = \frac{i}{2} \Omega_1^*(t) e^{-i\alpha} e^{-i\Delta_1 t} C_a + \frac{i}{2} \Omega_2^*(t) e^{-i\beta} e^{-i(\Delta_1 + \Delta_2)t} C_b. \quad (38c)$$

It is possible to eliminate the exponentials from Eqs. (38) by making the following change of variables

$$C_a = e^{i\phi_a t} \tilde{C}_a, \quad C_b = e^{i\phi_b t} \tilde{C}_b, \quad C_c = e^{i\phi_c t} \tilde{C}_c. \quad (39)$$

By differentiating with respect to time, we obtain

$$\dot{C}_a = e^{i\phi_a t} \dot{\tilde{C}}_a + i\phi_a e^{i\phi_a t} \tilde{C}_a, \quad (40a)$$

$$\dot{C}_b = e^{i\phi_b t} \dot{\tilde{C}}_b + i\phi_b e^{i\phi_b t} \tilde{C}_b, \quad (40b)$$

$$\dot{C}_c = e^{i\phi_c t} \dot{\tilde{C}}_c + i\phi_c e^{i\phi_c t} \tilde{C}_c. \quad (40c)$$

Now plugging Eqs. (39) and (40) into Eqs. (38) gives

$$\dot{\tilde{C}}_a = -i\phi_a \tilde{C}_a + i \frac{\Omega_1(t)}{2} e^{i\alpha} e^{i(\Delta_1 + \phi_c - \phi_a)t} \tilde{C}_c, \quad (41a)$$

$$\dot{\tilde{C}}_b = -i\phi_b \tilde{C}_b + i \frac{\Omega_2(t)}{2} e^{i\beta} e^{i(\Delta_1 + \Delta_2 + \phi_c - \phi_b)t} \tilde{C}_c, \quad (41b)$$

$$\begin{aligned} \dot{\tilde{C}}_c = & -i\phi_c \tilde{C}_c + i \frac{\Omega_1^*(t)}{2} e^{-i\alpha} e^{-i(\Delta_1 + \phi_c - \phi_a)t} \tilde{C}_a \\ & + i \frac{\Omega_2^*(t)}{2} e^{-i\beta} e^{-i(\Delta_1 + \Delta_2 + \phi_c - \phi_b)t} \tilde{C}_b. \end{aligned} \quad (41c)$$

Because we want the phases to cancel out, they must satisfy the conditions

$$\Delta_1 + \phi_c - \phi_a = 0, \quad (42a)$$

$$\Delta_1 + \Delta_2 + \phi_c + \phi_b = 0. \quad (42b)$$

Solving this system of equations for  $\phi_a$ ,  $\phi_b$ , and  $\phi_c$  gives

$$\phi_a = \Delta_1 + \phi_c, \quad \phi_b = \Delta_1 + \Delta_2 + \phi_c, \quad \phi_c \text{ arbitrary}. \quad (43)$$

By choosing  $\phi_c = 0$ , and plugging these phases into Eqs. (41), we get

$$i\dot{C}_a(t) = \Delta_1 C_a(t) - \frac{\Omega_1(t)}{2} e^{i\alpha} C_c(t), \quad (44a)$$

$$i\dot{C}_b(t) = (\Delta_1 + \Delta_2) C_b(t) - \frac{\Omega_2(t)}{2} e^{i\beta} C_c(t), \quad (44b)$$

$$i\dot{C}_c(t) = -\frac{\Omega_1^*(t)}{2} e^{-i\alpha} C_a(t) - \frac{\Omega_2^*(t)}{2} e^{-i\beta} C_b(t). \quad (44c)$$

Finally, the phases  $\alpha$  and  $\beta$  allow us to flip the signs of the terms by choosing suitable values. If  $\alpha = \beta = \pi$ , Eqs. (44) become

$$i\dot{C}_a(t) = \Delta_1 C_a(t) + \frac{\Omega_1(t)}{2} C_c(t), \quad (45a)$$

$$i\dot{C}_b(t) = (\Delta_1 + \Delta_2) C_b(t) + \frac{\Omega_2(t)}{2} C_c(t), \quad (45b)$$

$$i\dot{C}_c(t) = \frac{\Omega_1^*(t)}{2} C_a(t) + \frac{\Omega_2^*(t)}{2} C_b(t). \quad (45c)$$

# Appendix B: The instantaneous Hamiltonian eigenstates

Let us find the eigenvalues and eigenvectors of the instantaneous RWA Hamiltonian ( $\hbar = 1$ )

$$H(t) = \frac{1}{2} \begin{bmatrix} 0 & 0 & \Omega_1(t) \\ 0 & 0 & \Omega_2(t) \\ \Omega_1(t) & \Omega_2(t) & 0 \end{bmatrix}. \quad (46)$$

Solving the characteristic equation

$$\det(H - \omega I) = \begin{vmatrix} -\omega & 0 & \frac{1}{2}\Omega_1 \\ 0 & -\omega & \frac{1}{2}\Omega_2 \\ \frac{1}{2}\Omega_1 & \frac{1}{2}\Omega_2 & -\omega \end{vmatrix} = 0, \quad (47)$$

or

$$\omega^3 - \frac{1}{4}(\Omega_1^2 + \Omega_2^2)\omega = 0, \quad (48)$$

we find the eigenvalues

$$\omega^+ = +\frac{1}{2}\sqrt{\Omega_1^2 + \Omega_2^2}, \quad \omega^0 = 0, \quad \omega^- = -\frac{1}{2}\sqrt{\Omega_1^2 + \Omega_2^2}, \quad (49)$$

For  $\omega^+$  the eigenvector can be determined from the system

$$\begin{aligned}\Omega_1 z &= \Omega x, \\ \Omega_2 z &= \Omega y, \\ \Omega_1 x + \Omega_2 y &= \Omega z,\end{aligned}\tag{50}$$

where  $\Omega = \sqrt{\Omega_1^2 + \Omega_2^2}$ . Thus

$$x = \frac{\Omega_1}{\Omega} z, \quad y = \frac{\Omega_2}{\Omega} z, \quad z \text{ arbitrary}.\tag{51}$$

Assuming the representation

$$|a\rangle = \begin{bmatrix} 1 \\ 0 \\ 0 \end{bmatrix}, \quad |b\rangle = \begin{bmatrix} 0 \\ 1 \\ 0 \end{bmatrix}, \quad |c\rangle = \begin{bmatrix} 0 \\ 0 \\ 1 \end{bmatrix},\tag{52}$$

the eigenvector associated with  $\omega^+$  can be written as

$$|W^+\rangle = \frac{1}{\sqrt{2}} \left[ \frac{\Omega_1}{\Omega} |a\rangle + \frac{\Omega_2}{\Omega} |b\rangle + |c\rangle \right].\tag{53a}$$

Similarly, for  $\omega^0$  and  $\omega^-$ , the associated eigenvectors are

$$|W^0\rangle = \frac{\Omega_2}{\Omega} |a\rangle - \frac{\Omega_1}{\Omega} |b\rangle,\tag{53b}$$

$$|W^-\rangle = \frac{1}{\sqrt{2}} \left[ \frac{\Omega_1}{\Omega} |a\rangle + \frac{\Omega_2}{\Omega} |b\rangle - |c\rangle \right],\tag{53c}$$

respectively. By using the trigonometric relations

$$\sin \Phi(t) = \frac{\Omega_1(t)}{\Omega(t)}, \quad \cos \Phi(t) = \frac{\Omega_2(t)}{\Omega(t)}, \quad \tan \Phi(t) = \frac{\Omega_1(t)}{\Omega_2(t)},\tag{54}$$

we can rewrite Eqs. (53) as follows

$$|W^+\rangle = \frac{1}{\sqrt{2}} [\sin \Phi(t)|a\rangle + \cos \Phi(t)|b\rangle + |c\rangle], \quad (55a)$$

$$|W^0\rangle = \cos \Phi(t)|a\rangle - \sin \Phi(t)|b\rangle, \quad (55b)$$

$$|W^-\rangle = \frac{1}{\sqrt{2}} [\sin \Phi(t)|a\rangle + \cos \Phi(t)|b\rangle - |c\rangle]. \quad (55c)$$

# Appendix C: The forced harmonic oscillator

The equation of motion for a particle of mass  $m$  moving under the combined influence of a linear restoring force  $-kx$ , a resisting force  $-b\dot{x}$ , and an external driving force  $F(t)$  is given by

$$m\ddot{x} + b\dot{x} + kx = F(t). \quad (56)$$

The most general solution to this differential equation is composed of the *complementary* and *particular* solutions (see [MT95]):

$$x(t) = x_c(t) + x_p(t). \quad (57)$$

## Complementary solution

The complementary solution has the general form

$$x_c(t) = e^{-\gamma t} \left[ C_1 \exp\left(i\sqrt{\omega_0^2 - \gamma^2} t\right) + C_2 \exp\left(-i\sqrt{\omega_0^2 - \gamma^2} t\right) \right], \quad (58)$$

where

$$\gamma = \frac{b}{2m}, \quad \text{and} \quad \omega_0 = \sqrt{\frac{k}{m}}. \quad (59)$$

There are three general cases of interest:

$$\text{Underdamping:} \quad \gamma^2 < \omega_0^2$$

$$\text{Critical damping:} \quad \gamma^2 = \omega_0^2$$

$$\text{Overdamping:} \quad \gamma^2 > \omega_0^2$$



For the case of underdamped motion, the exponents in the brackets of Eq. (58) are imaginary, and the solution can be written as

$$x_c(t) = [A \sin \omega_1 t + B \cos \omega_1 t], \quad (60)$$

where

$$\omega_1 = \sqrt{\omega_0^2 - \gamma^2}. \quad (61)$$

For the case of critical damping, the roots of the auxiliary equation ( $r^2 + 2\gamma r + \omega_0^2 r = 0$ ) are equal, and the complementary function must be written in the form

$$x_c(t) = e^{-\gamma t} (A + Bt). \quad (62)$$

Finally, for the case of overdamped motion, the exponents in the brackets of Eq. (58) become real quantities:

$$x_c(t) = e^{-\gamma t} [C_1 e^{\omega_1 t} + C_2 e^{-\omega_1 t}]. \quad (63)$$

## Particular solution

Now we seek a particular solution to the inhomogeneous equation in the form

$$x_p(t) = \int_{-\infty}^{\infty} F(t') G(t, t') dt', \quad (64)$$

where  $F(t')$  is the applied external force (inhomogeneity), and  $G(t, t')$  is the Green's function for Eq. (56). We define

$$G(t, t') = \begin{cases} \frac{1}{m\omega_1} e^{-\gamma(t-t')} \sin[\omega_1(t-t')] & \text{if } t \geq t', \\ 0 & \text{if } t < t'. \end{cases} \quad (65)$$

Then, the particular solution can be expressed as

$$x_p(t) = \int_{-\infty}^t \frac{F(t')}{m\omega_1} e^{-\gamma(t-t')} \sin[\omega_1(t-t')] dt'. \quad (66)$$

## The simple analytical model

For the simple analytical model studied in Sec. 3.1, we obtained a second-order linear differential equation of the form

$$\frac{d^2}{d\tau^2}\delta\theta[\tau] + \delta\theta[\tau] = -\frac{d}{d\tau}\Phi[\tau]. \quad (67)$$

On comparing Eqs. (56) and (67), we have

$$m = 1, \quad b = 0, \quad k = 1, \quad F(\tau) = -\frac{d}{d\tau}\Phi. \quad (68)$$

Upon substitution of these parameters into Eq. (59) and Eq. (61), we get

$$\omega_0 = 1, \quad \gamma = 0, \quad \omega_1 = 1. \quad (69)$$

For this case we have  $\omega_0^2 > \gamma^2$  (underdamping). Therefore the most general solution to Eq. (67) can be expressed as

$$\delta\theta[\tau] = A \sin[\tau] + B \cos[\tau] - \int_{-\infty}^{\tau} \sin[\tau - \tau'] \frac{d\Phi(\tau')}{d\tau'} d\tau'. \quad (70)$$